

## Chapter I.4

### Longitudinal beam dynamics

*Alexandre Lasheen*

CERN, Geneva, Switzerland

---

Longitudinal beam dynamics in particle accelerators treats the acceleration as well as the focusing (bunching) of the particles in the longitudinal direction. In this lecture, general aspects of particle acceleration are first exposed before focusing on acceleration with RF systems and the synchrotron design. The concept of synchronous particle and the relevant differential equations for that reference point are demonstrated. Longitudinal equations of motion for non-synchronous particles are derived to analyze the motion of all non-ideal particles in the longitudinal phase space (synchrotron motion). Derivations are done first by solving linearized equations, followed by solutions relying on non-linear terms to put in evidence the concepts of RF bucket and acceptance. A final part is devoted to real life applications and examples of operational aspects. All along, exercises are proposed to guide the reader and provide insights in practical accelerator parameters encountered for CERN synchrotrons.

---

#### I.4.1 Introduction

##### I.4.1.1 Foreword

The following lecture on longitudinal beam dynamics is the product of many contributions and evolutions over the past thirty years of the JUAS, by the following lecturers: L. Rinolfi (1994–2002), R. Corsini (2003–2009), F. Tecker (2010), E. Métral (2011–2021), A. Lasheen (2022–present), and with essential help from teaching assistants: E. Benedetto, B. Salvant, D. Amorim, S. Joly, D. Quartullo, B. E. Karlsen-Baeck and L. Intelisano. Colleagues across the Accelerator Sector at CERN, in particular from the Accelerator and Beam Physics and the Radio Frequency groups are also gratefully acknowledged for their direct and indirect contributions. Notably, H. Damerou and E. Shaposhnikova for the recent lectures done for the CAS and F. Batsch, J. Flowerdew, M. Marchi, M. Schwarz, A. Vanel, T. Van Rijswijk for proofreading. The content of the lecture is greatly inspired by the work of the authors provided in the bibliography.

##### I.4.1.2 Course layout

The introductory lesson (Section I.4.1) provides a shallow overview of the concepts around longitudinal beam dynamics and how this lecture connects with the rest of the JUAS program.

Lesson 1 (Section I.4.2) is devoted to the fundamentals of particle acceleration. This includes an exploration of fields and forces, a review of various accelerator designs, and an understanding of relativistic relationships.

---

This chapter should be cited as: Longitudinal beam dynamics, A. Lasheen, DOI: [10.23730/CYRSP-2024-003.167](https://doi.org/10.23730/CYRSP-2024-003.167), in: Proceedings of the Joint Universities Accelerator School (JUAS): Courses and exercises, E. Métral (ed.), CERN Yellow Reports: School Proceedings, CERN-2024-003, DOI: [10.23730/CYRSP-2024-003](https://doi.org/10.23730/CYRSP-2024-003), p. 167. © CERN, 2024. Published by CERN under the [Creative Commons Attribution 4.0 license](https://creativecommons.org/licenses/by/4.0/).

Lesson 2 (Section I.4.3) focuses on synchrotron design, presenting the equations for the synchronous particle. It also describes the momentum compaction factor and the differential relationships together with a brief outlook on betatronic acceleration, synchrotron radiation, and self-induced fields.

Lesson 3 (Section I.4.4) is dedicated to the longitudinal equations of motion. It covers the equations for non-synchronous particles and introduces the concept of particle tracking for numerical simulations.

In Lesson 4 (Section I.4.5), the longitudinal equations of motion are used to describe the synchrotron motion. First in the linear regime to demonstrate phase stability, synchrotron frequency/tune; then in the non-linear synchrotron regime to introduce the RF bucket characteristics, the longitudinal emittance, and the non-linear synchrotron frequency.

In Lesson 5 (Section I.4.6), we apply these concepts to real-life applications. This includes longitudinal bunch profile measurements and the description of injection oscillations together with their optimization. A final word on more advanced topics is given on RF manipulations and beam instabilities.

The main formulas, concepts and assumptions are finally summarized in Section I.4.7, followed by the correction of the exercises.

Towards the end of the course, students should have a clear understanding of how a beam is effectively accelerated in a particle accelerator and understand the fundamental concepts of longitudinal beam dynamics, such as synchrotron motion, the RF bucket, and its parameters. They should also understand how main equations and formulae are derived, including the underlying assumptions.

Finally, students should be able to compute RF parameters and basic design parameters of a synchrotron and interpret the longitudinal motion of a measured bunch of particles, to apply their acquired knowledge to practical scenarios.

### I.4.1.3 Key aspects of longitudinal beam dynamics

The main objective of a particle accelerator is to increase particle energies for various applications, from fixed target experiments, colliders, and light sources. Longitudinal beam dynamics addresses the acceleration of the particles along the longitudinal direction, along the reference trajectory of the accelerator. It also describes the focusing of the particles as bunches, which depends on the relative motion of the particles around a reference point, called the synchronous particle.

In order to understand the basics of longitudinal beam dynamics, we first need to describe the layout of an accelerator. To do so, the example of the Low Energy Ion Ring (LEIR) at CERN is used. A picture of the accelerator together with a schematic drawing are shown in Fig. I.4.1. More accelerators can be virtually visited from the CERN web site<sup>1</sup>. A second simplified representation is given in Fig. I.4.2 together with the coordinate system that will be used as a basis for the rest of the course.

---

<sup>1</sup><https://panoramas-outreach.cern.ch/index.html>

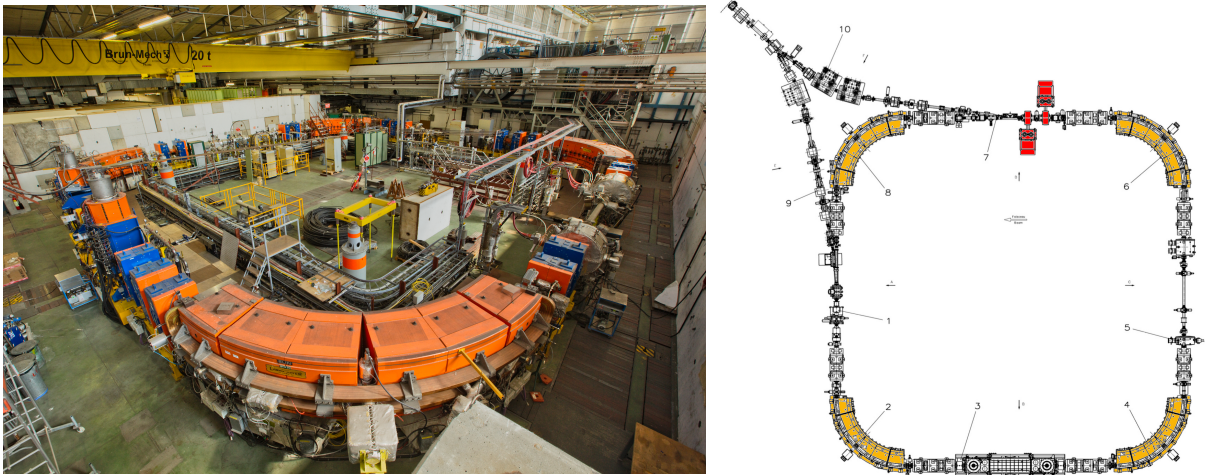


**Fig. I.4.1:** The Low Energy Ion Ring (LEIR) at CERN, as seen from a platform, and its drawing to the right. The dipole bending magnets to steer the beam are in orange, the RF system to accelerate the beam in red.

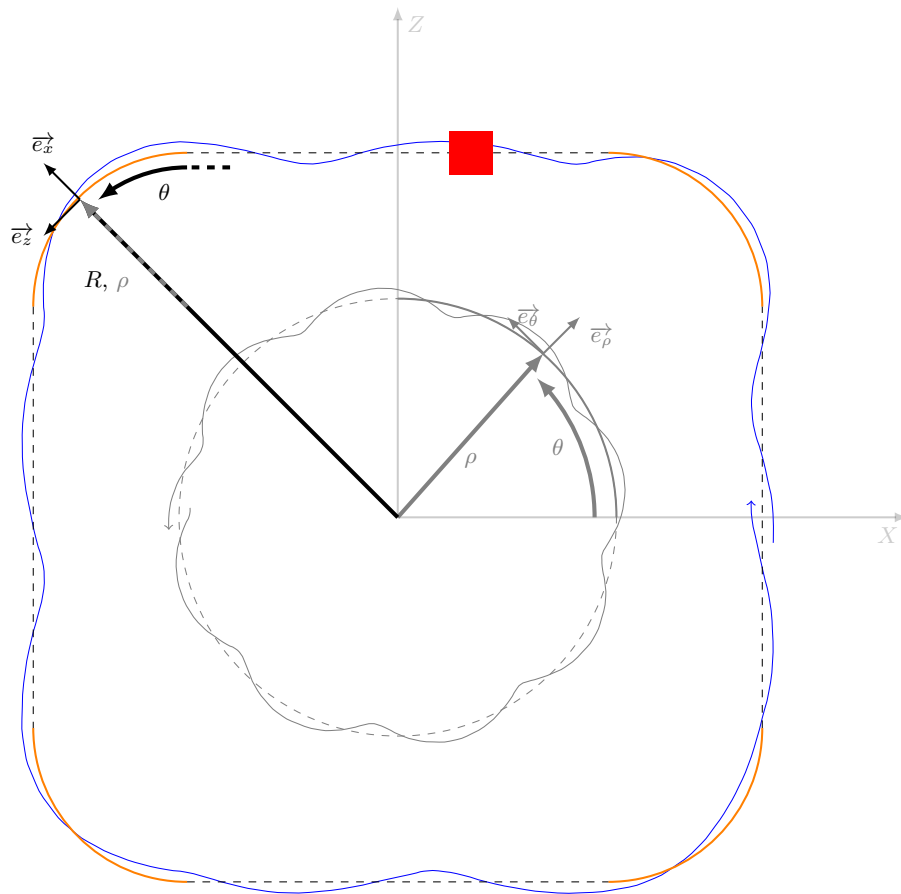


**Fig. I.4.2:** A simplified view of a synchrotron, seen from above (along the vertical axis  $\vec{Y}$  in a Cartesian coordinate system), together with the coordinate system used for the rest of the lecture. The bending magnets are still represented in orange and the RF systems in red. An arbitrary particle trajectory is represented in blue.

### I.4.1.3.1 Coordinate system

In this section we will introduce the coordinate system to describe the particle motion in the longitudinal direction. The black dashed line represents the (ideal) design trajectory of the beam around which a particle oscillates (in blue). The accelerator layout can be described in fixed Cartesian coordinates  $(\vec{X}, \vec{Z}, \vec{Y})$  where the  $\vec{Y}$  direction is the vertical direction. However, this coordinate system is not suited to describe particle motion in circular accelerators.

A particle trajectory is a curved path, which can be described in the Frenet-Serret coordinate system. In terms of particle coordinates, they are defined as offsets relative to the design trajectory, and are categorized as follows:  $x$  for the horizontal position pointing outwards,  $y$  for the vertical position pointing upwards, and  $z$  for the longitudinal coordinate, as depicted in Fig. I.4.3. This forms a  $(\vec{x}, \vec{z}, \vec{y})$  right-handed coordinate system for a particle rotating counter-clockwise along the design trajectory (NB: the normal vector in the Frenet-Serret coordinate system is usually defined pointing towards the center of the curve, which is not the case here). This coordinate system will be used for the rest of the lecture. In the arcs, the local bending radius of the reference trajectory is denoted as  $\rho$ , and the  $x$  will therefore coincide to a radial offset on top of the design curvature.

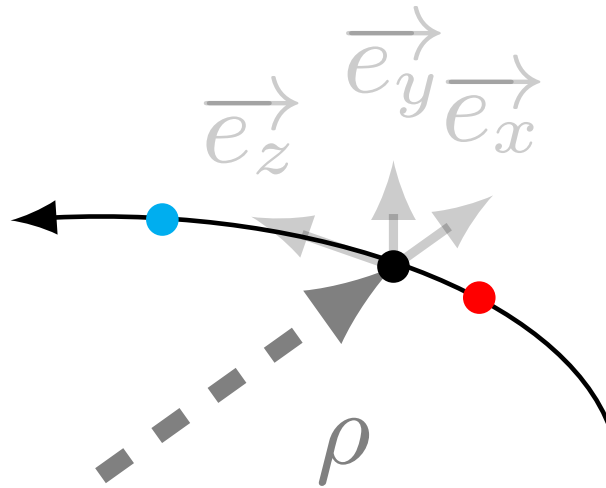


**Fig. I.4.3:** The Frenet-Serret coordinate system along a curved path. Relative to the black reference particle, the blue particle is in front and the red particle is behind in the longitudinal direction.

Note that different conventions can be found in the literature and depending on the use-case. Indeed, some references prefer a left-handed  $(\vec{x}, \vec{z}, \vec{y})$  coordinate system to describe a clockwise rotating beam (the horizontal direction still pointing outwards and the vertical one pointing upwards). In the early literature, the preference was to have a system  $(\vec{x}, \vec{y}, \vec{z})$  where  $z$  represented the vertical direction instead of the longitudinal one [1].

We introduce the concept of the mean radius, defined as  $R = C/(2\pi)$ , where  $C$  represents the full path circumference, including the straight sections. Alongside this, we define the generalized azimuth  $\theta \in [0, 2\pi]$ , also representing the longitudinal coordinate along the accelerator.

It is important to distinguish between  $\rho$  and  $R$ . As a reminder,  $\rho$  represents the local bending radius in curved paths, whereas  $R$  is the radius of the particle orbit, which includes straight sections of

total length  $L$ . We express this relationship as  $C = 2\pi R = L + 2\pi\rho$ .

#### 1.4.1.3.2 Particle acceleration

The primary purpose of a particle accelerator is to produce a beam of particles with a precise energy  $E$ . This energy is imparted on the charged particles by applying the Lorentz force, described by the equation

$$\frac{d\vec{p}}{dt} = \vec{F} = q(\vec{\mathcal{E}} + \vec{v} \times \vec{\mathcal{B}}), \quad (1.4.1)$$

where  $\vec{p} = m\vec{v}$  represents the particle momentum,  $q$  the particle charge,  $m$  the particle's relativistic mass,  $\vec{v}$  the particle velocity,  $\vec{F}$  the force,  $\vec{\mathcal{E}}$  an electric field, and  $\vec{\mathcal{B}}$  a magnetic field.

An electric field can effectively accelerate (or decelerate) particles, and can also be used to deflect particles if applied transversely to the particle trajectory. The force applied by a magnetic field is always orthogonal to the particle trajectory and therefore cannot provide energy to the beam, it can only steer the beam.

The acceleration process in a particle accelerator involves applying an electric field tangential to the beam trajectory, which can be represented as  $\vec{\mathcal{E}} = \mathcal{E}_z \vec{e}_z$ . It is important to note that, with the exception of extremely low energies (such as in particle sources), the momentum of a particle is predominantly directed towards the longitudinal  $z$  direction, with only small deviations in the transverse  $x$  and  $y$  directions. Based on these observations, we make the following assumptions:  $p_z \gg p_{x,y}$  and  $p \approx p_z$ .

The steering of the beam trajectory in a horizontal direction is achieved by applying a vertical magnetic field, expressed as  $\vec{\mathcal{B}} = \mathcal{B}_y \vec{e}_y$ . The force applied depends on the particle velocity  $v_z$ . Consequently, for particles with different momenta, the steering and their trajectories will deviate from the design path. This is known as dispersion and is covered in both the transverse and longitudinal beam dynamics lectures.

#### 1.4.1.3.3 Relative particle position and synchrotron motion

The relative longitudinal position of the particles will evolve as a function of time due to the relative change of trajectory length over one revolution in the accelerator and the difference in relative velocity. This is referred to as the ‘‘synchrotron motion’’, which is the essence of longitudinal beam dynamics.

The synchrotron motion can be described in the longitudinal phase space  $(z, p_z)$  where the particle coordinates are represented at a given instant in time, with respect to a reference particle. Other particles can be in front/early in time (right side), or behind/late in time (left side), have higher momentum/velocity (above) or lower momentum/velocity (below). This is illustrated in Fig. 1.4.4. The blue/red particles are respectively in front/behind the reference particle in black, and have a smaller/larger velocity (i.e., a smaller/larger momentum). A real bunch of particles (right plot in Fig. 1.4.4) is composed of many particles (typically  $\mathcal{O} \sim 10^{10} - 10^{12}$ ) that, as an ensemble, perform coherent oscillations.

#### Quiz 1.4.1

From the three particles (blue: slower and shorter path, red: faster and longer path), which one would arrive first after one full revolution in the accelerator?

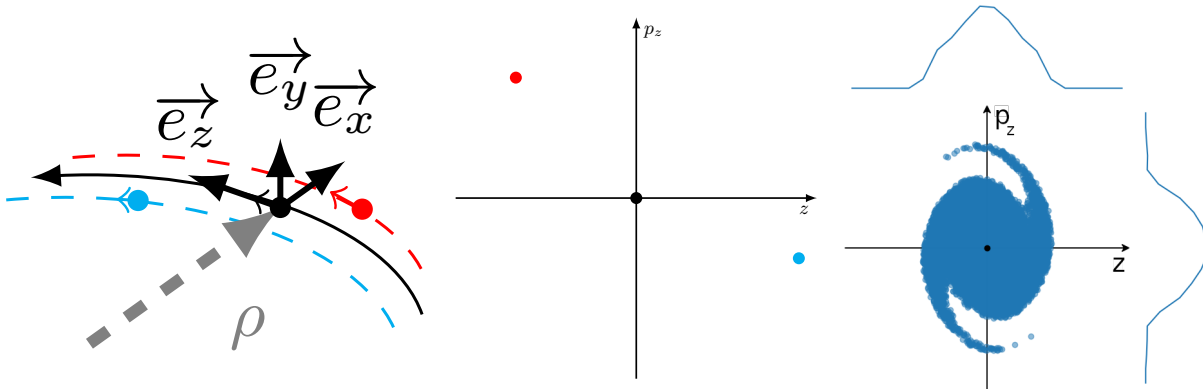


**Fig. I.4.4:** Three particles in the Frenet–Serret coordinate system (left) and in the  $(z, p_z)$  longitudinal phase space (middle). The blue/red particles are respectively in front/behind and slower/faster than the reference particle in black. The right plot shows the case for a bunch composed of many particles, as well as the distributions in position and momentum (phase space, animated in Ref. [2]).

Finally, controlling the synchrotron motion allows for defining the temporal structure and the longitudinal beam parameters of a pulse of particles. The beam current is expressed as  $I = \frac{dQ}{dt}$ , where  $dQ$  represents the total charge passing in a time  $dt$ . Depending on the specific requirements of the destination, whether it is an experiment or the next machine in a chain, the parameters defining the synchrotron motion can be adjusted to deliver either a continuous or a bunched beam.

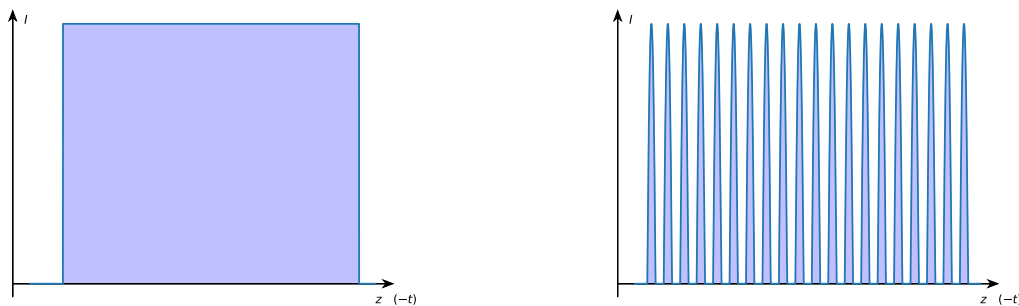


**Fig. I.4.5:** The longitudinal (temporal) distribution of a beam of particles. A continuous beam is represented to the left, and a bunched beam to the right.

#### I.4.1.3.4 Relationship with other courses

Although this course intends to teach longitudinal beam dynamics in a self-consistent way, it remains nonetheless tightly linked to other JUAS courses. Notably, the following questions are covered in the other courses:

- How do we focus the beam in the horizontal and vertical directions, how do we transport the beam to a target?
- Chapter I.3 on transverse beam dynamics

- Can we use the beam in another way than colliding with a target, what is the principle behind light sources?  
→ Chapter [I.10](#) on **synchrotron radiation**
- Do charged particles interact with each other, can we accelerate an infinite amount of particles?  
→ Chapter [I.12](#) on **collective effects**
- What systems do we use to provide the beam with an electric field, how are they designed?  
→ Chapters [II.2](#) on **RF engineering** and [II.5](#) on **superconducting RF cavities**
- How do we measure a bunch profile, specifically in the longitudinal plane?  
→ Chapter [II.9](#) on **beam instrumentation**

Moreover, this course is devoted to describing the fundamentals of longitudinal beam dynamics with specifics linked to the design of **synchrotrons**. Dedicated chapters on **linacs** and **cyclotrons** can be found elsewhere in these proceedings (see Chapters [I.11](#) and [I.13](#)). Similar concepts are covered in the other courses but possibly with different definitions, conventions, and assumptions to derive formulas.

## I.4.2 Fundamentals of particle acceleration

### I.4.2.1 Fields and forces

This section introduces key concepts of particle acceleration in electric fields. It starts with an overview of acceleration in electrostatic fields, where stationary electric charges create potentials that increase the kinetic energy of charged particles. Next, the focus shifts to induction and Radio Frequency (RF) acceleration, which use time-varying electromagnetic fields for more efficient and continuous acceleration of particles. The final part of this section covers circular accelerators, examining the concept of magnetic rigidity. This term refers to the relationship between a particle's momentum and the magnetic field needed to keep it on a circular path. Together, these topics provide a foundational understanding of particle acceleration techniques used in physics.

#### I.4.2.1.1 Maxwell's equations

Maxwell's equations are first reminded in this section as a base for the following derivations. More details are provided in Chapter [I.1](#) on electromagnetism, introducing all the necessary basis of electromagnetism required for the design and studies related to particle accelerators.

The differential Maxwell's equations in vacuum are

$$\nabla \cdot \vec{\mathcal{E}} = \frac{\rho_q}{\epsilon_0} \quad (\text{Gauss' law}) \quad (\text{I.4.2})$$

$$\nabla \cdot \vec{\mathcal{B}} = 0 \quad (\text{Flux/Thomson's law}) \quad (\text{I.4.3})$$

$$\nabla \times \vec{\mathcal{E}} = -\frac{\partial \vec{\mathcal{B}}}{\partial t} \quad (\text{Faraday's law}) \quad (\text{I.4.4})$$

$$\nabla \times \vec{\mathcal{B}} = \mu_0 \left( \vec{j} + \epsilon_0 \frac{\partial \vec{\mathcal{E}}}{\partial t} \right) \quad (\text{Ampère's law}) \quad (\text{I.4.5})$$

where  $\epsilon_0$  is the vacuum permittivity,  $\mu_0$  the vacuum permeability,  $\rho_q$  the charge density, and  $\vec{j}$  the current density. The corresponding integral forms in vacuum are

$$\oiint_S \vec{\mathcal{E}} \cdot d\vec{S} = \frac{1}{\epsilon_0} \iiint \rho_q dV \quad (\text{Gauss' law}) \quad (\text{I.4.2})$$

$$\oiint_S \vec{\mathcal{B}} \cdot d\vec{S} = 0 \quad (\text{Flux/Thomson's law}) \quad (\text{I.4.3})$$

$$\oint_C \vec{\mathcal{E}} \cdot d\vec{z} = -\frac{d}{dt} \iint_S \vec{\mathcal{B}} \cdot d\vec{S} \quad (\text{Faraday's law}) \quad (\text{I.4.4})$$

$$\oint_C \vec{\mathcal{B}} \cdot d\vec{z} = \mu_0 \iint_S \vec{j} \cdot d\vec{S} + \mu_0 \epsilon_0 \iint_S \frac{\partial \vec{\mathcal{E}}}{\partial t} \cdot d\vec{S} \quad (\text{Ampère's law}) \quad (\text{I.4.5})$$

where  $dz$  is the line element,  $dS$  the surface element, and  $dV$  the volume element.

### I.4.2.1.2 Acceleration in electrostatic fields (DC)

The simplest form of acceleration can be obtained using electrostatic fields along the longitudinal direction. This can be obtained across a charged capacitor of length  $g$ , as represented in Fig. I.4.6. Applying the Lorentz force from Eq. (I.4.1) with a static electric field along the longitudinal direction, the momentum increases as

$$\frac{dp}{dt} = \frac{dE}{dz} = q \mathcal{E}_z,$$

leading to an increment in energy over the gap of

$$\delta E = \int q \mathcal{E}_z dz = q \mathcal{E}_z g = qV_g, \quad (\text{I.4.6})$$

where the scalar potential  $V$  (or voltage) is defined as

$$\vec{\mathcal{E}} = -\nabla V \implies \mathcal{E}_z = -\frac{\partial V}{\partial z}.$$

There are numerous designs for extracting particles from a source and accelerating them using high field DC methods, such as the Cockroft–Walton, Van de Graaf (Fig. I.4.7, left), and Tandem accelerators. These technologies find applications in a variety of fields, including the cathode ray tubes used in older television models (Fig. I.4.7, right) and various industrial and medical applications. For more detailed information on these electrostatic accelerators, you can refer to the resource available from the dedicated CAS lecture [3].

The maximum electric field in electrostatic accelerators is limited to the MV range due to discharges or arcing. The maximum achievable voltage is influenced by the nature of the gas and its pressure in the vessel where the electric field is generated, following Paschen's law. The curves of the maximum voltage as a function of gas pressure for different gas types are represented in Fig. I.4.8.

Additionally, Faraday's law for static electromagnetic fields yields that the closed-loop integral of

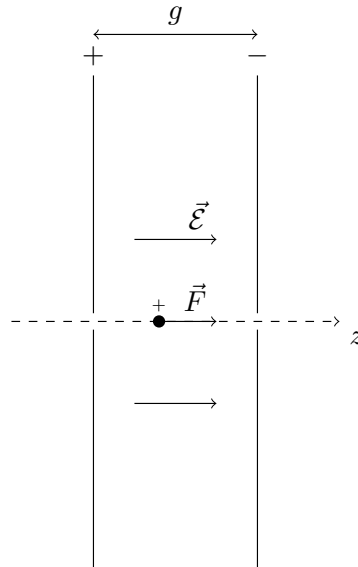


**Fig. I.4.6:** A particle accelerated in a gap of length  $g$  with electrostatic fields. The setup is comparable to a charged capacitor where holes would be made on each side to allow for the passage of a particle.

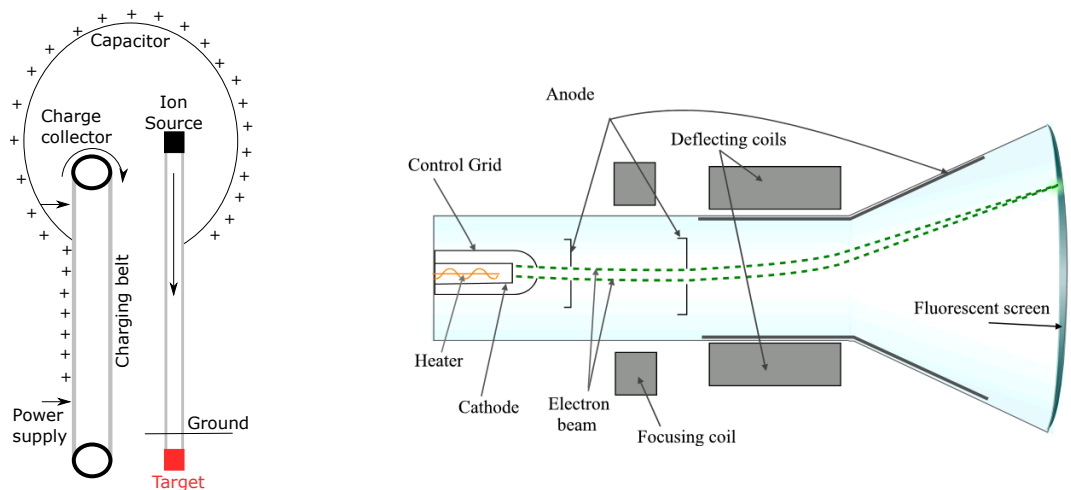


**Fig. I.4.7:** Applications of electrostatic accelerators. A Van De Graaf generator is displayed on the left, for which a belt charges a metallic cup and generates an electrostatic field between the cup and the ground allowing for ion particles to be accelerated. A cathode ray tube is displayed on the right [4], where an electron beam is extracted from the cathode and steered on a screen and was used for display in old monitors.

the electric field along a closed loop  $C$  is zero. From Eq. (I.4.4), we get

$$\oint_C \vec{\mathcal{E}} \cdot d\vec{z} = 0,$$

implying that there cannot be energy gain in a circular accelerator with DC fields, therefore restricting their maximum energy reach. This design is typically not applicable for high energy hadron colliders which can reach  $\mathcal{O}(10^6)$  higher energy levels.

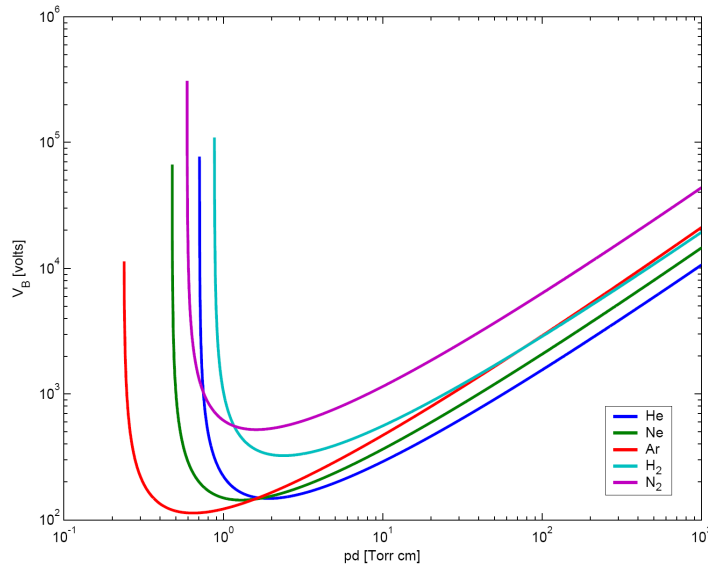


**Fig. I.4.8:** The Paschen curves, representing the maximum voltage as a function of the gas type and pressure, limiting the maximum capabilities in electrostatic accelerators [5].

#### I.4.2.1.3 Definitions of the electronvolt and beam power

We will now introduce the electronvolt (eV) unit which conveniently links the increment in energy of a particle passing through a gap with a given electric potential following Eq. (I.4.6). The eV unit corresponds to the energy gained by a particle with elementary charge  $e$  in a potential  $V_g = 1$  V, giving a value of

$$1 \text{ eV} = 1.602\,176\,634 \times 10^{-19} \text{ J.} \quad (\text{I.4.7})$$

Another important parameter is the average power transferred to the beam  $\langle P_b \rangle$ , expressed in watts. The beam power is defined as the total accelerated beam energy  $N_p E_{\text{acc}}$  ( $N_p$  being the number of particles and  $E_{\text{acc}}$  expressed in joule) delivered in an acceleration time  $T_{\text{acc}}$

$$\langle P_b \rangle = \frac{N_p E_{\text{acc}}}{T_{\text{acc}}}. \quad (\text{I.4.8})$$

A few questions are proposed in the following exercise to get familiar with these units.

#### Exercise I.4.2

- An accelerator has a potential of 20 MV, what is the corresponding energy gain of a particle in joules?
- What is the total energy of the beam stored in the LHC? The beam is composed of 2808 bunches of  $1.15 \times 10^{11}$  protons, each at 7 TeV.
- What is the equivalent speed of a high speed train? Assume a 400 tons (200 m long) TGV train.

- What is the beam power delivered to the LHC beam? Consider an acceleration from 450 GeV to 7 TeV in 30 minutes.

#### 1.4.2.1.4 Induction acceleration

Another way to produce an accelerating electric field is through induction. From Faraday's law for induction and applying a ramping magnetic field, we obtain

$$\oint_C \vec{\mathcal{E}} \cdot d\vec{z} = -\frac{d}{dt} \iint_S \vec{\mathcal{B}} \cdot d\vec{S}. \quad (\text{I.4.4})$$

This is the principle behind the betatron accelerator design, illustrated in Fig. I.4.9.

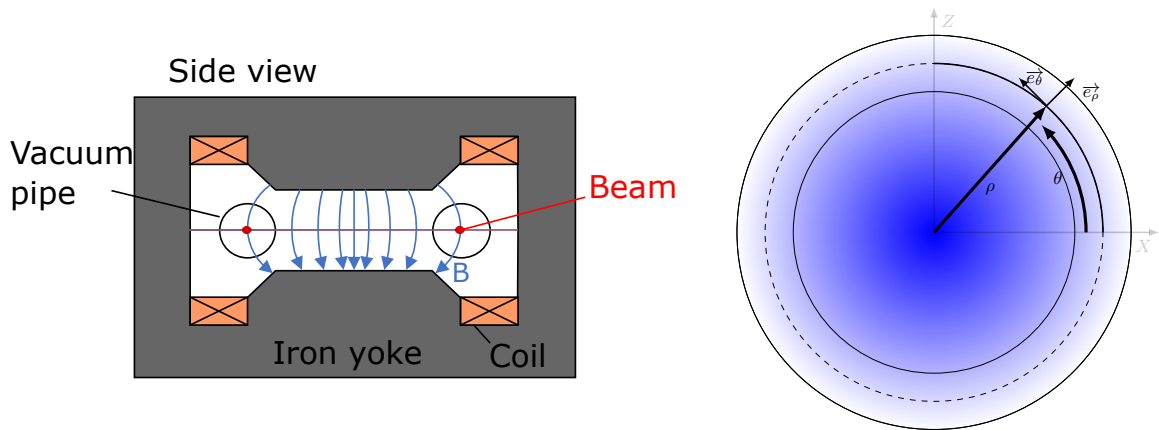


**Fig. I.4.9:** Schematics of a betatron accelerator. A transversal cut of the betatron is shown on the left. The beam circulates in the vacuum pipe within a large magnet, which shape is adjusted to provide a radially dependent magnetic field  $\mathcal{B}_y(\rho, t)$ . The magnetic field depends on the radial position, as represented on the right schematic with a view from the top of the betatron (the beam pipe is in thick black lines, the reference orbit in dashed, the magnetic field in blue with its opacity proportional to the amplitude of the field).

A vertical magnetic field is applied to the particle trajectory and serves two purposes. The first one is to bend the trajectory of the particles in a circular orbit, and the second is to induce an accelerating electric field in the azimuthal direction  $\theta$ .

Assuming azimuthal symmetry and a vertical magnetic field  $\vec{\mathcal{B}} = -\mathcal{B}_y(\rho, t) \vec{e}_y$ , we get the following condition for particles to be accelerated at a constant radius  $\rho_0$

$$\mathcal{B}_y(\rho_0) = \frac{1}{2} \frac{\Phi_{S, \rho_0}}{\pi \rho_0^2} = \frac{1}{2} \langle \mathcal{B}_y \rangle_{S, \rho_0}, \quad (\text{I.4.9})$$

with  $\Phi_{S, \rho_0}$  being the magnetic flux through the surface  $S$  enclosed by the orbit  $\rho_0$  and  $\langle \mathcal{B}_y \rangle_{S, \rho_0}$  the corresponding average magnetic field.

For the particles to move in a circular path with a radius  $\rho_0$ , the averaged magnetic field (flux) through the surface enclosed by the orbit should be twice the magnetic field on the particle trajectory. This is also referred to as the 2:1 rule.

The main limitations of the betatron accelerator are the size of the large magnet covering the

whole accelerator and the magnetic saturation of the iron yoke. Moreover, limiting the size of the accelerator leads to strong synchrotron radiation for electron beams (small radius), further limiting the maximum reachable energy. In terms of its operational capacity, these accelerators achieve a maximum energy output of approximately 300 MeV when accelerating electrons, compared to high-energy lepton synchrotrons which are capable of reaching energies in the range of hundreds of GeV (e.g. the Large Electron Positron collider).

### Derivation I.4.3

Let's derive the 2:1 rule stated in Eq. (I.4.9).

Assuming an azimuthal symmetry and a vertical magnetic field  $\vec{B} = -\mathcal{B}_y(\rho, t) \vec{e}_y$  at a constant orbit  $\rho_0$ , can you derive an equation for  $\mathcal{E}_\theta$  and the corresponding  $dp_\theta/dt$  ?

We will introduce the magnetic flux  $\Phi_{S,\rho_0}$  and an averaged magnetic field in the betatron core  $\langle \mathcal{B}_y \rangle_{S,\rho_0}$  with

$$\Phi_{S,\rho_0} = 2\pi \int_0^{\rho_0} \mathcal{B}_y(\rho) \rho d\rho = \pi \rho_0^2 \langle \mathcal{B}_y \rangle_{S,\rho_0}.$$

What is the equilibrium condition for a constant  $p_\theta$  if we assume that

$$\mathcal{B}_y \rho = \frac{p_\theta}{q} = \frac{p}{q} \text{ (this will be demonstrated later on) ?}$$

#### I.4.2.1.5 Acceleration with electromagnetic RF waves

A third way to accelerate particles is applying electromagnetic waves. Combining Maxwell's equations (I.4.4) and (I.4.5) in vacuum (no charge or current), a propagating electric wave can be obtained on the following form

$$\Delta \vec{\mathcal{E}} - \frac{1}{c^2} \frac{\partial^2 \vec{\mathcal{E}}}{\partial t^2} = 0, \quad \left( c = \frac{1}{\sqrt{\mu_0 \epsilon_0}} \right).$$

To accelerate particles in modern accelerators, electromagnetic waves in the frequency range  $\mathcal{O}$  (MHz, GHz) are produced and confined in resonant cavities, with the electric field pointing towards the longitudinal direction of the beam. The main components of a complete RF system are provided in Fig. I.4.10, while a real RF cavity integrated in an accelerator is shown together with its drawing in Fig. I.4.11. All the necessary information relating to the design of RF systems are provided in Chapters II.2 and II.5 on RF engineering and superconducting RF cavities.

Within the cavity, the standing wave can be described by

$$\vec{\mathcal{E}} = \mathcal{E}_z(\rho, z) \cos(\omega_{\text{rf}} t) \vec{e}_z, \quad (\text{I.4.10})$$

where  $\omega_{\text{rf}} = 2\pi f_{\text{rf}}$  is the (angular) frequency of the field, which depends on the geometry of the cavity. The maximum amplitude of the field depends on the radial position of the particle  $\rho$ , as well as the longitudinal position  $z$  at a given time  $t$ . To produce the standing wave, a low-power RF signal is first amplified and then coupled into the cavity. The amplitude and phase of the wave with respect to the beam can be controlled.

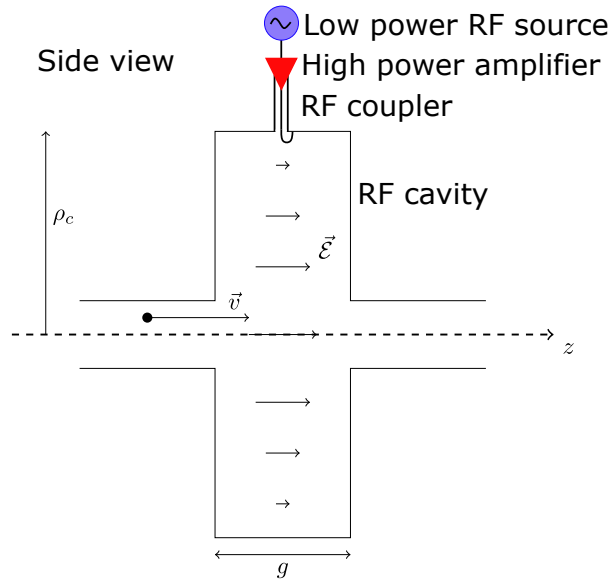


**Fig. I.4.10:** Schematic of a complete RF system. The RF cavity of radius  $\rho_c$  is used to confine the electromagnetic wave, with the electric field pointing towards the longitudinal direction of the beam. The wave is produced by a low-power RF source to control the amplitude, frequency and phase, then amplified using high-power amplifiers and coupled into the cavity (from the top in this schematic).

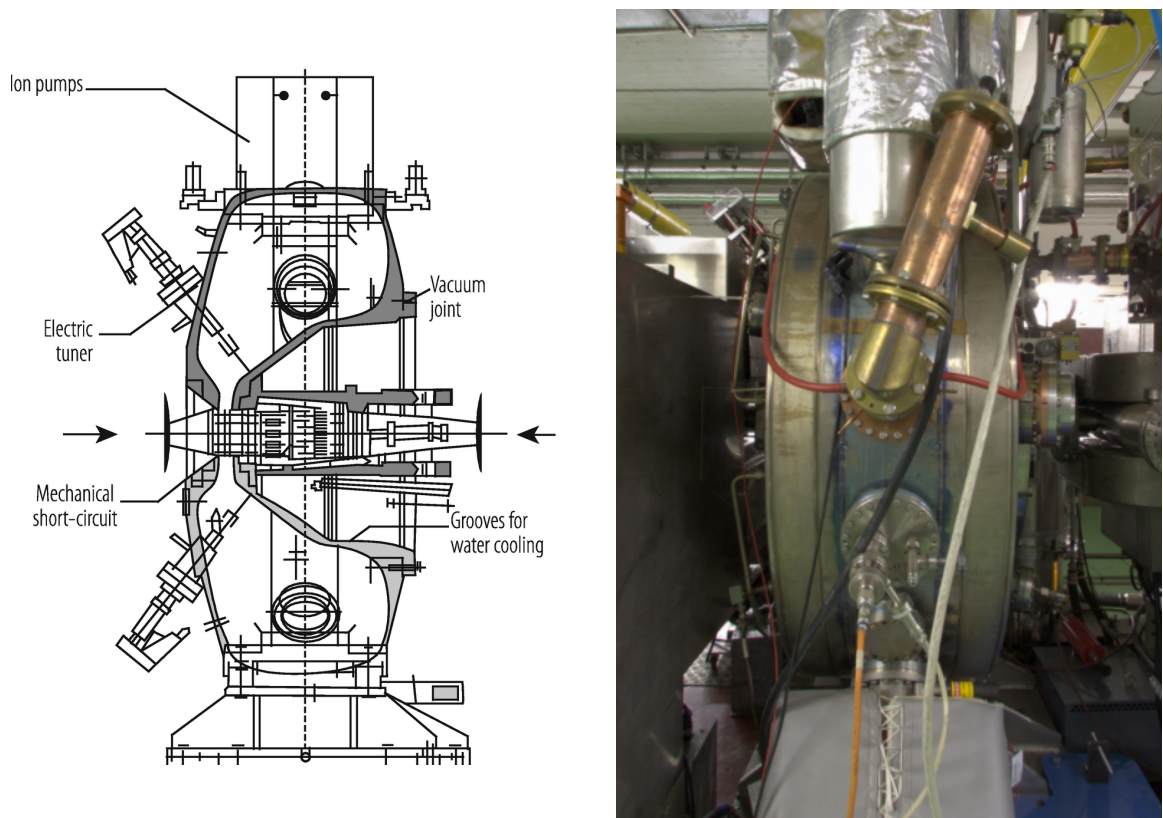


**Fig. I.4.11:** The 80 MHz RF cavity of the Proton Synchrotron at CERN. The engineering drawing is displayed on the left to reveal the different components [6], and a picture of the real cavity is given on the right. A panoramic view of the cavity within the Proton Synchrotron is available from Ref. [7].

An opening is made to let the beam pass through the oscillating electric field. The increase in energy of a particle passing through an RF cavity gap is

$$\delta E_{\text{rf}} = \int q\mathcal{E}_z(\rho, z, t)dz = qV_{\text{rf}}(\rho, \tau), \quad (\text{I.4.11})$$

where  $V_{\text{rf}}$  is the total accelerating potential for a particle arriving at a time  $\tau$  in the cavity. Note that this expression is very similar to the one obtained for electrostatic accelerators in Eq. (I.4.6) where the net electric potential is the integrated RF waveform along the path of the particle. A convenient expression of  $V_{\text{rf}}(\rho, \tau)$  for a simple form of RF cavity (pillbox cavity) is provided in Section I.4.3.1.1.

Unlike electrostatic accelerators, several RF systems can be stacked together linearly to reach higher energies. This is the principle of linear accelerators (linac), where the particles are passing a single time in many RF cavities, carefully spaced so that particles experience an accelerating field at each gap. A complete overview is offered in Chapter I.11 on linacs.

The maximum reachable energy then scales with the length of the linac and the RF accelerating gradient. Further increasing the maximum energy, or making the accelerator more compact, requires reaching higher gradients which is limited by field emission and eventually breakdown. This phenomenon is dependent on the cavity surface quality and conditioning. The observed frequency dependence was formulated empirically by Kilpatrick and can be seen in Fig. I.4.12. Present cavities go beyond the first established Kilpatrick criterion as a ratio expressed in ‘‘Kilpatrick’’ unit. A typical range for RF cavities nowadays is  $\mathcal{O}(1 - 10^2 \text{ MV/m})$ .

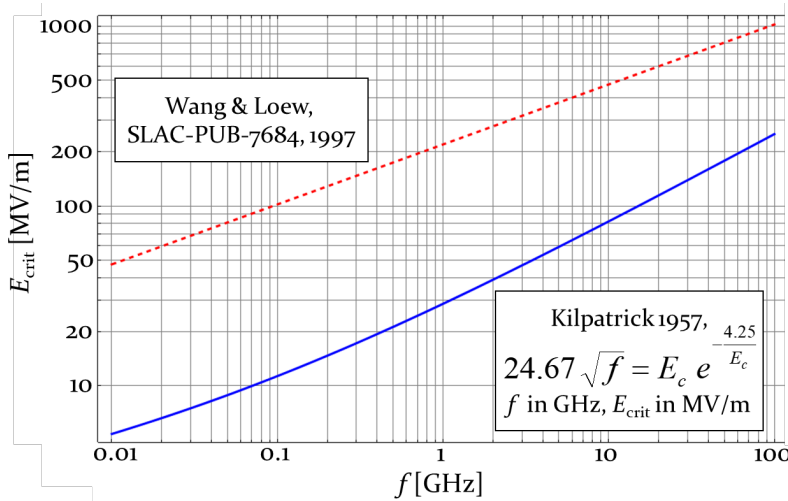


**Fig. I.4.12:** The maximum achievable accelerating gradient as a function of the resonant frequency of the RF cavity. The first empirical limit in blue corresponds to the Kilpatrick unit, which was then increased with an improved understanding of surface physics [8].

To go beyond the present limits imposed by RF systems, accelerating structures using fields provided by lasers and plasmas are being studied. An example is provided in Chapter III.15 describing the AWAKE experiment. In this lecture, we concentrate on conventional RF acceleration in circular accelerators.

### I.4.2.1.6 Circular accelerators

Another approach to linear accelerators is to use a single RF system and to steer the beam on a closed orbit back to the accelerating gap, as depicted in the introduction in Fig. I.4.2. The beam passes the same RF system multiple times, which is the main principle behind circular accelerators. At that stage, we need to introduce the concept of magnetic rigidity.

The force exerted in bending magnets on the beam to steer it on a circular orbit is

$$\vec{F}_B = q(\vec{v} \times \vec{B}).$$

Thus, the required vertical magnetic field  $\mathcal{B}_y$  to keep particles with a given momentum  $p$  and charge  $q$  on a given orbit  $\rho$  is

$$\mathcal{B}_y \rho = \frac{p}{q}. \quad (\text{I.4.12})$$

This relationship is called the magnetic rigidity or more trivially the “ $\mathcal{B}\rho$ ”. Two possibilities are then available to reach high energies:

- Increase  $\mathcal{B}_y$  at fixed  $\rho \rightarrow$  Synchrotron design,
- Increase  $\rho$  at fixed  $\mathcal{B}_y \rightarrow$  Cyclotron design.

Chapter I.13 on cyclotrons provides all the details of the cyclotron design. In this course, we will focus on synchrotron design.

The maximum energy of a circular accelerator is in principle limited by the maximum  $\mathcal{B}_y$  in the bending magnets or the radial size of the accelerator (e.g., the Future Circular Collider with a circumference of 100 km! See Chapter III.4.1 on introduction to colliders. The typical range for bending magnetic fields is  $\sim \mathcal{O}(1 - 10 \text{ T})$ , and an important effort is conducted to reach higher magnetic fields (see Chapters II.3 and II.5 on normal and superconducting magnets). In the presence of synchrotron radiation (for lepton machines, see Chapter I.10 on synchrotron radiation), the maximum energy is limited by RF power.

#### Derivation I.4.4

Demonstrate that

$$\mathcal{B}_y \rho = \frac{p_\theta}{q} = \frac{p}{q}.$$

Remember that the force from a magnetic field is always orthogonal to the particle direction. Demonstration can be done in cylindrical coordinates, assuming a constant  $v = v_\theta$  (implying  $p = p_\theta$ ,  $\dot{m} = 0$ ), and using as magnetic field  $\vec{B} = -\mathcal{B}_y \vec{e}_y$ .

### I.4.2.2 Relativistic kinematics

In this section, we will revisit the relevant relationships of relativistic mechanics that will be used throughout the lecture. For a more complete overview, see Chapter I.2 on special relativity.

The reader is reminded that until the rest of the lecture we will assume that the momentum of the particle is  $p \approx p_z$ . The total energy of the particle is then

$$E = E_{\text{kin}} + E_0 = \sqrt{P^2 + E_0^2}, \quad (\text{I.4.13})$$

where  $E$  is the total energy,  $E_0 = m_0 c^2$  the rest energy (particle rest mass  $m_0$ ),  $p = P/c$  the momentum. We also reiterate the following parameters

$$\beta = \frac{v}{c} = \frac{P}{E}, \quad (\text{I.4.14})$$

$$\gamma = \frac{1}{\sqrt{1 - \beta^2}} = \frac{E}{E_0} = \frac{m}{m_0}, \quad (\text{I.4.15})$$

where  $\beta$  is the relativistic velocity ratio,  $\gamma$  is the Lorentz factor and  $p = mv = \beta\gamma m_0 c$ . These parameters are linked together with the relationship

$$\beta^2 + \frac{1}{\gamma^2} = 1. \quad (\text{I.4.16})$$

The parameters  $E$ ,  $E_{\text{kin}}$ ,  $E_0$ , and  $P$  can be expressed in units of eV. The momentum  $p$  is commonly represented in units of eV/c. Additionally, the relativistic mass  $m$  is often expressed in eV/c<sup>2</sup>. Finally,  $\beta$  and  $\gamma$  are unitless quantities. The momentum can be obtained in units of eV/c from Eq. I.4.12 using the following approximate formula

$$p [\text{GeV}/c] \approx 0.3 Z \mathcal{B}_y [\text{T}] \rho [\text{m}], \quad (\text{I.4.17})$$

where  $Z$  is the number of elementary charges  $e$  ( $Z = +1$  for protons and electrons).

The relativistic velocity ratio  $\beta$  and mass  $\gamma m_0$  depend on the particle rest mass. Their respective evolution as a function of the particle kinetic energy for different species is given in Fig. I.4.13. Electrons can be considered with  $v \approx c$  at moderate kinetic energy, but not heavier particles. The evolution of the particle velocity during acceleration has an important influence on the design of an accelerator.

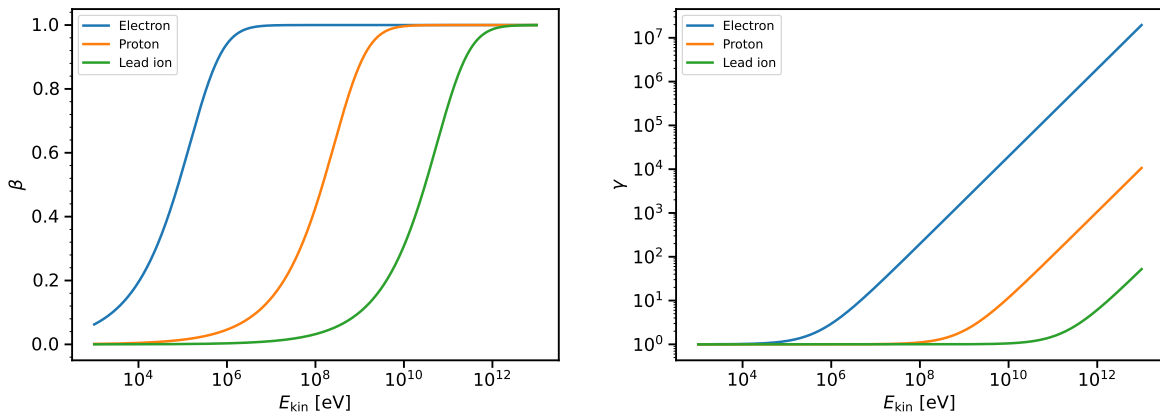


**Fig. I.4.13:** The relativistic velocity ratio  $\beta$  and mass  $\gamma m_0$  as a function of the kinetic energy  $E_{\text{kin}}$  for different particle species (electron, proton and lead ion).

In the next sections, we will make use of differential relationships between the various relativistic parameters to express their evolution in time, or to address small differences between particles. The following relationships will be used

$$\frac{dE}{dp} = \beta c = v, \tag{I.4.18}$$

$$\frac{dp}{p} = \frac{1}{\beta^2} \frac{dE}{E} = \frac{1}{\beta^2} \frac{d\gamma}{\gamma}, \tag{I.4.19}$$

$$\frac{dp}{p} = \gamma^2 \frac{d\beta}{\beta}. \tag{I.4.20}$$

Finally, the next exercises are given to gather experience with numerical applications and derivations of the relationships that will be used throughout the course.

**Exercise I.4.5**

Derive the approximate formula

$$p [\text{GeV}/c] \approx 0.3 Z \mathcal{B}_y [\text{T}] \rho [\text{m}].$$

**Exercise I.4.6**

Compute the relativistic parameters for the CERN accelerators in the table.

Machine	$E_0$ [MeV]	$E_{\text{kin}}$ [GeV]	$E$ [GeV]	$\gamma$	$\beta$	$p$ [GeV/c]	$\mathcal{B}_y \rho$ [Tm]
PSB inj (p+)		0.160					
PSB ext (p+)		2					
SPS ( $^{208}\text{Pb}^{82+}$ )							86.4
LHC (p+)			7000				
LEP (e+/e-)			100				

**Derivation I.4.7**

Demonstrate the differential relationships from Eqs. (I.4.18), (I.4.19) and (I.4.20).

**I.4.3 Synchrotron design**

**I.4.3.1 Acceleration in a synchrotron**

We will now dive into the details of the synchrotron design. More specifically, we will focus on the so-called “synchronous particle” serving as a reference. We will need an RF system to effectively accelerate the beam. As a start, we will use the pillbox cavity as a simplified model for the RF system, and look at how the accelerator parameters are adjusted to accelerate the synchronous particle.

**I.4.3.1.1 The pillbox cavity**

In this section, we will describe the pillbox cavity design. Although simplified, the cavity geometry is already extremely convenient to represent the main features of a resonating cavity. We will focus on key

aspects such as the fundamental mode of operation, formulating the energy gain for each passage through the cavity and define the transit time factor. Other sources of energy gain or loss across the accelerator will be introduced.

The pillbox cavity consists of a cylinder placed such that the parallel plates are in the longitudinal direction. An opening is made on-axis on each end to allow the particles to pass through the center of the cylinder where the accelerating RF wave is resonating. A representation of a pillbox cavity is available in Fig. I.4.14. The time-varying electric field along the longitudinal direction, and azimuthal magnetic field in the cavity are defined by

$$\mathcal{E}_z(\rho, t) = \mathcal{E}_0 J_0 \left( \chi_0 \frac{\rho}{\rho_c} \right) \cos(\omega_{\text{rf}} t), \tag{I.4.21}$$

$$\mathcal{B}_\theta(\rho, t) = -\frac{\mathcal{E}_0}{c} J_1 \left( \chi_0 \frac{\rho}{\rho_c} \right) \sin(\omega_{\text{rf}} t), \tag{I.4.22}$$

where  $J_n$  is the Bessel function of the first kind,  $\chi_0 \approx 2.405$  is the first zero of the Bessel function. The maximum electric field  $\mathcal{E}_0$  achievable in a cavity depends on many parameters including the cavity material, power amplification, coupling in transmission lines and reflections. The frequency of a pillbox cavity is

$$\omega_{\text{rf}} = \frac{\chi_0 c}{\rho_c}. \tag{I.4.23}$$

It is worth noticing that the frequency depends on the radial size but not on the cavity gap length  $g$ . More detailed information is provided in Chapter II.2 on RF.

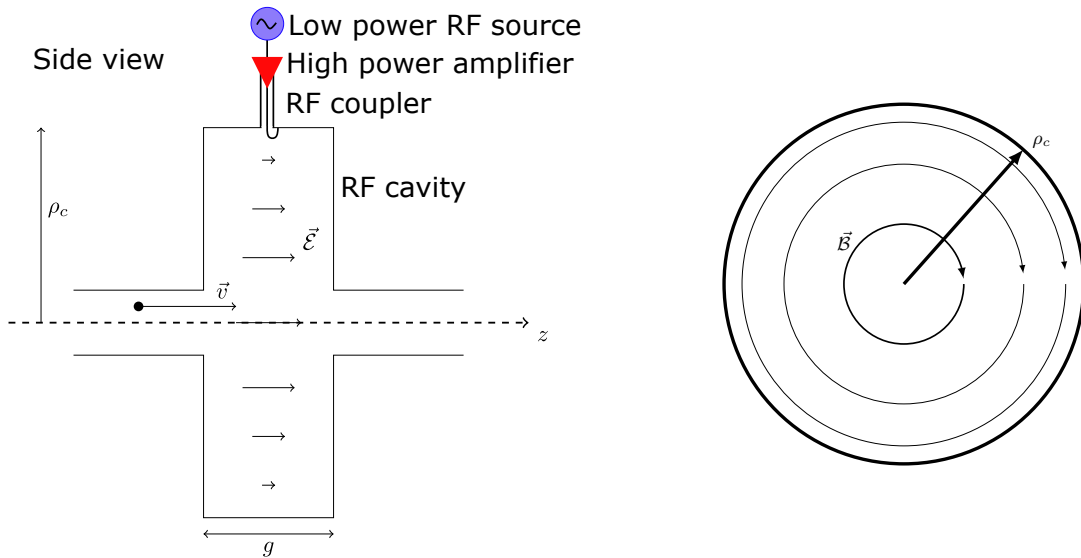


**Fig. I.4.14:** The pillbox cavity seen from the side (left plot), with the beam circulating from the left to the right, and seen in the direction of the beam (right plot). The electric field is longitudinal, and the magnetic field is transverse to the particle direction.

### Derivation I.4.8

Demonstrate that the electric and magnetic fields

$$\mathcal{E}_z(\rho, t) = \mathcal{E}_0 J_0 \left( \chi_0 \frac{\rho}{\rho_c} \right) \cos(\omega_{\text{rf}} t)$$

$$\mathcal{B}_\theta(\rho, t) = -\frac{\mathcal{E}_0}{c} J_1 \left( \chi_0 \frac{\rho}{\rho_c} \right) \sin(\omega_{\text{rf}} t)$$

are solutions of the wave equation

$$\Delta \vec{\mathcal{E}} - \frac{1}{c^2} \frac{\partial^2 \vec{\mathcal{E}}}{\partial t^2} = 0.$$

Two conditions on the fields on the boundaries of the cavity (conductor material) are:

- The electric field is orthogonal to the surface.
- The magnetic field is parallel to the surface.

Many modes of oscillation can exist in the cavity, we are interested only in the fundamental mode for which  $\vec{\mathcal{E}} = \mathcal{E}_z \vec{e}_z$  and  $\vec{\mathcal{B}} = \mathcal{B}_\theta \vec{e}_\theta$ .

#### 1.4.3.1.2 Energy gain in an RF cavity

We express the energy gain of a particle passing through a cavity as

$$\delta E_{\text{rf}} = \int q \mathcal{E}_z(\rho, z, t) dz = q \int_{-g/2}^{g/2} \mathcal{E}_0(\rho, z) \cos(\omega_{\text{rf}} t) dz. \quad (\text{I.4.24})$$

For a particle passing through the center of the cavity ( $\rho = 0$ ), the energy gain becomes

$$\begin{aligned} \delta E_{\text{rf}}(\tau) &= q V_{\text{rf},0} T_t \cos(\omega_{\text{rf}} \tau) && \text{Linac convention} \\ \delta E_{\text{rf}}(\tau) &= q V_{\text{rf},0} T_t \sin(\omega_{\text{rf}} \tau) && \text{Synchrotron convention.} \end{aligned}$$

where a new parameter called the transit time factor is introduced and defined as

$$T_t = \frac{\int_{-g/2}^{g/2} \mathcal{E}_0(\rho, z) \cos\left(\frac{\omega_{\text{rf}} z}{\beta c}\right) dz}{\int_{-g/2}^{g/2} \mathcal{E}_0(\rho, z) dz}. \quad (\text{I.4.25})$$

The transit time factor is the ratio between the effective accelerating potential including the time variation of the field (top term) and the maximum potential if a particle would pass instantaneously in the cavity (bottom term,  $V_{\text{rf},0}$ ).

The transit time factor is  $T_t \leq 1$  and depends in principle on the transverse position of the particle.

For a pillbox cavity, the transit time factor becomes

$$T_t = \frac{\sin\left(\frac{\chi_0 g}{2\beta\rho_c}\right)}{\left(\frac{\chi_0 g}{2\beta\rho_c}\right)} \quad (\text{I.4.26})$$

and is plotted as a function of the gap length in Fig. I.4.15.

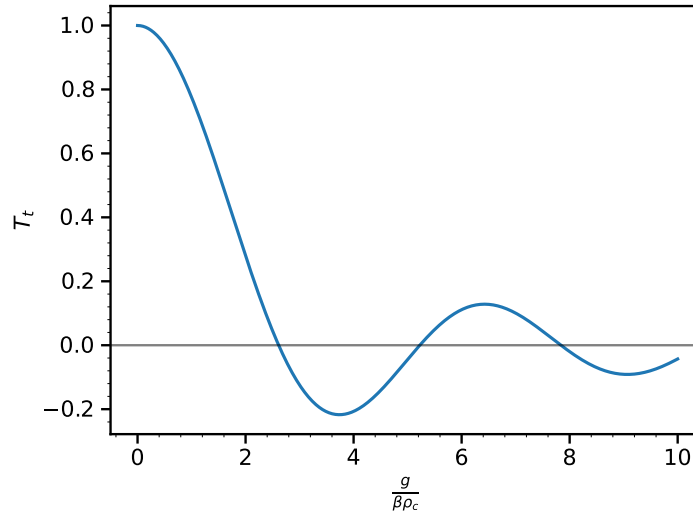


**Fig. I.4.15:** The transit time factor for a pillbox cavity, depending on the gap length  $g/\beta\rho_c$  geometrical ratio.

The electric field oscillates while the particle goes through the RF cavity. If the gap is too long, the effective acceleration potential is reduced. A compromise in the design of a cavity is needed to maximize the accelerating potential.

**Derivation I.4.9**

Derive the energy gain and the expression of the transit time factor starting from

$$\delta E_{\text{rf}} = q \int_{-g/2}^{g/2} \mathcal{E}_0(\rho, z) \cos(\omega_{\text{rf}} t) dz.$$

The longitudinal position of the particle with respect to the cavity is

$$z(t) = \int_{\tau}^t \beta(t) c dt \approx \beta c (t - \tau).$$

**Assumption:** The change in velocity of the particle is neglected here. This is not valid for high gradient cavities with non-relativistic particles!

**Derivation I.4.10**

Derive the transit time factor for a pillbox cavity using the expression of the electric field

$$\mathcal{E}_0 J_0(\rho) \cos\left(\frac{\omega_{\text{rf}} z}{\beta c}\right).$$

For the rest of the course we will use

$$\delta E_{\text{rf}}(\tau) = qV_{\text{rf}} \sin(\omega_{\text{rf}}\tau) \quad \rightarrow \quad \delta E_{\text{rf}}(\phi) = qV_{\text{rf}} \sin(\phi), \quad (\text{I.4.27})$$

where the transit time factor is included in the definition of  $V_{\text{rf}}$  (this parameter is often noted  $\hat{V}_{\text{rf}}$  in the literature) and  $\phi$  is the phase of arrival in the cavity.

**Assumption:** The transit time factor depends on the particle radial position and  $\beta$ . These dependencies will be neglected in the coming derivations.

### 1.4.3.1.3 Other sources of energy variations in a synchrotron

#### 1.4.3.1.3.1 Induction forces

During acceleration in a synchrotron, the magnetic field is ramped to keep the beam on a constant orbit with

$$\dot{p} = q\dot{\mathcal{B}}_y \rho.$$

With the same principle as in the betatron, an azimuthal electric field is induced. This leads to the energy gain (assuming  $\rho$  constant)

$$\delta E_{\text{b}}(\rho) = q \oint_C \vec{\mathcal{E}} \cdot d\vec{z} = q \int_0^{2\pi} \int_0^\rho \frac{\partial \mathcal{B}_y(\rho', \theta, t)}{\partial t} \rho' d\rho' d\theta. \quad (\text{I.4.28})$$

**Note:** This force is usually negligible in large synchrotrons, although it may not be overlooked to derive precisely longitudinal equations of motion.

#### 1.4.3.1.3.2 Synchrotron radiation

In curved trajectories in the accelerator, particles lose energy by emitting synchrotron radiation. The corresponding power lost due to synchrotron radiation is

$$P_{\text{sr}} = \frac{q^2 c}{6\pi\epsilon_0} \frac{(\beta\gamma)^4}{\rho^2}. \quad (\text{I.4.29})$$

The energy loss over a turn is obtained by multiplying the power by the time spent in the bending magnet  $T_b$

$$\delta E_{\text{sr}}(E, \rho) = \frac{q^2}{3\epsilon_0} \frac{\beta^3 E^4}{\rho E_0^4}, \quad \left(T_b = \frac{2\pi\rho}{\beta c}\right). \quad (\text{I.4.30})$$

Note the important dependence on  $1/E_0^4$ . Synchrotron radiation is usually neglected for hadron synchrotrons and is predominant for lepton machines. Nonetheless, the dependence with  $E^4$  implies that synchrotron radiation is still relevant for very high energy hadron accelerators (e.g. LHC, FCC), despite their larger radius ( $1/\rho$ ).

I.4.3.1.3.3 Self-induced fields

A real accelerator is composed of many pieces of equipment, which can lead to discontinuities in the beam pipe aperture. When passing through these cavity-like structures, particles will induce electric fields, leading to a change in energy of the particles.

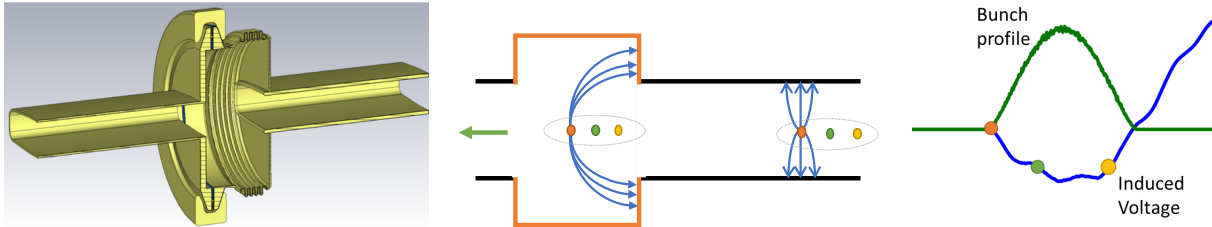


**Fig. I.4.16:** The beam induced voltage in a vacuum flange, which is a vacuum equipment providing continuity of the beam pipe. The geometry of the (cavity-like) flange is shown to the left. The single particles (orange, green, and yellow) induce wakefields (middle). The contribution of all particles sum up as a convolution to generate a collective induced voltage (right).

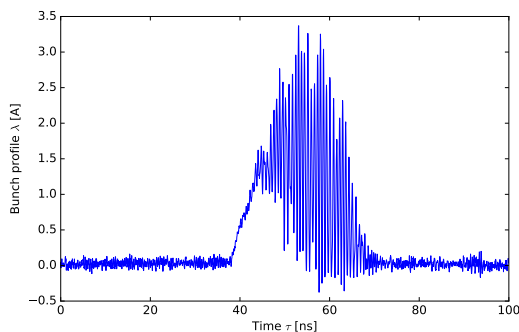
In the example from Fig I.4.16, a single particle passing through a cavity-like gap induces a wakefield  $\mathcal{W}(\tau)$ . A bunch with a longitudinal charge density  $\lambda(\tau)$  and number of particles  $N_b$  induces a voltage  $V_{\text{ind}}(\tau)$ , which is the convolution product of all the particles' single wakes

$$\delta E_{\text{ind}}(\tau) = qV_{\text{ind}}(\tau) = -qN_b(\lambda * \mathcal{W}). \quad (\text{I.4.31})$$

Collective effects are discussed in Chapter I.12.

**Exercise I.4.11**

- Compute the expected radius of the 80 MHz cavity shown in Fig. I.4.11, assuming it is a pillbox cavity.
- The image below to the left is a bunch during an instability. A 1.4 GHz modulation grows within the bunch. What is the size of the device responsible for the wakefields (compare to the size of the SPS in the image below to the right)?



**I.4.3.2 The synchronous particle**

Now that a model of the RF system is defined, we will make use of it to evaluate how particles can effectively be accelerated. In this section, we will define the synchronism condition in synchrotrons and the notion of the synchronous particle. This reference will be used to establish the rate at which the

particles can be accelerated, and the corresponding programs for the bending fields and RF frequency to accelerate the beam while staying on the reference orbit.

#### 1.4.3.2.1 Synchronism condition, energy gain

Using the layout of the accelerator from Fig. 1.4.2, we first define the time it takes for particles to circulate around the accelerator. The revolution period of an arbitrary particle in a circular machine is

$$T_{\text{rev}} = \frac{C}{v} = \frac{2\pi R}{\beta c}, \quad (\text{I.4.32})$$

while the corresponding revolution (angular) frequency is

$$\omega_{\text{rev}} = 2\pi f_{\text{rev}} = \frac{2\pi}{T_{\text{rev}}} = \frac{\beta c}{R}. \quad (\text{I.4.33})$$

We will derive the relationships for the synchronous particle (subscript  $s$ ).

A particle is synchronous with the RF waveform if

$$\omega_{\text{rf}} = h\omega_{\text{rev},s} = h \frac{\beta_s c}{R_s}, \quad (\text{I.4.34})$$

where  $h$  is the RF harmonic number (integer number). There are  $h$  different synchronous particles in a synchrotron (and effectively up to  $h$  bunches forming trains as represented in Fig. 1.4.5). The synchronous particle is fictitious and serves a reference point.

The total energy variation over one turn, accounting for all the potential sources described in the previous section, is

$$\delta E_s = \delta E_{\text{rf},s} + \delta E_{\text{b},s} + \delta E_{\text{sr},s} + \delta E_{\text{ind},s}. \quad (\text{I.4.35})$$

For the following derivations we will only consider the RF contribution. The energy gain per turn of the synchronous particle becomes

$$\delta E_s = qV_{\text{rf}} \sin(h\omega_{\text{rev},s}\tau_s) = qV_{\text{rf}} \sin(\phi_s), \quad (\text{I.4.36})$$

where  $\phi_s$  is the synchronous phase.

**Assumption:** The acceleration rate of the synchronous particle is assumed to be a smooth function of time. The energy gain per turn is usually small (not in Rapid Cycling Synchrotrons!). The acceleration rate is

$$\dot{E}_s \approx \frac{\delta E_s}{T_{\text{rev},s}} \rightarrow \dot{E}_s = \frac{qV_{\text{rf}}}{T_{\text{rev},s}} \sin(\phi_s). \quad (\text{I.4.37})$$

The bending field must be increased synchronously, keeping a constant orbit ( $\rho_s$  and  $R_s$ )

$$\dot{B}_y \rho_s = \frac{\dot{p}_s}{q}. \quad (\text{I.4.38})$$

Using the differential relationship from Eq. (I.4.18), we obtain

$$\frac{dE}{dp} = \beta c \quad \rightarrow \quad \dot{E} = \beta c \dot{p}.$$

Assuming that  $\dot{\rho}_s = 0$ , we get

$$\delta E_s = 2\pi q \rho_s R_s \dot{\mathcal{B}}_y \quad \text{and} \quad \phi_s = \arcsin \left( 2\pi \rho_s R_s \frac{\dot{\mathcal{B}}_y}{V_{\text{rf}}} \right), \quad (\text{I.4.39})$$

linking the energy gain per turn  $\delta E_s$  provided by the RF system applying an RF voltage  $V_{\text{rf}}$  with the expected  $\dot{\mathcal{B}}_y$  ramp rate. Note that this equation is not related to the induction acceleration. Here, the acceleration is obtained from the electric field in the RF cavity.

An important constraint given by Eq. (I.4.39) is that in order to accelerate the beam,  $\phi_s$  must be between  $[0, \pi/2]$ . This sets a minimal RF voltage  $V_{\text{rf}}$  for a given ramp rate  $\dot{\mathcal{B}}_y$ , defining how fast the synchronous particle can be accelerated.

#### Derivation I.4.12

Derive the acceleration per turn and the synchronous phase assuming  $\dot{\rho}_s = 0$

$$\delta E_s = 2\pi q \rho_s R_s \dot{\mathcal{B}}_y \quad \text{and} \quad \phi_s = \arcsin \left( 2\pi \rho_s R_s \frac{\dot{\mathcal{B}}_y}{V_{\text{rf}}} \right).$$

To preserve the synchronism condition, the RF frequency must also be adjusted to follow the evolution of  $\beta_s$  during acceleration

$$\omega_{\text{rf}}(t) = \frac{hc}{R_s} \beta_s(t). \quad (\text{I.4.40})$$

The RF frequency program is finally linked to the magnetic field by

$$f_{\text{rf}}(t) = \frac{hc}{2\pi R_s} \sqrt{\frac{\mathcal{B}_y^2(t)}{\mathcal{B}_y^2(t) + \left(\frac{m_0 c}{\rho_s q}\right)^2}}. \quad (\text{I.4.41})$$

#### Derivation I.4.13

From

$$\omega_{\text{rf}}(t) = \frac{hc}{R_s} \beta_s(t),$$

express  $\beta_s(t)$  as a function of  $\mathcal{B}_y(t)$  using the definition of the magnetic rigidity with constant  $\rho_s$  (and  $R_s$ ). Obtain

$$f_{\text{rf}}(t) = \frac{hc}{2\pi R_s} \sqrt{\frac{\mathcal{B}_y^2(t)}{\mathcal{B}_y^2(t) + \left(\frac{m_0 c}{\rho_s q}\right)^2}}.$$

The set of equations derived earlier is already sufficient to define the main accelerator parameters. These are:

- The required bending field to keep the beam on orbit from low to high momenta.
- The range in RF frequency to be covered by the RF system.
- The RF voltage needed to accelerate the synchronous particle.

#### ***1.4.3.2.2 Example for an existing synchrotron***

In Fig. 1.4.17, a cycle from the Super Proton Synchrotron (SPS) at CERN is illustrated as an example. The synchronous particle is accelerated from a momentum of 26 to 450  $Z$  GeV/ $c$ , where  $Z$  represents the charge number of the particle species (1 for protons and 82 for Lead ions). To do so, the bending field is ramped from 0.1 T to 2 T, in about 5 s (top left plot). The acceleration is done smoothly by defining linear segments in  $\dot{\mathcal{B}}_y$  (bottom left), providing a parabolic ramp in  $\mathcal{B}_y$ . In parallel, the RF frequency is adjusted (top right) to follow the evolution in  $\beta_s$ . Finally, the RF system provides the energy to the synchronous particle, which arrives at the synchronous phase  $\phi_s$  in the RF system, following the evolution of  $\dot{\mathcal{B}}_y$  (bottom right). The minimal RF voltage is set by the requirement to have  $\phi_s \in [0, \pi/4]$ . More RF voltage allows for a faster acceleration of the particles (up to the limit defined by the ramping of the magnets), but also allows for more particles to be accelerated, as it will be described in Section 1.4.5.

#### **Exercise I.4.14**

Compute the following parameters for protons in the SPS at injection and extraction energies (momentum 26 GeV/ $c \rightarrow$  450 GeV/ $c$ ):

- Revolution period/frequency of the SPS ( $\rho_0 = 741.25$  m,  $C_0 = 6911.50$  m)
- RF frequency of the SPS (using  $h = 4620$ )
- Energy gain per turn in the SPS (using  $\dot{\mathcal{B}}_y$  T/s)
- The smallest RF voltage to accelerate the synchronous particle.
- Compute the same parameters with Lead ions  $^{208}\text{Pb}^{82+}$ .

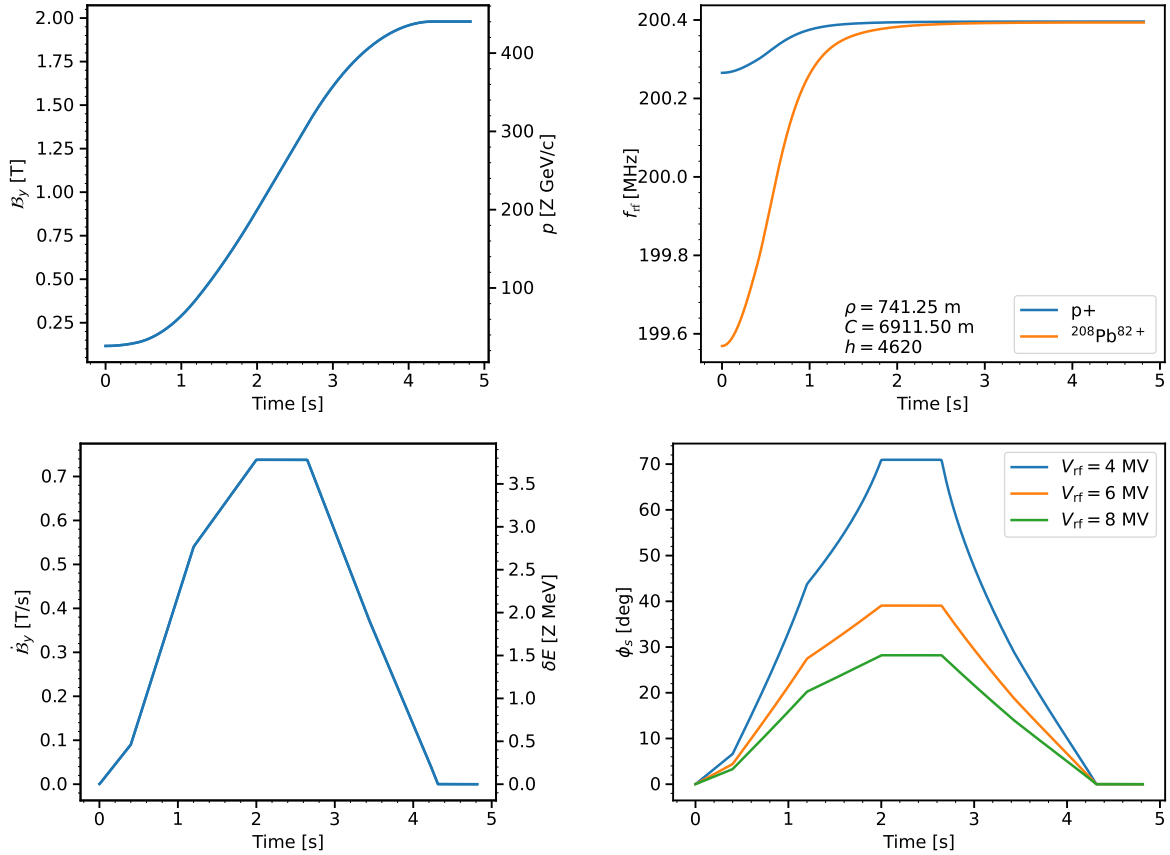


**Fig. I.4.17:** The magnetic field (upper left) and RF frequency (upper right) programs to bring the beam momentum from 26 Z GeV/c to 450 Z GeV/c, together with the corresponding magnetic ramp rate evolution (lower left) and the synchronous phase for different RF voltage (lower right), with the voltage kept constant during the whole acceleration. Due to their larger mass, the Lead ions have a lower  $\beta_s$  and hence  $f_{rf}$  for the same  $B_y \rho_s$  (NB:  $\phi_s$  is independent of the charge Z!).

### I.4.3.3 Differential relationships in a synchrotron

Now that the conditions to accelerate the synchronous particle are established, we will describe how the particle energy, its orbit and revolution frequency change for any independent variation of the other accelerator parameters. A few more accelerator parameters depending on the optics and relevant for longitudinal dynamics will be introduced. Namely the momentum compaction factor, the phase slip factor, and the transition  $\gamma_t$ .

#### I.4.3.3.1 The momentum compaction factor

In the previous module we assumed acceleration with a constant  $\rho_s$ . Nonetheless, like in cyclotrons, a particle can also be accelerated at a fixed magnetic field with

$$\begin{aligned} dp_s &= q(d\mathcal{B}_y\rho_s + \mathcal{B}_y d\rho_s) \\ &= q\mathcal{B}_y d\rho_s. \end{aligned}$$

The synchronism condition  $\omega_{\text{rf}} = h\omega_{\text{rev},s}$  remains valid, and the RF frequency has to be adjusted to accelerate the beam. In synchrotrons, the small beam pipe aperture only allows for small orbit changes. Nonetheless, this is used to steer the beam radially or to do very fine adjustments of the beam energy.

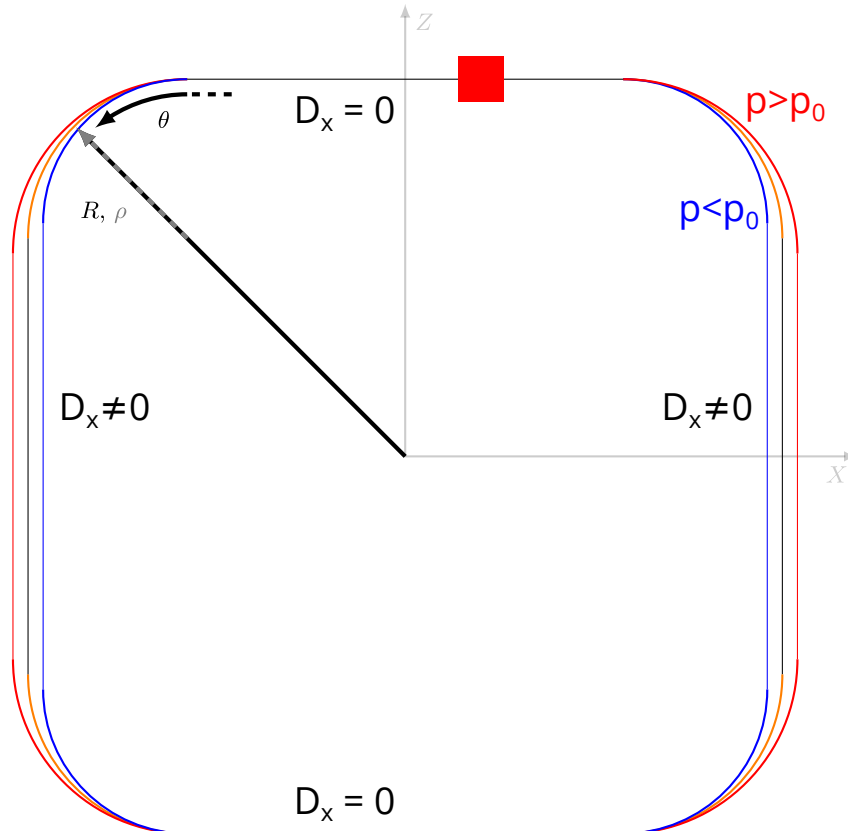


**Fig. I.4.18:** Trajectories for particles with  $p \neq p_0$  where  $p_0$  is the momentum on the reference trajectory. Due to dispersion in the bending regions, the particles with  $p \neq p_0$  will follow an outer or inner trajectory hence having a different orbit  $R$  and revolution period  $T_{\text{rev}}$ . The radial offset is represented by the dispersion function  $D_x$  and is large where the dispersion function  $D_x$  is not zero. The RF cavity is represented as a red box and ideally place in locations with zero dispersion.

An important consideration for the rest of the lecture is that the longitudinal dynamics is tightly linked to the particle orbit, defining the time of flight in the circular accelerator and hence the phase of arrival in the RF system after a turn. Indeed, as shown in Fig. I.4.18, any particle with a slight offset in momentum to the expected  $p_0$  has a small radial/horizontal offset due to dispersion. The radial offset is given by the transverse dispersion function

$$x_D(z) = D_x(z) \frac{dp}{p_0}, \quad (\text{I.4.42})$$

which depends on the accelerator optics. Full details on the definition of the dispersion function are provided in Chapter I.3 on transverse beam dynamics.

The relative elongation of the mean radius corresponding to a momentum relative offset is represented with the “momentum compaction factor” parameter denoted

$$\alpha_p = \frac{dR/R}{dp/p}. \quad (\text{I.4.43})$$

#### To go beyond: General definition of the momentum compaction factor

A more general definition of the momentum compaction factor can be obtained through differential equations. The momentum is a function of  $(\rho, \mathcal{B}_y)$ , and consequently of  $(R, \mathcal{B}_y)$ . It can be differentiated as

$$\begin{aligned} \frac{dp}{p} &= \left( \frac{\partial p}{\partial R} \right)_{\mathcal{B}_y} \frac{R}{p} \frac{dR}{R} + \left( \frac{\partial p}{\partial \mathcal{B}_y} \right)_R \frac{\mathcal{B}_y}{p} \frac{d\mathcal{B}_y}{\mathcal{B}_y} \\ &\implies \frac{dp}{p} = \frac{1}{\alpha_p} \frac{dR}{R} + \frac{d\mathcal{B}_y}{\mathcal{B}_y}. \end{aligned} \quad (\text{I.4.44})$$

The momentum compaction factor **assumes a constant**  $\mathcal{B}_y$  and is defined as

$$\alpha_p = \left( \frac{\partial p}{\partial R} \right)_{\mathcal{B}_y}^{-1} \frac{p}{R} = \left( \frac{\partial R}{\partial p} \right)_{\mathcal{B}_y} \frac{p}{R}. \quad (\text{I.4.45})$$

It is reminded that  $p = \mathcal{B}_y \rho q$ , therefore

$$\left( \frac{\partial p}{\partial \mathcal{B}_y} \right)_R \frac{\mathcal{B}_y}{p} = \rho q \frac{\mathcal{B}_y}{p} = 1.$$

The momentum compaction factor can then be computed from the dispersion function using the relationship, where the radial offset is integrated over the circumference of the accelerator

$$\alpha_p = \frac{1}{2\pi R} \int_0^{2\pi R} \frac{D_x(z)}{\rho(z)} dz = \frac{\langle D_x \rangle_\rho}{R}. \quad (\text{I.4.46})$$

Here,  $\langle D_x \rangle_\rho$  is an averaged dispersion value in the bending magnets (*NB*:  $\rho \rightarrow \infty$  in straight sections, and  $\alpha_p = 0$  in linacs). For azimuthally symmetric fields,  $\alpha_p = 1/Q_x^2$  where  $Q_x$  is the horizontal tune (note that the horizontal tune can be used as a reasonable scaling law to get an approximate value of the

momentum compaction factor).

#### Derivation I.4.15

Demonstrate that

$$\alpha_p = \frac{1}{2\pi R} \int_0^{2\pi R} \frac{D_x(z)}{\rho(z)} dz = \frac{\langle D_x \rangle_\rho}{R}.$$

Start by using the total path length increase due to dispersion

$$dC = 2\pi dR = \int_0^{2\pi} x_D(z) d\theta.$$

*Reminder:*  $x_D$  is a horizontal (radial) offset.

#### I.4.3.3.2 The momentum compaction factor for an existing synchrotron

To better grasp the concept of the momentum compaction factor, the example of the Low Energy Ion Ring (LEIR) at CERN is taken. A representation of the particle trajectories with a momentum offset  $p \neq p_0$  together with the optics is given in Fig. I.4.19.

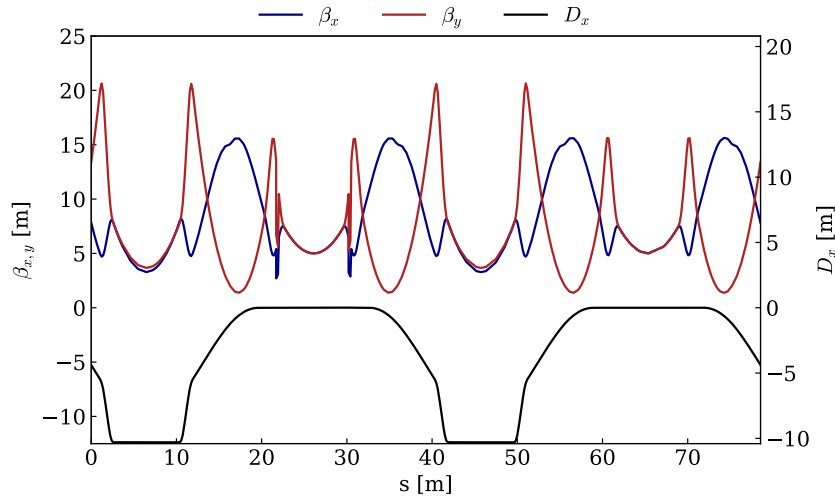


**Fig. I.4.19:** The optics of the LEIR accelerator, corresponding to the illustration in Fig. I.4.18. The trajectory of particles with a momentum offset is shown to the left with the corresponding optics functions to the right. More details on the LEIR optics in [9].

Following the calculation of the optics functions, the momentum compaction can be obtained by integrating the dispersion along the ring using Eq. (I.4.46). Note that the dispersion function  $D_x$  is displayed as negative. Due to conventions, and as the beam is rotating counter clock-wise in the LEIR synchrotron, the Eq. (I.4.46) should be integrated from  $2\pi R \rightarrow 0$ , yielding a positive  $\alpha_p$ . For LEIR, the obtained momentum compaction factor is  $\alpha_p = 0.124$  and the circumference of the accelerator is  $C = 78.54$  m.

**Exercise I.4.16**

For the following exercise, the dispersion function from Fig. I.4.19 can be taken as positive for simplification.

- What is the local radial offset for a particle with  $\frac{\Delta p}{p_0} = 10^{-3}$  at large dispersion?
- What is the elongation of the trajectory  $\Delta C$  for a particle with  $\frac{\Delta p}{p_0} = 10^{-3}$ ?

The momentum compaction factor is computed in synchrotrons with respect to the design orbit  $R_0$  (subscript for design synchrotron parameters 0). Note that the synchronous particle can be offset in orbit with respect to the design trajectory.

The momentum compaction factor can be expanded in series around  $p_0$  and coefficients computed from the nonlinear dispersion function (more details in Chapter I.9 on nonlinear transverse dynamics)

$$\alpha_{p_0} = \alpha_0 + \alpha_1 \frac{\Delta p}{p_0} + \alpha_2 \left( \frac{\Delta p}{p_0} \right)^2 + \dots \quad (I.4.47)$$

**Assumption:** We will consider for the rest of the lecture only linear dispersion, momentum compaction factor  $\alpha_0 = (\Delta R/R_0) / (\Delta p/p_0)$ , phase slip factor  $\eta_0 = -(\Delta\omega_{\text{rev}}/\omega_{\text{rev},0}) / (\Delta p/p_0)$ .

**To go beyond: The magnetic field index**

Another parameter found in the literature is the magnetic field index, linking the effective bending magnetic field to the orbit of the particle. Although common for cyclotrons and FFAs (see Chapter I.13), it is less often used in the context of synchrotrons.

The magnetic rigidity formula can also be written as

$$p = q\mathcal{B}_y\rho = q \langle \mathcal{B}_y \rangle R, \quad (I.4.48)$$

where we define the average magnetic field along a particle path as

$$\langle \mathcal{B}_y \rangle = \frac{1}{2\pi R} \int_0^{2\pi R} \mathcal{B}_y dz. \quad (I.4.49)$$

We define the average magnetic field index

$$\langle n \rangle = -\frac{d \langle \mathcal{B}_y \rangle / \langle \mathcal{B}_y \rangle}{dR/R} = 1 - \frac{1}{\alpha_p}. \quad (I.4.50)$$

**Derivation I.4.17**

Show that the definition of the average magnetic field leads to Eq. (I.4.48) and demonstrate the definition of the average magnetic field index Eq (I.4.50).

### I.4.3.3 The phase slip factor and transition energy

As the orbit varies with the momentum offset, the revolution period/frequency of the particle also changes. This causes a slippage in the phase of the particle with respect to the synchronous phase. Hence, the RF frequency needs to be changed to continue fulfilling the synchronism condition. The phase slip factor is defined as

$$\eta = -\frac{d\omega_{\text{rev}}/\omega_{\text{rev}}}{dp/p} = \frac{dT_{\text{rev}}/T_{\text{rev}}}{dp/p}. \quad (\text{I.4.51})$$

The phase slip factor is also a property of the accelerator optics and can be obtained from the momentum compaction factor. Differentiating the revolution frequency

$$\omega_{\text{rev}} = \frac{\beta c}{R} \quad \rightarrow \quad \frac{d\omega_{\text{rev}}}{\omega_{\text{rev}}} = \frac{d\beta}{\beta} - \frac{dR}{R} \left( = -\frac{dT_{\text{rev}}}{T_{\text{rev}}} \right), \quad (\text{I.4.52})$$

we can obtain the phase slip factor

$$\eta = \alpha_p - \frac{1}{\gamma^2}. \quad (\text{I.4.53})$$

*Note:* The phase slip factor can be defined differently in the literature (e.g. opposite sign), beware of the used conventions!

With this newly introduced parameter, we will now be able to answer the question raised in Ex. I.4.1, thanks to the concept of transition energy. Using Eq. (I.4.53), and knowing that the momentum compaction is a constant depending on the optics configuration, we introduce the transition energy parameter

$$\alpha_p = \frac{1}{\gamma_t^2} \rightarrow \gamma_t = \frac{1}{\sqrt{\alpha_p}}. \quad (\text{I.4.54})$$

This allows us to outline three regimes based on the sign of  $\eta$ , together with the Fig. I.4.18:

1.  $\eta < 0$  if  $\alpha_p < \frac{1}{\gamma^2}$ ,  $\gamma < \gamma_t$ , below transition energy

The particles with **increasing orbit/momentum arrives earlier** as the velocity gain is more important than the increased path length. This happens in particular in **low energy synchrotrons**.

2.  $\eta > 0$  if  $\alpha_p > \frac{1}{\gamma^2}$ ,  $\gamma > \gamma_t$ , above transition energy

The particles with **increasing orbit/momentum arrives later** as the velocity gain is less important than the increased path length. This happens in particular in **high energy synchrotrons**.

3.  $\eta = 0$  if  $\alpha_p = \frac{1}{\gamma^2}$ ,  $\gamma = \gamma_t$ , at transition energy

At transition energy, all particles circulate with the same revolution period. This change of regime during acceleration requires special treatment which requires further derivations. To avoid transition crossing, special optics with  $\langle D_x \rangle < 0 \rightarrow \alpha_p < 0$  can be made, leading mathematically to an imaginary  $\gamma_t$ .

#### Exercise I.4.18

Fill the table for the SPS ( $C_0 = 6911.50$  m) with  $\gamma_t = 18$  for a proton beam ( $E_t$  is the energy at transition crossing). Is transition crossed in the SPS during acceleration?

	SPS injection	SPS extraction
Momentum [GeV/c]	14	450
$E$ [GeV]		
$\gamma$		
$T_{\text{rev}}$ [ $\mu\text{s}$ ]		
$\alpha_p$ [ $10^{-3}$ ]		
$E_t$ [GeV]		
$\eta$ [ $10^{-3}$ ]		

#### I.4.3.3.4 Set of useful differential equations

Now that the momentum compaction and phase slip factors are defined, a complete set of differential equations describing how the parameters of the synchronous particle evolve with the adjustments of the accelerator settings. Specifically, these differential equations describe how the momentum  $p$ , the orbit  $R$ , and the revolution frequency  $f_{\text{rev}}$  are changing together with the RF frequency  $f_{\text{rf}}$  (directly related to  $f_{\text{rev}}$  through the synchronism condition  $f_{\text{rf}} = h f_{\text{rev}}$ ) and the bending field  $\mathcal{B}_y$ . The four fundamental equations are given in Table I.4.1 and are self-consistent.

(1) $\mathcal{B}_y, p, R$	$\frac{dp}{p} = \gamma_t^2 \frac{dR}{R} + \frac{d\mathcal{B}_y}{\mathcal{B}_y}$	(I.4.55)
(2) $f_{\text{rev}}, p, R$	$\frac{dp}{p} = \gamma^2 \frac{df_{\text{rev}}}{f_{\text{rev}}} + \gamma^2 \frac{dR}{R}$	(I.4.56)
(3) $\mathcal{B}_y, f_{\text{rev}}, p$	$\frac{d\mathcal{B}_y}{\mathcal{B}_y} = \gamma_t^2 \frac{df_{\text{rev}}}{f_{\text{rev}}} + \frac{\gamma^2 - \gamma_t^2}{\gamma^2} \frac{dp}{p}$	(I.4.57)
(4) $\mathcal{B}_y, f_{\text{rev}}, R$	$\frac{d\mathcal{B}_y}{\mathcal{B}_y} = \gamma^2 \frac{df_{\text{rev}}}{f_{\text{rev}}} + (\gamma^2 - \gamma_t^2) \frac{dR}{R}$	(I.4.58)

**Table I.4.1:** The synchrotron differential equations linking variations of the magnetic field, the particle orbit, its momentum and revolution frequency. The RF frequency is directly analogous to the revolution frequency via the synchronism condition [10].

The equations can then be exploited to express how all the parameters evolve in a self consistent manner. Here are some specific examples:

1.  $dR = 0$

This represents the acceleration on orbit as described in Section I.4.3.2. The beam can be accelerated by ramping the bending field (Eq. (I.4.55)) while increasing the RF frequency (Eq. (I.4.58)).

2.  $dp = 0$

This represents the case with RF off, where the beam is not accelerated/decelerated. In that case, the variations of the magnetic field will adjust the beam orbit (Eq. (I.4.55)) as well as the revolution

frequency (Eq. (I.4.57)).

3.  $d\mathcal{B}_y = 0$

This represents the case where the beam orbit is steered by adjusting the RF frequency (Eq. (I.4.58)), with also a variation of the momentum (Eq. (I.4.57)). Note that the sign of the steering is changing depending on whether the accelerator is above/below transition energy. This can be used to facilitate the extraction of the beam or fine-adjust the beam energy.

4.  $df_{\text{rev}} = 0$

This represents the case where the RF frequency is fixed (e.g. during synchronization with a downstream experiment or accelerator). Any small variation of the magnetic field will directly translate in a change of the beam energy (Eq. (I.4.57)) and orbit (Eq. (I.4.58)). The sign also depends on the transition energy.

Finally, other useful relationships are provided here:

$$\frac{dp}{p} = \frac{d\rho}{\rho} + \frac{d\mathcal{B}_y}{\mathcal{B}_y}, \quad (\text{I.4.59})$$

$$\frac{dp}{p} = \frac{dR}{R} + \frac{d\langle\mathcal{B}_y\rangle}{\langle\mathcal{B}_y\rangle}, \quad (\text{I.4.60})$$

$$\frac{dR}{R} = \alpha_p \frac{d\rho}{\rho}. \quad (\text{I.4.61})$$

**Exercise I.4.19**

- What is the mean radial offset  $\Delta R$  of a particle with  $\Delta p/p_0 = -10^{-4}$  with a constant  $\mathcal{B}_y$ ?
- What is the corresponding change in the revolution period  $\Delta T_{\text{rev}}$ ? Is the particle delayed or in advance after a turn, with respect to the reference?

**Derivation I.4.20**

Demonstrate the differential equations Eqs. (I.4.55) (I.4.56) (I.4.57) (I.4.58).

## I.4.4 Longitudinal equations of motion

### I.4.4.1 The non-synchronous particles

As specified in the previous section, the synchronous particle (denoted with the subscript  $s$ ) is a fictitious particle serving as ideal reference for all the particles composing a bunch. In this section, we treat the equations describing the motion of the non-synchronous particles, for which the energy and longitudinal

coordinate are expressed relative to the synchronous particle as

$$\begin{aligned}
 E &= E_s + \Delta E \\
 \omega_{\text{rev}} &= \omega_{\text{rev},s} + \Delta\omega_{\text{rev}} \\
 \theta &= \theta_s + \Delta\theta \\
 \rho(z) &= \rho_s(z) + x_D(z) \quad (\text{Dispersion}) \\
 &\dots
 \end{aligned}$$

Note that all following  $\Delta$  for the rest of the course will relate the offset of an arbitrary particle property to that of the synchronous reference.

We describe the evolution of the energy gain of an arbitrary particle arriving at a phase  $\phi$  in the cavity

$$\frac{d(\Delta E)}{dt} = f(\phi).$$

We then derive the evolution of the phase of an arbitrary particle with an energy offset  $\Delta E$  with respect to the synchronous particle

$$\frac{d\phi}{dt} = g(\Delta E).$$

#### I.4.4.1.1 Energy gain for an arbitrary particle

In the previous lesson, we derived the acceleration rate of the synchronous particle. The acceleration rate is first approximated to consider only the RF contribution (no induction force, synchrotron radiation, wakefields...). For the synchronous particle one obtains

$$\dot{E}_s \approx \frac{\delta E_s}{T_{\text{rev},s}} \rightarrow \dot{E}_s = \frac{qV_{\text{rf}}}{T_{\text{rev},s}} \sin \phi_s = \omega_{\text{rev},s} \frac{qV_{\text{rf}}}{2\pi} \sin \phi_s.$$

The acceleration rate for an arbitrary particle is

$$\dot{E} = \omega_{\text{rev}} \frac{qV_{\text{rf}}}{2\pi} \sin \phi.$$

The difference in acceleration rate is

$$\frac{\dot{E}}{\omega_{\text{rev}}} - \frac{\dot{E}_s}{\omega_{\text{rev},s}} = \frac{qV_{\text{rf}}}{2\pi} (\sin \phi - \sin \phi_s). \quad (\text{I.4.62})$$

Re-organizing the term on the left-hand side provides us with the following equation of motion:

$$\frac{d}{dt} \left( \frac{\Delta E}{\omega_{\text{rev},s}} \right) = \frac{qV_{\text{rf}}}{2\pi} (\sin \phi - \sin \phi_s). \quad (\text{I.4.63})$$

This is the first fundamental longitudinal equation of motion. Note that  $\omega_{\text{rev}} \neq \omega_{\text{rev},s}$  and that  $\omega_{\text{rev},s}$  is inside the time derivative. This is obtained following thorough derivations and is not as simple as it may first appear!

### Derivation I.4.21

Demonstrate for the first longitudinal equation of motion (I.4.63) the following relationship

$$\frac{\dot{E}}{\omega_{\text{rev}}} - \frac{\dot{E}_s}{\omega_{\text{rev},s}} \approx \frac{d}{dt} \left( \frac{\Delta E}{\omega_{\text{rev},s}} \right).$$

Hints: Remember that  $\omega_{\text{rev}}$  and  $\omega_{\text{rev},s}$  are functions of time. It may be easier to handle  $T_{\text{rev}}$  than  $\omega_{\text{rev}}$  for the initial derivations. Expand the parameters describing the non-synchronous particle as  $E = E_s + \Delta E$ , drop second order terms in  $\Delta$ , and consider that

$$\Delta T_{\text{rev}} \approx \left( \frac{dT_{\text{rev}}}{dE} \right)_s \Delta E.$$

### To go beyond: When the betatron meets the synchrotron

A more accurate approach to obtain Eq. (I.4.63) requires us to include the induction forces due to the ramping of the bending field during acceleration.

Let's first reformulate the left-hand side of Eq. (I.4.62) without using the approximation that

$$\Delta T_{\text{rev}} \approx \left( \frac{dT_{\text{rev}}}{dE} \right)_s \Delta E.$$

The reorganization of the terms then leads to

$$\frac{\dot{E}}{\omega_{\text{rev}}} - \frac{\dot{E}_s}{\omega_{\text{rev},s}} = \frac{d}{dt} \left( \frac{\Delta E}{\omega_{\text{rev},s}} \right) + \alpha_p \frac{\Delta E}{\omega_{\text{rev},s}} \frac{\dot{\mathcal{B}}_{y,s}}{\mathcal{B}_{y,s}}. \quad (\text{I.4.64})$$

Additionally, by adding the contribution from the induction forces with ramping  $\mathcal{B}_y$ , the acceleration rate for an arbitrary particle becomes

$$\dot{E} = \frac{\omega_{\text{rev}}}{2\pi} \left[ qV_{\text{rf}} \sin \phi + q \int_0^{2\pi} \int_0^\rho \frac{\partial \mathcal{B}_y}{\partial t} \rho' d\rho' d\theta \right]. \quad (\text{I.4.65})$$

Note that for the synchronous particle the induction force should be modified by replacing  $\rho$  in the integral interval with  $\rho_s$ . Reformulating the difference of the acceleration rate due to induction forces between an arbitrary particle to the synchronous one finally leads to

$$\frac{d}{dt} \left( \frac{\Delta E}{\omega_{\text{rev},s}} \right) = \frac{qV_{\text{rf}}}{2\pi} (\sin \phi - \sin \phi_s) \quad (1)$$

$$- \alpha_p \frac{\dot{\mathcal{B}}_{y,s}}{\mathcal{B}_{y,s}} \left( \frac{\Delta E}{\omega_{\text{rev},s}} \right) \quad (2)$$

$$+ \frac{q}{2\pi} \int_0^{2\pi} \frac{\partial \mathcal{B}_{y,s}}{\partial t} \rho_s x_D d\theta. \quad (3)$$

It can be demonstrated that (3) is equal to (2) to the first order and hence both cancel out with no further assumption! We then finally get

$$\frac{d}{dt} \left( \frac{\Delta E}{\omega_{\text{rev},s}} \right) = \frac{qV_{\text{rf}}}{2\pi} (\sin \phi - \sin \phi_s). \quad (\text{I.4.63})$$

**Derivation I.4.22**

Demonstrate the relationship from Eq. (I.4.64). Hint: Use the relativistic relationships from Sec. I.4.2.2 to convert energies to momenta, etc. Use the linear momentum compaction factor and phase slip factor from Sec. I.4.3.3.

**Derivation I.4.23**

Demonstrate that the difference in induction force for an arbitrary particle can be written as

$$\frac{q}{2\pi} \int_0^{2\pi} \frac{\partial \mathcal{B}_{y,s}}{\partial t} \rho_s x_D d\theta,$$

and that it compensates exactly the term

$$\alpha_p \frac{\dot{\mathcal{B}}_{y,s}}{\mathcal{B}_{y,s}} \left( \frac{\Delta E}{\omega_{\text{rev},s}} \right).$$

**I.4.4.1.2 Phase slippage for an arbitrary particle**

In the previous lesson, we considered the synchronous particle which is by definition always synchronous to the RF and arrives at the phase  $\phi_s$ . We will now consider the phase evolution of an arbitrary particle  $\phi$ , relative to the RF wave.

The azimuth of an arbitrary particle revolving around the ring at a time  $t$  is

$$\theta(t) = \int \omega_{\text{rev}} dt.$$

The phase of an arbitrary particle with respect to the RF wave at all time is

$$\phi(t) = \int \omega_{\text{rf}} dt - h\theta(t) = -h \int \Delta\omega_{\text{rev}} dt.$$

Remember that  $\omega_{\text{rf}} = h\omega_{\text{rev},s}$ . Notice the minus sign, a particle in front azimuthally (higher  $\theta$ ) will arrive earlier in the cavity (lower  $\phi$ ).

By differentiating for the time and including the phase slip factor  $\eta$ , one gets

$$\begin{aligned} \frac{d\phi}{dt} &= -h\Delta\omega_{\text{rev}} \\ &= h\eta\omega_{\text{rev},s} \frac{\Delta p}{p_s}. \end{aligned}$$

Using the differential relationship  $dE/E = \beta^2 dp/p$  (Eq. (I.4.19)), we finally obtain

$$\frac{d\phi}{dt} = \frac{h\eta\omega_{\text{rev},s}^2}{\beta_s^2 E_s} \left( \frac{\Delta E}{\omega_{\text{rev},s}} \right). \quad (\text{I.4.66})$$

This is the second fundamental longitudinal equation of motion. From now on we will describe the motion in the longitudinal phase space  $\left(\phi, \frac{\Delta E}{\omega_{\text{rev},s}}\right)$  instead of  $(z, p_z)$ .

#### I.4.4.2 Introduction to particle tracking

Now that the equations of motion are established, the motion of the particles in phase space can be analyzed. A first approach proposed here is to implement the equations of motion numerically. The objective will be to track the particle coordinates as a function of time. This method is complementary to the analytical derivations described in the following Section I.4.5. Since the synchrotron motion can be complex to grasp, a tracking code can help to visualize easily the longitudinal motion in phase space. Tracking was also established as an essential tool for accelerator and beam dynamics studies because high level complexity can be implemented with moderate effort.

We will start with the simplest configuration, a single RF system, and assuming no longitudinal energy gain/loss in the rest of the ring. A simplified layout is shown in Fig. I.4.20.

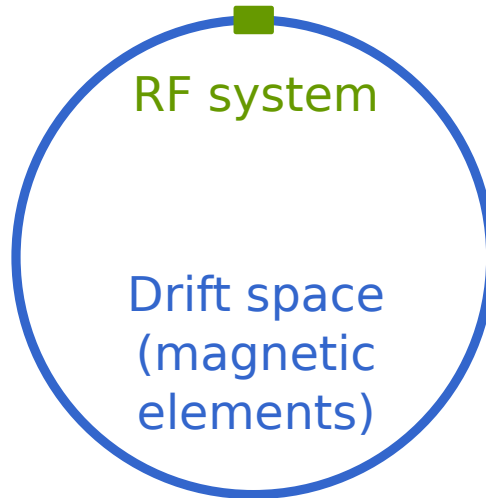


**Fig. I.4.20:** A very simplified schematic of a synchrotron, with only a single RF system and no electric field contribution in the magnetic elements (pure drift space).

##### I.4.4.2.1 Discretizing the equations of motion

In the context of the tracking code, we will use the  $(\phi, \Delta E)$  coordinate system.<sup>2</sup> The (continuous) equations of motion obtained previously need to be discretized to be implemented in code.

The energy gain from Eq. (I.4.63) is commonly called the “kick” equation (NB: we neglect  $\dot{\omega}_{\text{rev},s}$  for simplicity)

$$\frac{d}{dt} \left( \frac{\Delta E}{\omega_{\text{rev},s}} \right) = \frac{qV_{\text{rf}}}{2\pi} (\sin \phi - \sin \phi_s) \approx \frac{\Delta E^{(n+1)} - \Delta E^{(n)}}{\omega_{\text{rev},s} T_{\text{rev},s}},$$

<sup>2</sup>Note that  $(\phi, \Delta E)$  are not canonical variables,  $(\tau, \Delta E)$  or  $(\phi, \Delta E/\omega_{\text{rev},s})$  are canonical.

where  $n$  represents the iteration turn corresponding to one revolution in the accelerator (note that  $n$  is a superscript to indicate the turn index and not an exponent). The equation of motion is actually discrete by nature, the relative energy of a particle changes from one turn to the next as

$$\Delta E^{(n+1)} = \Delta E^{(n)} + qV_{\text{rf}} \sin \phi - \delta E_s^{(n \rightarrow n+1)}. \quad (\text{I.4.67})$$

The energy gain of the synchronous particle at a turn  $n$  is

$$\delta E_s^{(n \rightarrow n+1)} = 2\pi q \rho_s R_s \frac{\mathcal{B}_y^{(n+1)} - \mathcal{B}_y^{(n)}}{T_{\text{rev},s}}. \quad (\text{I.4.68})$$

An example of the applied energy change when passing through an RF system is given in Fig. I.4.21. Note the fact that the coordinate system is relative to the energy of the synchronous particle, the relative energy  $\Delta E$  of any particle sitting exactly on  $\phi_s$  would remain unchanged.

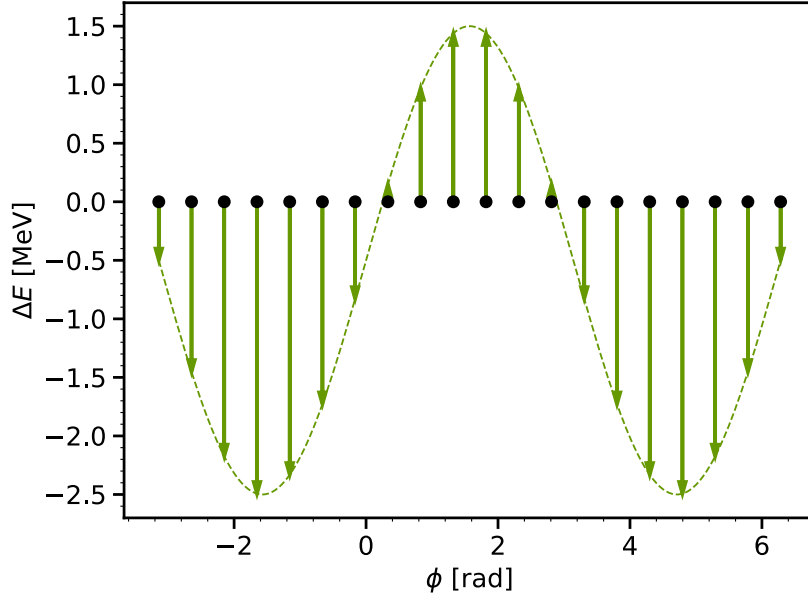


**Fig. I.4.21:** Example of energy change for protons passing through an RF system with  $V_{\text{rf}} = 2$  MV,  $f_{\text{rf}} = 200$  MHz,  $\delta E_s = 0.5$  MeV (animated in [2]).

The phase slip from Eq. (I.4.66) is commonly called the “drift” equation. Neglecting any source of change in  $\Delta E$  along the magnetic elements, only the phase of the particle relative to the RF will change as

$$\frac{d\phi}{dt} = \frac{h\eta\omega_{\text{rev},s}^2}{\beta_s^2 E_s} \left( \frac{\Delta E}{\omega_{\text{rev},s}} \right) = \frac{\phi^{(n+1)} - \phi^{(n)}}{T_{\text{rev},s}}.$$

The corresponding discrete equation becomes

$$\phi^{(n+1)} = \phi^{(n)} + \left( \frac{2\pi h\eta}{\beta_s^2 E_s} \right) \Delta E, \quad (\text{I.4.69})$$

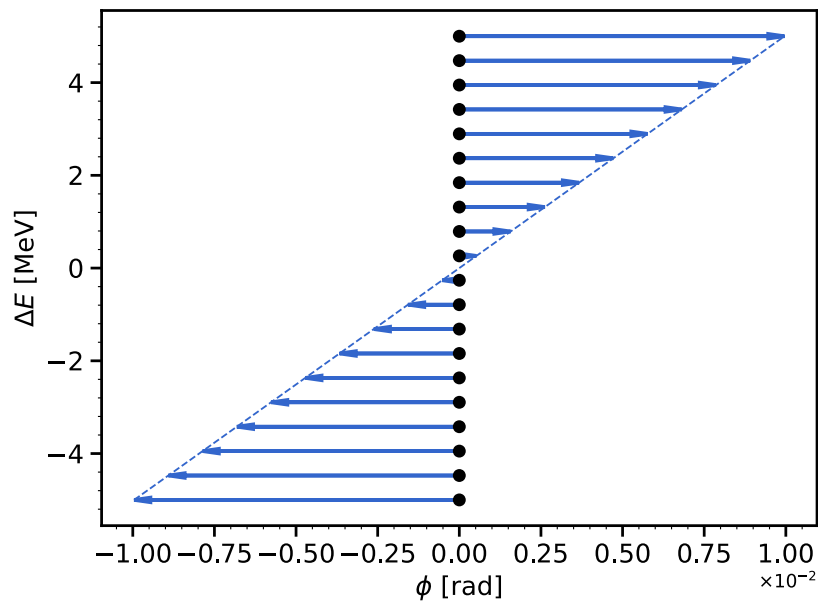


**Fig. I.4.22:** Example for the phase slippage of protons passing along a ring with  $C_0 = 6911.50$  m,  $E_s = 26$  GeV,  $\gamma_t = 18$  (animated in [2]).

using the linear momentum compaction and phase slip factors

$$\eta = \frac{1}{\gamma_t^2} - \frac{1}{\gamma_s^2} = \alpha_p - \frac{1}{\gamma_s^2}.$$

An example of the applied phase slippage while circulating through the ring is shown in Fig. I.4.22. In that configuration, all particles with an offset in energy drift away linearly from the synchronous particle.

#### I.4.4.2.2 A working tracking code

The two equations of motion are sufficient to build a simple (yet very useful) tracking code. For any coding language, the computation boils down to two functions applied in two nested loops (one to loop over particles, the second for each turn). A pseudocode valid for any programming language is

```

1 for n_turns:
2     for n_particles:
3         dE += rf_kick(phi)
4         phi += drift(dE)

```

where the equations of motion are defined as

```

1 def rf_kick(phi):
2     return q*Vrf*sin(phi) - q*Vrf*sin(phi_s)
3
4 def drift(dE):
5     return 2*pi*h*eta_0 / (beta**2 * E) * dE

```

In the following, a complete example using Python together with the packages Numpy, Scipy and Matplotlib is provided. This example can be reproduced as an exercise and allows us to have a working tracking code.

1. We first import useful libraries.

```

1 import numpy as np # Numerical computation package
2 import matplotlib.pyplot as plt # A plotting library
3 from scipy.constants import m_p, c, e # Physics constants
4

```

2. We then define the accelerator parameters.

```

1 Ekin = 26e9 # Kinetic energy [eV]
2
3 charge = 1 # Proton charge [e]
4 E0 = m_p * c**2.0 / e # Proton mass [eV/c**2]
5 circumference = 6911.5 # Accelerator circumference [m]
6 energy = Ekin + E0 # Total energy [eV]
7 momentum = np.sqrt(energy**2.0 - E0**2.0) # Momentum [eV/c]
8 beta = momentum / energy # Relativistic velocity ratio
9 gamma = energy / E0 # Lorentz factor
10
11 t_rev = circumference / (beta * c) # Revolution period [s]
12 f_rev = 1 / t_rev # Revolution frequency [Hz]
13
14 harmonic = 4620 # RF harmonic number
15 voltage = 4.5e6 # RF voltage [V]
16 f_rf = harmonic * f_rev # RF frequency [Hz]
17 t_rf = 1 / f_rf # RF period [s]
18
19 gamma_t = 18 # Transition gamma
20 alpha_p = 1 / gamma_t**2.0 # Momentum compaction factor
21 eta = alpha_p - 1 / gamma**2.0 # Phase slip factor
22
23 # The values can be printed for verification
24 print("Beta: " + str(beta))
25 print("Gamma: " + str(gamma))
26 print("Revolution period: " + str(t_rev * 1e6) + " mus")
27 print("RF frequency: " + str(f_rf / 1e6) + " MHz")
28 print("RF period: " + str(t_rf * 1e9) + " ns")
29 print("Momentum compaction factor: " + str(alpha_p))
30 print("Phase slippage factor: " + str(eta))
31

```

3. Define your tracking functions from Eqs. (I.4.67) (I.4.69), at this place more complex configurations (non-linear momentum compaction, several RF systems) can be included.

```

1 def rf_kick(phi, charge, voltage, phi_s=0):
2     '''The equation of motion describing the
3     energy gain in the RF system'''
4     return charge * voltage * (np.sin(phi) - np.sin(phi_s))
5
6 def drift(dE, harmonic, eta, beta, energy):
7     '''The equation of motion describing the
8     phase slippage in the ring'''

```

```

9     return 2 * np.pi * harmonic * eta * dE / (beta**2 * energy)
10

```

4. Define your initial particle positions. In that example we simply distribute few particles in the first period of the RF waveform with the same energy. The number of particles can be increased to have a better statistical representation of the dynamics.

```

1     n_particles = 10
2     # Two arrays representing the phase and energy coordinates of each
3     # particle
4     phase_coordinates = np.linspace(0, 2 * np.pi, n_particles)
5     dE_coordinates = np.zeros(n_particles)

```

5. Define the number of turns to track for and iterate over all the particles and turns (note that the loop over the particles is implicit thanks to the Numpy package).

```

1     n_turns = 25
2     for idx_turn in range(n_turns):
3         # Adding the energy and phase offsets to the existing coordinates
4         # Note the += term which consists in adding values to the particles
5         # coordinates at the turn idx_turn
6         dE_coordinates += rf_kick(phase_coordinates, charge, voltage)
7         phase_coordinates += drift(dE_coordinates, harmonic, eta, beta, energy)

```

6. The particle coordinates can then be monitored at each turn during the tracking by modifying the previous entry.

```

1     n_turns = 25
2
3     # Generating empty arrays with two dimensions to then save all particles
4     # coordinates at each turn
5     saved_positions_phi = np.zeros((n_particles, n_turns))
6     saved_positions_dE = np.zeros((n_particles, n_turns))
7
8     for idx_turn in range(n_turns):
9         dE_coordinates += rf_kick(phase_coordinates, charge, voltage)
10        phase_coordinates += drift(dE_coordinates, harmonic, eta, beta, energy)
11
12        # Recording the particles coordinates at each turn
13        saved_positions_dE[:, idx_turn] = dE_coordinates
14        saved_positions_phi[:, idx_turn] = phase_coordinates

```

7. The trajectory of the particles can finally be visualized.

```

1     plt.figure('phase space')
2     plt.clf()
3     for idx_particle in range(n_particles):
4         # Plotting the evolution of the particles coordinates for each particle
5         # one by one

```

```

5     plt.plot(
6         saved_positions_phi[idx_particle, :],
7         saved_positions_dE[idx_particle, :],
8         '-o')
9     plt.xlabel('Phase [rad]')
10    plt.ylabel('Energy [eV]')
11    plt.savefig('tracking_result.png')
12

```

The result of the script is given in Fig. I.4.23. In less than 100 lines of code, a complete representation of the longitudinal dynamics is obtained allowing us to perform studies. One can already observe that the particle trajectories form closed trajectories around a reference point ( $\phi = \pi$  in that case), that particles take a different number of turns to perform a complete oscillation in the  $(\phi, \Delta E)$  phase space, and that particles at the very edge  $\phi = 0, 2\pi$  remain static. All these observations will be carefully analyzed in the next section devoted to the analytical description of the synchrotron motion. Further animations are proposed in [2].

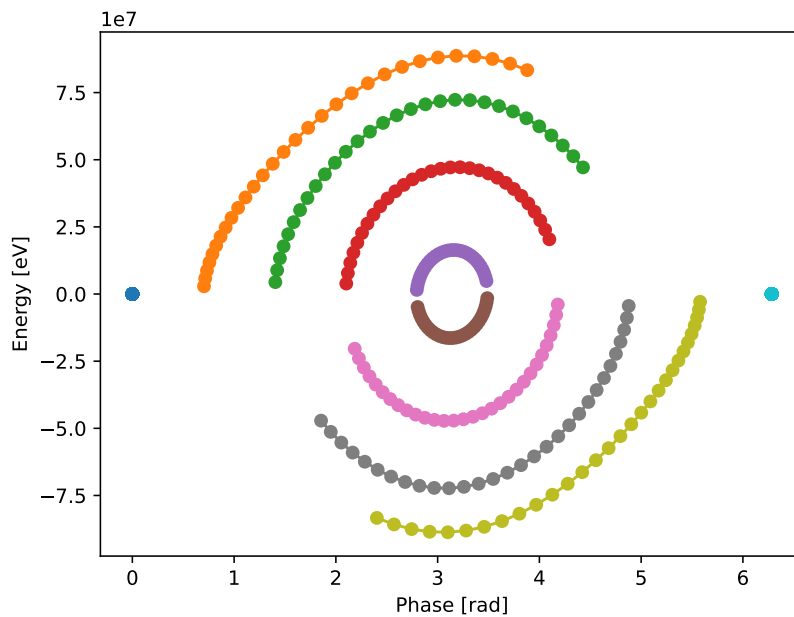


**Fig. I.4.23:** Result of the tracking code described earlier in the section (example of the SPS). Particles were initiated with an RF phase  $\phi \in [0, 2\pi]$  and an energy offset of  $\Delta E = 0$  and tracked for 25 turns in the accelerator (animated in [2]).

Advanced tracking codes are set on the same basis as the description above. Nonetheless, an important work consists in ensuring that the coordinate system is composed of canonical variables, and allows for more complex simulations. Moreover, one improvement to the code above would be to express the coordinate system around “design” values rather than the synchronous particle. For instance, as described in Section I.4.3.3, the beam can be radially displaced at fixed  $\mathcal{B}_y$  by manipulating the RF frequency  $f_{\text{rf}}$ . This case is better handled by using the reference energy and orbit rather than the synchronous energy that will also be slightly offset. More exact versions of the discrete equations of motion

are used in the BLoND simulation code [12]:

$$\Delta E^{(n+1)} = \Delta E^{(n)} + \sum_{k=1}^{n_{\text{rf}}} qV_{\text{rf},k}^{(n)} \sin\left(\omega_{\text{rf},k}^{(n)} \Delta\tau^{(n)} + \phi_k^{(n)}\right) - \delta E_s^{(n \rightarrow n+1)} + \delta E_{\text{other}}, \quad (\text{I.4.70})$$

which can include several RF systems and where  $k$  denotes the index of the RF system. The coordinate  $\Delta\tau$  is the time of arrival in the RF system, relative to the external time reference based on the design revolution period

$$\Delta\tau = \tau - \sum_{d=1}^n T_{\text{rev},d}^{(n)}. \quad (\text{I.4.71})$$

The design revolution period (denoted with the subscript  $d$ ) is the expected value for the momentum on the reference orbit. The RF frequency  $\omega_{\text{rf},k}^{(n)}$  and phase  $\phi_k^{(n)}$  can then vary arbitrarily with respect to that absolute reference (e.g. for the implementation of feedback loops). The drift equation taking into account the non-linear momentum compaction factors is

$$\Delta\tau^{(n+1)} = \Delta\tau^{(n)} + T_{\text{rev},d}^{(n+1)} \left[ \left[ 1 + \sum_l \alpha_l^{(n+1)} \left( \frac{\Delta p}{p_d^{(n+1)}} \right)^l \right] \frac{\Delta p/p_d^{(n+1)}}{\Delta E/E_d^{(n+1)}} - 1 \right], \quad (\text{I.4.72})$$

where the non-linear momentum compaction factors (up to the order  $l$ ) is obtained from Eq. (I.4.47) with the full optics of the accelerator. The relative momentum and  $\Delta p$  can be computed from Eq. (I.4.19).

Numerous codes were made to include more complex longitudinal beam dynamics aspects (collective effects, feedback loops...) with high computational performance and accuracy. Notable codes are the legacy ESME code developed at Fermilab [11] and the more recent BLoND simulation code developed at CERN [12]. Some tracking codes combine transverse and longitudinal dynamics such as PyHEADTAIL [13], Xsuite [14], or Py-ORBIT [15] specializing in different aspects (simulations of transverse instabilities, electron-clouds, space charge effects...). A hands-on tutorial using PyHEADTAIL is proposed in the framework of the JUAS (see Chapter I.6).

## I.4.5 Synchrotron motion

### I.4.5.1 Linear synchrotron motion

We will now describe analytically the motion of the arbitrary particles in the longitudinal phase space  $(\phi, \Delta E/\omega_{\text{rev},s})$ , which is also called the synchrotron motion. As detailed in Section I.4.4, the longitudinal equations of motion form a system of two interdependent differential equations to describe the evolution of the particles' phase  $\phi$  and energy  $\Delta E/\omega_{\text{rev},s}$  with respect to the synchronous particle. These two equations of motion can be combined to analyze the synchrotron motion.

#### I.4.5.1.1 Combining the equations of motion

By incorporating Eq. (I.4.66) in Eq. (I.4.63), and replacing  $\omega_{\text{rev},s}$  by  $\omega_{\text{rf}}/h$  (this is equivalent and will become relevant later), we get

$$\frac{d}{dt} \left( \frac{d\phi}{dt} \frac{\beta_s^2 E_s}{\eta \omega_{\text{rf}}^2} \right) = \frac{qV_{\text{rf}}}{2\pi h} (\sin \phi - \sin \phi_s). \quad (\text{I.4.73})$$

We will first make two important approximations:

1. The synchronous machine and beam parameters denoted with  $s$  are changing slowly with time (only  $\phi$  and  $\Delta E$  are functions of time).
2. We consider small phase oscillations  $\Delta\phi = \phi - \phi_s$  (reminder:  $\dot{\phi}_s = 0$  by definition).

The sine functions on the right-hand side are linearized:

$$\begin{aligned}\sin \phi - \sin \phi_s &= \sin(\phi_s + \Delta\phi) - \sin \phi_s \\ &= \sin \phi_s \cos \Delta\phi + \cos \phi_s \sin \Delta\phi - \sin \phi_s \\ &\approx \cos \phi_s \Delta\phi.\end{aligned}$$

The approximations lead to

$$\begin{aligned}\frac{d^2 \Delta\phi}{dt^2} &= \frac{qV_{\text{rf}}\eta\omega_{\text{rf}}^2}{2\pi h\beta_s^2 E_s} \cos \phi_s \Delta\phi \\ \implies \frac{d^2 \Delta\phi}{dt^2} + \omega_{s_0}^2 \Delta\phi &= 0,\end{aligned}\tag{I.4.74}$$

where the linear synchrotron frequency is defined as (**beware**  $\omega_{s_0} \neq \omega_{\text{rev},s}$ )

$$\omega_{s_0} = 2\pi f_{s_0} = \sqrt{-\frac{qV_{\text{rf}}\omega_{\text{rf}}^2\eta \cos \phi_s}{2\pi h\beta_s^2 E_s}}.\tag{I.4.75}$$

The motion of particles in the longitudinal phase space (synchrotron motion) is the motion of a harmonic oscillator for small  $\Delta\phi$ , under the condition that

$$\eta \cos \phi_s < 0.\tag{I.4.76}$$

It is reminded that the phase stability condition depends on the definition of  $\eta$ , which can be found in the literature with an opposite sign in Eq. (I.4.53).

#### I.4.5.1.2 Phase stability and transition crossing

The phase stability condition  $\eta \cos \phi_s < 0$  imposes that the synchronous phase for a positively charged particle is

$$\begin{aligned}\eta < 0 &\rightarrow \phi_s \in \left[-\frac{\pi}{2}, \frac{\pi}{2}\right] \quad \text{below transition energy} \\ \eta > 0 &\rightarrow \phi_s \in \left[\frac{\pi}{2}, \frac{3\pi}{2}\right] \quad \text{above transition energy}\end{aligned}$$

and vice versa for a negatively charged particle. A non-synchronous particle oscillates around the synchronous particle only if the phase stability condition is fulfilled. A representation of the RF phase fulfilling the phase stability condition to accelerate and decelerate a particle is given in Fig. I.4.24.

An illustration of the motion of a particle in phase space is given in Fig. I.4.25. The phase stability condition can be explained intuitively, with a non-synchronous particle starting with the same energy as the synchronous particle ( $\Delta E = 0$ ), but a different phase of arrival in the RF system  $\phi \neq \phi_s$ . In

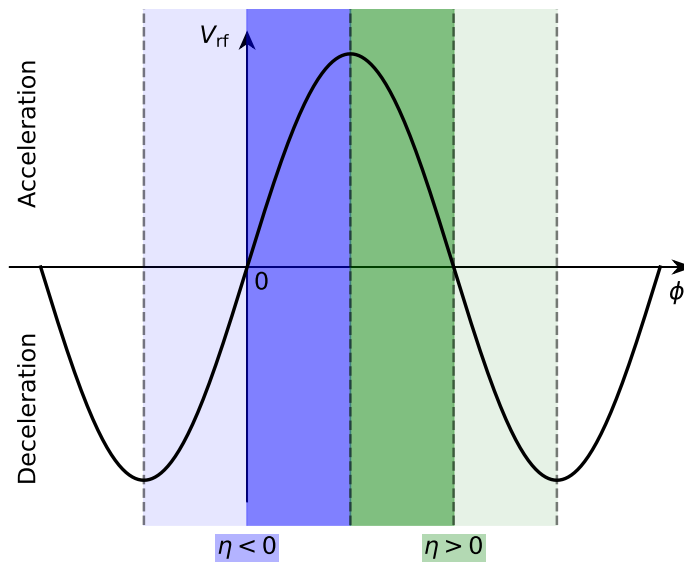


**Fig. I.4.24:** The phase stability condition from Eq. (I.4.76) represented on top of the RF waveform. To fulfill the phase stability condition, a positively charged particle should arrive at a phase where the RF voltage is positive, i.e., in the purple area for  $\eta < 0$  and green area for  $\eta > 0$ . The picture should be mirrored vertically for a negatively charged particle.

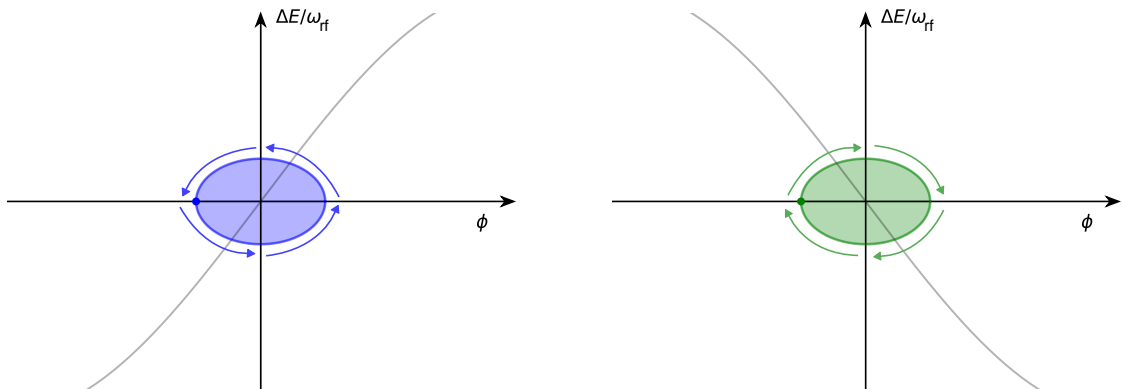


**Fig. I.4.25:** Trajectory in the longitudinal phase space for a positively charged particle below (left,  $\eta < 0$ ) and above (right,  $\eta > 0$ ) transition energy. The particle trajectory and direction is shown together with the RF waveform (light gray). The surface of the enclosed area is the longitudinal emittance for that given particle (animated in [2]).

Fig. I.4.25, the motion of a particle represented by a dot with a starting position of  $\phi < \phi_s$  and  $\Delta E = 0$ , with the arrows representing the direction of the particle motion with time in the longitudinal phase space. Below transition  $\eta < 0$ , the early particle ( $\phi < \phi_s$ ) loses energy (and hence velocity) and gets delayed. The particle with  $\Delta E < 0$  then takes more time to make a full revolution in the accelerator (despite the shorter trajectory, see Section I.4.3.3.1) and becomes late with respect to the synchronous particle. Once  $\phi > \phi_s$ , the particle arrives at an accelerating phase, recovering the energy that was lost in the previous turns. The particle then gains too much energy (and velocity), and again becomes early with respect to the synchronous particle. The particle is finally decelerated and gets back to its starting position in

phase space. The particle oscillates around the synchronous phase located on the rising front of the RF waveform for  $\eta > 0$  ( $\phi_s = 0$  without acceleration). The motion is comparable above transition energy  $\eta > 0$ . In that case, as previously explained in Section I.4.3.3.3, the revolution period for a particle with  $\Delta E > 0$  is larger due to the longer path length, despite the increase in particle velocity. The trajectory in phase space is then reversed, implying that the particle oscillates around the synchronous phase that is located on the decreasing front of the RF waveform for  $\eta > 0$  ( $\phi_s = \pi$  without acceleration). This however describes the cases far below or above transition energy, a specific treatment is necessary to explain what is happening when the transition energy is crossed.

During acceleration and depending on the synchrotron optics, transition energy can be crossed and  $\eta$  changes sign as  $\eta(t) = \alpha_p - 1/\gamma_s^2(t)$ . When  $\gamma_s = \gamma_t$  (and  $\eta = 0$ ), the RF phase must be changed rapidly to maintain the phase stability condition, with an amplitude of  $\pi - 2\phi_s$  as displayed in Fig. I.4.26.

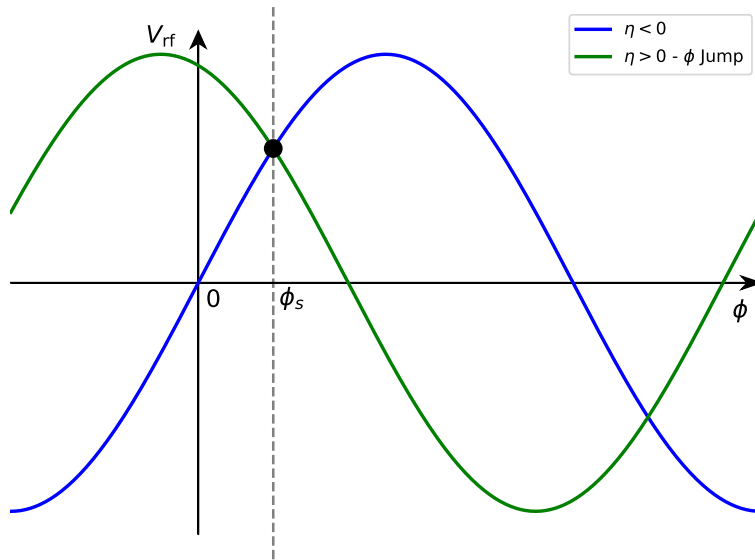


**Fig. I.4.26:** The synchronous phase jump at transition crossing. During acceleration, a rapid jump of the RF phase must be applied to maintain the phase stability condition.

### I.4.5.1.3 Linear parameters of the synchrotron motion

Equation (I.4.74) can then be used to derive the properties of the synchrotron motion from the accelerator parameters.

We first define the linear synchrotron tune as the ratio of the synchrotron frequency to the revolution frequency:

$$Q_{s0} = \frac{\omega_{s0}}{\omega_{\text{rev},s}} = \sqrt{-\frac{qV_{\text{rf}}h\eta \cos \phi_s}{2\pi\beta_s^2 E_s}}. \quad (\text{I.4.77})$$

The inverse of the synchrotron tune gives the number of machine turns needed to perform one full oscillation in longitudinal phase space and is analogous to the betatron tune defined in the transverse beam dynamics lecture. However, the synchrotron tune is usually much smaller than the betatron tune (longitudinal  $\mathcal{O}(10^{-3} - 10^{-2})$  with respect to transverse  $\mathcal{O}(1 - 10^2)$ ).

The amplitude of oscillations of the particle in the longitudinal phase space can also be obtained from Eq. (I.4.74). The solutions for the evolution of the parameters of the non-synchronous particle are

$$\begin{aligned}\Delta\phi(t) &= \Delta\phi_m \sin(\omega_{s0}t), \\ \left(\frac{\Delta E}{\omega_{\text{rf}}}\right)(t) &= \left(\frac{\Delta E}{\omega_{\text{rf}}}\right)_m \cos(\omega_{s0}t),\end{aligned}\quad (\text{I.4.78})$$

the maximum amplitudes of oscillations in phase and energy have the subscript  $m$ . The synchrotron angle is noted  $\psi = \omega_{s0}t$ . The ratio in the amplitudes of oscillation is

$$\frac{(\Delta E/\omega_{\text{rf}})_m}{\Delta\phi_m} = \frac{\beta_s^2 E_s}{|\eta| \omega_{\text{rf}}^2} \omega_{s0} = \frac{\beta_s^2 E_s}{|\eta| h^2 \omega_{\text{rev},s}} Q_{s0}. \quad (\text{I.4.79})$$

#### Derivation I.4.24

Demonstrate the ratio of maximum amplitudes in phase/energy

$$\frac{(\Delta E/\omega_{\text{rf}})_m}{\Delta\phi_m} = \frac{\beta_s^2 E_s}{|\eta| \omega_{\text{rf}}^2} \omega_{s0} = \frac{\beta_s^2 E_s}{|\eta| h^2 \omega_{\text{rev},s}} Q_{s0}. \quad (\text{I.4.79})$$

*Hint: Include the solution for  $\Delta\phi$  in the equation of motion as a start.*

The trajectory of the particles in phase space is an ellipse of the form

$$\left(\frac{\Delta\phi}{\Delta\phi_m}\right)^2 + \left(\frac{\Delta E/\omega_{\text{rf}}}{[\Delta E/\omega_{\text{rf}}]_m}\right)^2 = 1. \quad (\text{I.4.80})$$

The surface of the ellipse corresponds to the longitudinal emittance of a particle. A linear approximation is

$$\varepsilon_{l0} = \frac{\pi}{\omega_{\text{rf}}} \Delta E_m \Delta\phi_m = \pi \Delta E_m \Delta\tau_m, \quad (\text{I.4.81})$$

where  $\tau_m = \phi_m/\omega_{\text{rf}}$ . The longitudinal emittance (corresponding to the particle action in action/angle coordinates) is expressed in the unit [eV · s] and is constant for a particle as long as machine parameters are changed slowly (i.e., adiabatically).

For a bunch of particles composed of many particles, we express the bunch length as  $\tau_l = 2\Delta\tau_m$ , corresponding to the horizontal diameter of ellipse representing the trajectory of the particle with the largest amplitude. The linear longitudinal emittance becomes

$$\begin{aligned}\varepsilon_{l0} &= \pi \Delta E_m \frac{\tau_l}{2} = \frac{\pi \beta_s^2 E_s}{4 |\eta|} \omega_{s0} \tau_l^2 \\ &= \frac{\pi |\eta|}{\beta_s^2 E_s} \frac{1}{\omega_{s0}} \Delta E_m^2.\end{aligned}\quad (\text{I.4.82})$$

In practice, the longitudinal emittance of a bunch is estimated from the measured bunch length together with the machine parameters. The bunch momentum spread is

$$\delta_p = 2\Delta p_m/p_s = 2\Delta E_m/(\beta_s^2 E_s)$$

**Derivation I.4.25**

Demonstrate that

$$\varepsilon_{l_0} = \pi \Delta E_m \frac{\tau_l}{2} = \frac{\pi \beta_s^2 E_s}{4 |\eta|} \omega_{s_0} \tau_l^2 = \frac{\pi |\eta|}{\beta_s^2 E_s \omega_{s_0}} \Delta E_m^2. \quad (\text{I.4.82})$$

*Hint: Replace the phase or energy deviation with the one obtained from the energy/phase amplitude ratios.*

As mentioned previously, the longitudinal emittance of a bunch is preserved as long as the machine parameters are changed adiabatically. The relative variation of the synchrotron frequency with time should be small compared to the synchrotron frequency:

$$\left| \frac{\dot{\omega}_{s_0}}{\omega_{s_0}} \right| \ll \omega_{s_0}.$$

The adiabaticity parameter is then

$$\alpha_{\text{ad}} = \left| \frac{1}{\omega_{s_0}^2} \frac{d\omega_{s_0}}{dt} \right| \ll 1. \quad (\text{I.4.83})$$

Intuitively, the parameters of the machine (e.g., energy, RF voltage, RF phase...) must be changed slower than the synchrotron motion for the bunch to adapt to its new trajectory in phase space.

The following scaling laws allow to evaluate the change in bunch length and energy spread from relative variations in emittance and machine parameters (NB:  $E_s$  and  $\eta$  are interdependent).

**Bunch length:**

$$\tau_l \propto \varepsilon_{l_0}^{1/2} V_{\text{rf}}^{-1/4} h^{-1/4} E_s^{-1/4} \eta^{1/4} \quad (\text{I.4.84})$$

**Energy deviation:**

$$\Delta E_m \propto \varepsilon_{l_0}^{1/2} V_{\text{rf}}^{1/4} h^{1/4} E_s^{1/4} \eta^{-1/4} \quad (\text{I.4.85})$$

During acceleration, with all parameters constant except  $E_s$ , the bunch length reduces with  $\tau_l \propto E_s^{-1/4}$ . This evolution is often referred to as the adiabatic damping of phase oscillations. The energy spread scales inversely with  $\Delta E_m \propto E_s^{1/4}$ ,  $\varepsilon_{l_0}$  is therefore constant.

**Exercise I.4.26**

Following the parameter computation from Exercise I.4.18:

- Compute the linear synchrotron frequency and tune in the SPS at  $p = 14$  and  $450 \text{ GeV}/c$ , with an RF harmonic  $h = 4620$  and voltage  $V_{\text{rf}} = 4.5 \text{ MV}$  (find the other SPS parameters obtained in the exercises from Exercise I.4.18). The beam is not accelerated.
- Compute the approximate emittance and momentum spread at  $p = 14 \text{ GeV}/c$  for a bunch length of  $\tau_l = 3 \text{ ns}$ .
- What would be the bunch length at  $p = 450 \text{ GeV}/c$  if the emittance is preserved?
- What would be the bunch length and energy spread at transition energy?

- Evaluate the required increase in RF voltage to shorten the bunch length by a factor 2.

### 1.4.5.2 Non-linear synchrotron motion

In the following section, we will now consider the equations of motion including the non-linearity due to the sinusoidal nature of the RF waveform. This will reveal a limit to the phase stability condition and imply that non-synchronous particles with very large deviations in phase or energy (i.e., large longitudinal emittance) will not oscillate stably around the synchronous reference and will not be accelerated (and hence lost). The concept of bucket area will be introduced, providing more insights into what the RF voltage should be to accelerate all the particles composing the beam and not only the synchronous particle as described in Section 1.4.3.2.

#### 1.4.5.2.1 Non-linear motion and Hamiltonian

Starting from the same conditions as in the beginning of Section 1.4.5.1.1, we resume with the equation

$$\frac{d}{dt} \left( \frac{d\phi}{dt} \frac{\beta_s^2 E_s}{\eta \omega_{\text{rf}}^2} \right) = \frac{qV_{\text{rf}}}{2\pi h} (\sin \phi - \sin \phi_s). \quad (1.4.73)$$

We assume again that the change of machine parameters with time is negligible (adiabaticity condition), hence

$$\frac{d^2 \phi}{dt^2} + \frac{\omega_{s_0}^2}{\cos \phi_s} (\sin \phi - \sin \phi_s) = 0.$$

We can solve for  $\dot{\phi}$ . By multiplying by  $\dot{\phi}$  and integrating over time, we obtain

$$\frac{\dot{\phi}^2}{2\omega_{s_0}^2} - \frac{\cos \phi + \phi \sin \phi_s}{\cos \phi_s} = \mathcal{H}.$$

For the first term, we use the differential identity

$$d(x^2) = 2x dx \quad \rightarrow \quad \dot{\phi} \ddot{\phi} = \frac{1}{2} \frac{1}{dt} \frac{d(\dot{\phi}^2)}{dt}.$$

For the second term, we integrate

$$\begin{aligned} & \frac{\omega_{s_0}^2}{\cos \phi_s} \int (\sin \phi - \sin \phi_s) \frac{d\phi}{dt} dt \\ &= \frac{\omega_{s_0}^2}{\cos \phi_s} \left[ \int \sin \phi d\phi - \int \sin \phi_s d\phi \right] \\ &= - \frac{\omega_{s_0}^2}{\cos \phi_s} (\cos \phi + \phi \sin \phi_s). \end{aligned}$$

The integration constant  $\mathcal{H}$  can be offset so that its value is zero for the synchronous particle. Since  $\dot{\phi}_s = 0$ , we obtain

$$\mathcal{H} = \frac{\dot{\phi}^2}{2\omega_{s_0}^2} - \frac{\cos \phi - \cos \phi_s + (\phi - \phi_s) \sin \phi_s}{\cos \phi_s}.$$

Replacing  $\dot{\phi}$  using the phase differential equation definition and  $\omega_{s0}$ , we finally obtain

$$\mathcal{H} = \frac{\eta\omega_{\text{rf}}^2}{2\beta_s^2 E_s} \left( \frac{\Delta E}{\omega_{\text{rf}}} \right)^2 + \frac{qV_{\text{rf}}}{2\pi h} [\cos \phi - \cos \phi_s + (\phi - \phi_s) \sin \phi_s]. \quad (\text{I.4.86})$$

Linearized for small  $\Delta\phi$ , the equation describes the same ellipse as obtained in the previous module. The Hamiltonian of synchrotron oscillations is equivalent to that of the non-linear pendulum.

In the previous equations,  $\mathcal{H}$  effectively represents the Hamiltonian of a particle in our reference system, corresponding to the **energy of synchrotron oscillations** (beware: this is not the actual particle energy!) The Hamiltonian is composed of two parts

$$\mathcal{H} = \mathcal{T} \left( \frac{\Delta E}{\omega_{\text{rf}}} \right) + \mathcal{U}(\phi),$$

where  $\mathcal{T}$  is the “kinetic” energy of synchrotron oscillations and  $\mathcal{U}$  the “potential” energy.

### To go beyond: The Hamiltonian formalism applied to longitudinal dynamics

The Hamiltonian of a particle can be obtained from the canonical Hamilton equations

$$\frac{dq}{dt} = \frac{\partial \mathcal{H}}{\partial p} \quad \text{and} \quad \frac{dp}{dt} = -\frac{\partial \mathcal{H}}{\partial q},$$

with  $p$  and  $q$  the conjugate momentum and coordinate. A time invariant Hamiltonian is then expressed as

$$\mathcal{H} = \int \frac{\partial \mathcal{H}}{\partial p} dp + \int \frac{\partial \mathcal{H}}{\partial q} dq$$

and is a constant of motion.

The Eq. (I.4.86) can be obtained from the expression of the Hamiltonian replacing the conjugate variables with  $p \rightarrow \Delta E/\omega_{\text{rf}}$  and  $q \rightarrow \phi$ , giving

$$\frac{d\phi}{dt} = \frac{\partial \mathcal{H}}{\partial (\Delta E/\omega_{\text{rf}})} \quad \text{and} \quad \frac{d(\Delta E/\omega_{\text{rf}})}{dt} = -\frac{\partial \mathcal{H}}{\partial \phi}.$$

The Hamiltonian then becomes

$$\mathcal{H} = \int \frac{d\phi}{dt} d(\Delta E/\omega_{\text{rf}}) + \int \frac{d(\Delta E/\omega_{\text{rf}})}{dt} d\phi.$$

By replacing the differential in times by their corresponding Eqs. (I.4.63) and (I.4.66) and integrating allows to recover the result from Eq. (I.4.86). Note that the integration constant is adjusted such that  $\mathcal{H}(\phi = \phi_s, \Delta E = 0) = 0$ .

#### I.4.5.2.2 Properties of the RF bucket

We will now make use of the expression of the trajectories in the longitudinal phase space from Eq. (I.4.86) to detail the characteristics of the RF bucket.

The Hamiltonian gives the trajectory of the particle in phase space, as shown in Fig. I.4.27 for the

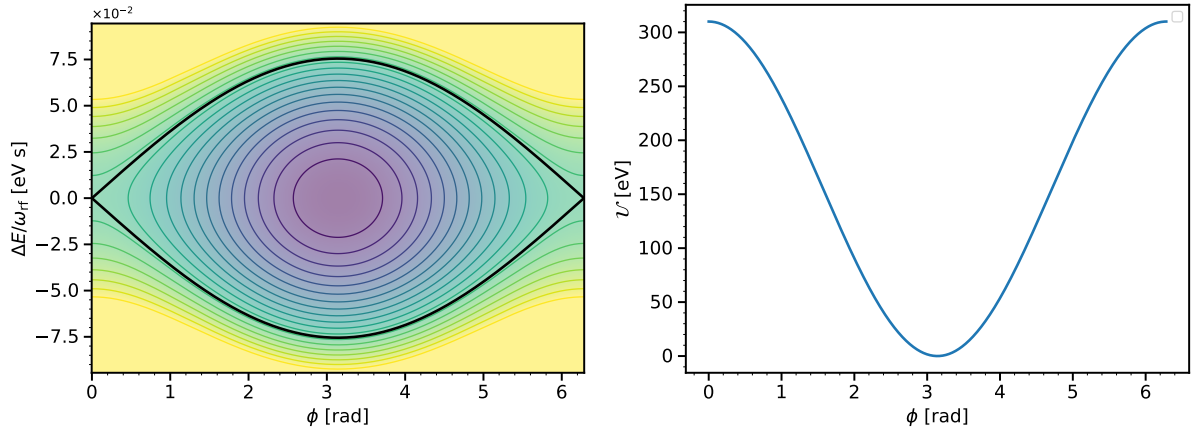


**Fig. I.4.27:** Trajectories in the longitudinal phase space for positively charged particles above transition energy (left) without acceleration ( $\phi_s = \pi$  rad), together with the RF potential well (right). The black line is referred to as the separatrix and delimitates the boundary of the RF bucket outside of which particles do not perform stable periodic oscillations around the synchronous particle. The separatrix corresponds to the limit defined by the maxima of the potential well. The parameters used were the same as for the tracking example in Section I.4.4.2.2.

example of above transition energy and positively charged particles. For small oscillation amplitudes (low  $\Delta\phi$ ), the trajectory of each particle forms an ellipse, as demonstrated in Section I.4.5.1. A particle oscillates in phase space and performs a bounded motion if its energy of synchrotron oscillations  $\mathcal{H}$  is lower than the maximum of the potential well. The center of the bucket (i.e., the minimum of the potential well) represents the stable fixed point of the synchrotron motion, here at  $\phi_s = \pi$  (above transition energy) and  $\Delta E = 0$ . The points  $\phi_s = 0$  and  $\phi_s = 2\pi$  are the unstable fixed points. For particles with too large  $\mathcal{H}$ , corresponding to particles with a too large deviation in energy, the trajectories do not form a closed contour around the synchronous particle. Instead, the particles drift above the limit represented in black in Fig. I.4.27. This limit is called the separatrix.

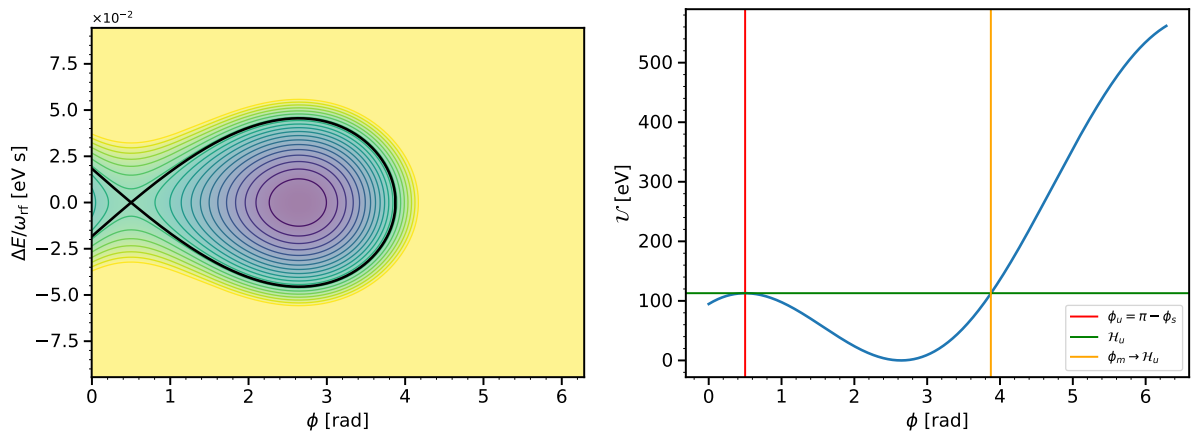


**Fig. I.4.28:** Trajectory in the longitudinal phase space for a positively charged particles above transition energy (left), together with the RF potential well (right). The case with acceleration ( $\phi_s = \pi - 0.5$  rad) is given. The edges of the separatrix are defined by the unstable fixed point (red) and the turnaround point (yellow).

During acceleration with  $\phi_s \neq 0$  (below transition) or  $\phi_s \neq \pi$  (above transition), the trajectories change in shape and amplitude as displayed in Fig. I.4.28. In that case, compared to Fig. I.4.27, the stable fixed point (center of the RF bucket) is shifted to a  $\phi_s < \pi$ . The shape of the potential well changes with  $\phi_s$  and gives an asymmetry to the trajectories depending on the sign of  $\eta$ . The limit of the separatrix is given by the unstable fixed point  $\phi_u = \pi - \phi_s$  (obtained from  $d\mathcal{U}/d\phi = 0$ ) on one side. On the other side, the phase  $\phi_m$  corresponds to the turning point where  $\mathcal{U}_m = \mathcal{U}(\pi - \phi_s) = \mathcal{H}_u(\pi - \phi_s, \Delta E = 0)$ .

#### I.4.5.2.2.1 The separatrix and the RF bucket height

As described before, the maximum contour in which the particles have a bounded motion around the synchronous phase is the separatrix. The separatrix is the limit of the RF bucket, where particles can be captured in a bunch.

The expression for the separatrix is then obtained from the Hamiltonian

$$\mathcal{H} = \frac{\eta\omega_{\text{rf}}^2}{2\beta_s^2 E_s} \left( \frac{\Delta E}{\omega_{\text{rf}}} \right)^2 + \mathcal{U}(\phi)$$

$$\mathcal{H}_u = \mathcal{U}(\pi - \phi_s),$$

giving the following relationship

$$\Delta E_{\text{sep}} = \pm \sqrt{\frac{2\beta_s^2 E_s}{|\eta|}} \sqrt{\mathcal{U}(\pi - \phi_s) - \mathcal{U}(\phi)}, \quad (\text{I.4.87})$$

where  $\Delta E_{\text{sep}}$  is the trajectory on the separatrix itself.

The RF bucket height is obtained from the maximum height of the separatrix at  $\Delta E_{\text{sep}}(\phi_s)$ . The RF bucket height in energy is (NB: this is the half size from 0 to  $\Delta E_{\text{sep,m}}$ , and should be  $\times 2$  for the full bucket height)

$$\Delta E_{\text{sep,m}} = \sqrt{\frac{2qV_{\text{rf}}\beta_s^2 E_s}{\pi h |\eta|}} Y(\phi_s), \quad (\text{I.4.88})$$

where

$$Y(\phi_s) = \left| -\cos \phi_s + \frac{(\pi - 2\phi_s)}{2} \sin \phi_s \right|^{1/2} \quad (\text{I.4.89})$$

is the reduction of the bucket height during acceleration  $Y \leq 1$ . The  $Y$  function as a function of the synchronous phase  $\phi_s$  is shown in Fig. I.4.29.

#### Derivation I.4.27

Demonstrate the expression of  $Y(\phi_s)$  from Eq. (I.4.89). Note that the absolute value of the function is taken as simplification with respect to the sign of  $\eta$ .

#### I.4.5.2.2.2 The acceptance or RF bucket area

The RF bucket area (or acceptance) corresponds to the surface enclosed within the separatrix, analogous to the longitudinal emittance. Note that the longitudinal emittance is constant given that modifications to the accelerator parameters and acceleration are done adiabatically. Therefore, the acceptance which is a

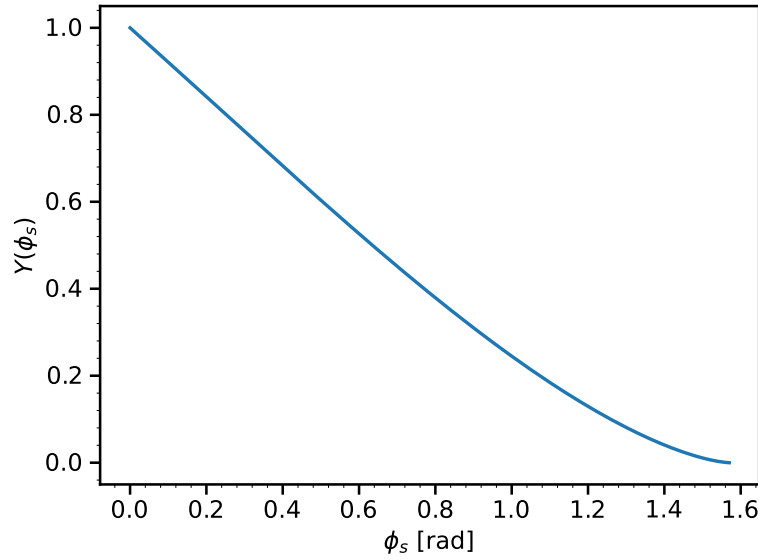


**Fig. I.4.29:** The reduction factor of the RF bucket height  $Y(\phi_s)$ . A too rapid acceleration (for all other parameters remaining constant) leads to a reduction of the maximum acceptable energy deviation  $\Delta E$  for an arbitrary particle.

property resulting from the accelerator parameters corresponds to the maximum emittance possible for a particle to be captured within the RF bucket. The accelerator parameters, in particular the RF voltage and harmonic, must be adapted to ensure that the acceptance always remains larger than the particle with the largest emittance to avoid particle losses.

The bucket area is obtained by integrating within the separatrix contour from Eq. (I.4.87)

$$A_{\text{bk}} = 2\sqrt{\frac{2\beta_s^2 E_s}{|\eta|\omega_{\text{rf}}^2}} \int_{\phi_u}^{\phi_m} \sqrt{\mathcal{U}(\pi - \phi_s) - \mathcal{U}(\phi)} d\phi.$$

The bucket area can be reformulated as

$$A_{\text{bk}} = \frac{8}{\omega_{\text{rf}}} \sqrt{\frac{2qV_{\text{rf}}\beta_s^2 E_s}{\pi h |\eta|}} \Gamma(\phi_s) \quad (\text{I.4.90})$$

with

$$\Gamma(\phi_s) = \frac{1}{4\sqrt{2}} \int_{\phi_u}^{\phi_m} \sqrt{-\cos \phi_s - \cos \phi + (\pi - \phi - \phi_s) \sin \phi_s} d\phi. \quad (\text{I.4.91})$$

The function  $\Gamma(\phi_s)$  is the reduction of the bucket area during acceleration,  $\Gamma \leq 1$  and can be approximated to give the following formula [16]

$$A_{\text{bk}} \approx \frac{8}{\omega_{\text{rf}}} \sqrt{\frac{2qV_{\text{rf}}\beta_s^2 E_s}{\pi h |\eta|}} \frac{1 - \sin \phi_s}{1 + \sin \phi_s}. \quad (\text{I.4.92})$$

The function  $\Gamma(\phi_s)$  is represented in Fig. I.4.30 both for the exact formulation from Eq. (I.4.91) and the approximate one from the last term of Eq. (I.4.92). For the stationary RF bucket, we get the exact

relationship  $\mathcal{A}_{\text{bk}} = 8\Delta E_{\text{sep,m}}/\omega_{\text{rf}}$ .

The modification of the RF potential well, the shape of the bucket area, the trajectories of the particles as well as the reduction of the bucket area and height are illustrated above and below transition in Figs. I.4.31 and I.4.32.

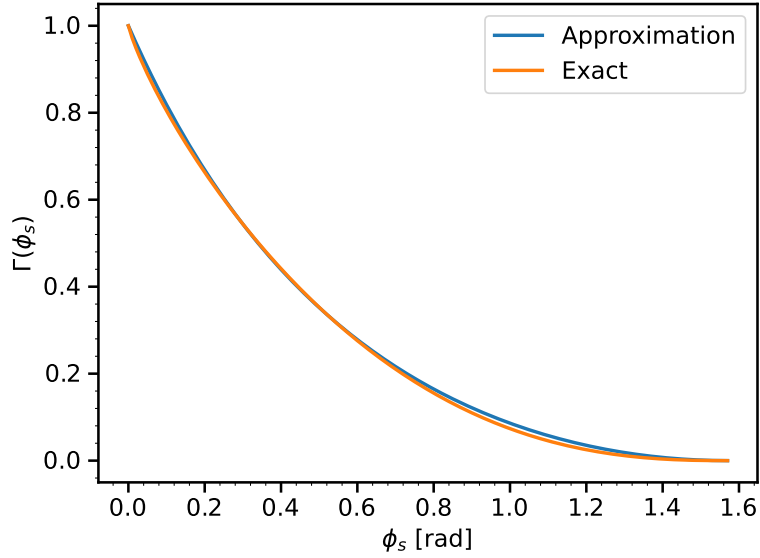


**Fig. I.4.30:** The reduction factor of the RF bucket area  $\Gamma(\phi_s)$ . Together with the reduction of the RF bucket height shown in Fig. I.4.29, a too rapid acceleration (for all other parameters remaining constant) leads to a reduction of the maximum acceptable longitudinal emittance and can lead to particle loss. The exact formulation (orange) corresponds to Eq. (I.4.91) and the approximate one is the last term of Eq. (I.4.92)

#### Derivation I.4.28

Demonstrate the expression of  $\Gamma(\phi_s)$  from Eq. (I.4.91).

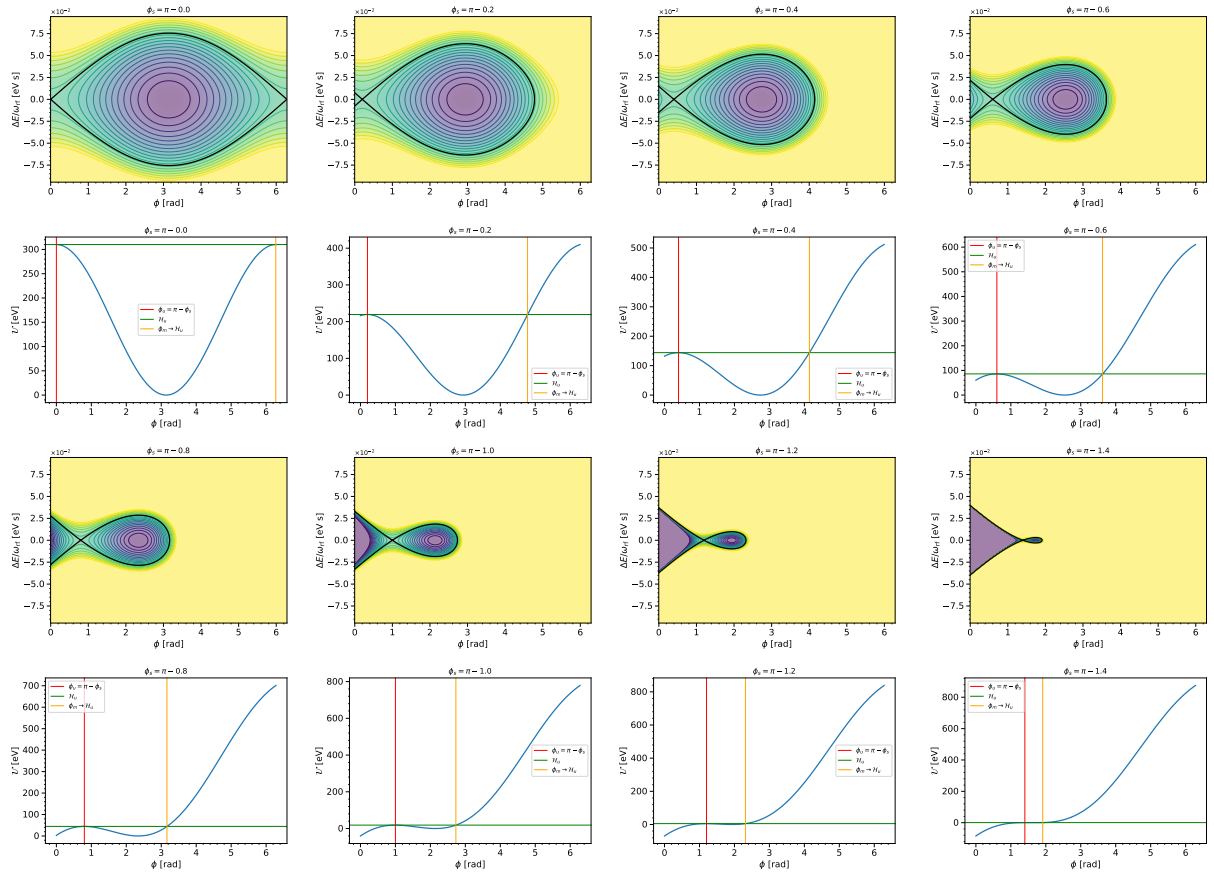


**Fig. I.4.31:** The RF bucket (first and third row) and corresponding RF potential wells (second and fourth row) for varying  $\phi_s$ , above transition energy (see Fig. I.4.28 for further description). The trajectories of the particles in longitudinal phase space are changed according to Eq. (I.4.86), while the amplitude and size of the RF bucket are changed according to Eqs. (I.4.89) and (I.4.90). The acceleration should remain moderate to ensure that the bucket area is not smaller than the longitudinal emittance of the bunch.

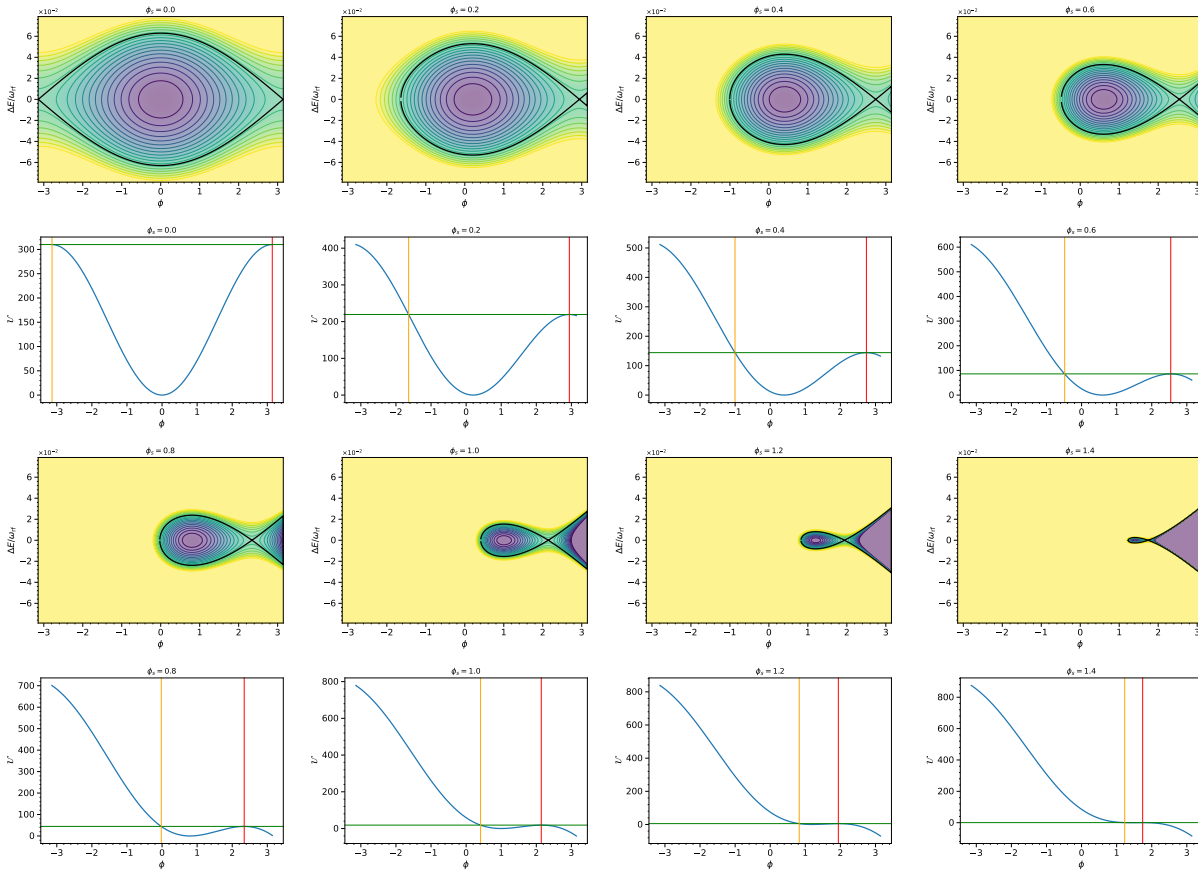


**Fig. I.4.32:** The RF bucket (first and third row) and corresponding RF potential wells (second and fourth row) for varying  $\phi_s$ , below transition energy (see Fig. I.4.28 for further description). The trajectories of the particles in longitudinal phase space are changed according to Eq. (I.4.86), while the amplitude and size of the RF bucket is changed according to Eqs. (I.4.89) and (I.4.90). The acceleration should remain moderate to ensure that the bucket area is not smaller than the longitudinal emittance of the bunch.

#### I.4.5.2.2.3 The longitudinal emittance

As described in Section I.4.5.1, the longitudinal emittance corresponds to the area enclosed by the trajectory of a particle in the longitudinal phase space. The longitudinal emittance can be calculated by accounting for the non-linearities of the RF bucket:

$$\varepsilon_l = 2\sqrt{\frac{2\beta_s^2 E_s}{|\eta| \omega_{\text{rf}}^2}} \int_{\phi_{b,l}}^{\phi_{b,r}} \sqrt{\mathcal{U}(\phi_{b,l,r}) - \mathcal{U}(\phi)} d\phi, \quad (\text{I.4.93})$$

where the indices  $b, l$  and  $b, r$  stand for the left and right edge of the bunch in phase (amplitude  $\phi_b$  and full length  $2\phi_b$ ). This longitudinal emittance, more exact than Eq. (I.4.82), is usually computed numerically.

For an ensemble of particles composing a bunch, as represented in Fig. I.4.33, the longitudinal emittance of the distribution can be computed either from the statistical distribution (e.g. standard deviation), or by taking the amplitude of the most outer particle as an evaluation of the maximal longitudinal emittance for the whole bunch. The maximum amplitude is usually obtained from the measured bunch profile in the longitudinal direction (see Section I.4.6 for details).

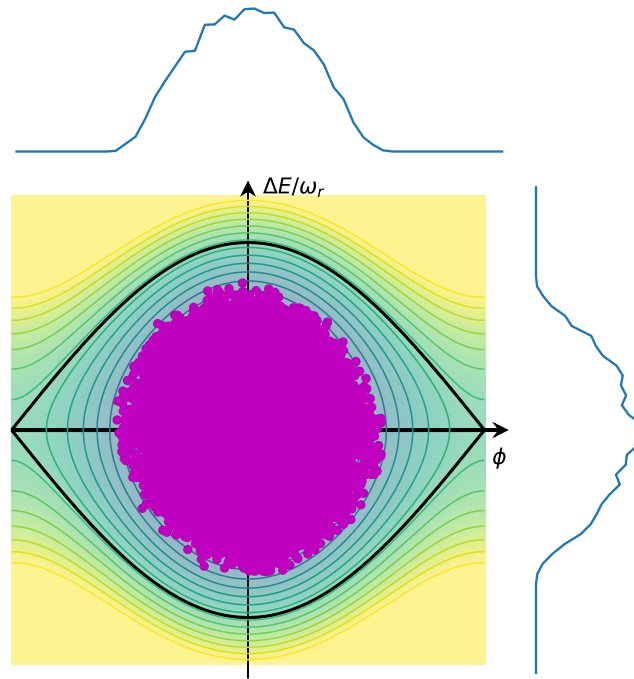


**Fig. I.4.33:** A distribution of particles in longitudinal phase space forming a bunch. Each particle oscillates in phase space following its trajectory of constant  $\mathcal{H}$ . The surface occupied by the bunch distribution is the longitudinal emittance  $\varepsilon_l$ . The profile to the top is the longitudinal particle density in the longitudinal direction ( $z$  or  $\phi$ ), while the curve to the right is the particle density in energy (animated in [2]).

To ensure that all the particles of the bunch are accelerated successfully, the bucket area should be sufficient to accommodate the longitudinal emittance. The RF bucket filling factor is commonly defined as a ratio of emittance over bucket area:  $\varepsilon_l/\mathcal{A}_{\text{bk}}$  or in as a ratio of the maximum energy deviation over the

separatrix amplitude:  $\Delta E_{b,m}/\Delta E_{sep,m}$ . Therefore, the RF voltage should be sufficient to have a large enough bucket area and the acceleration should be done slowly enough so that the bucket area reduction from Section I.4.5.2.2.2 is not too large.

#### I.4.5.2.2.4 The non-linear synchrotron frequency and bunch matching

Together with the modification of the trajectories in phase space due to the non-linearity, the synchrotron frequency is also changed at larger amplitudes in the RF bucket. The non-linear synchrotron period is the time taken by a particle to perform a full synchrotron revolution along its trajectory at constant  $\mathcal{H}$ :

$$T_s = \int_{\phi_{b,l}}^{\phi_{b,r}} \frac{d\phi}{\dot{\phi}}. \quad (\text{I.4.94})$$

It can be demonstrated that the integration leads to the relationship of the synchrotron frequency distribution

$$\frac{\omega_s}{\omega_{s0}} = \frac{\pi}{2K\left(\sin\frac{\phi_b}{2}\right)} \approx 1 - \frac{\phi_b^2}{16}, \quad (\text{I.4.95})$$

where  $\omega_s = 2\pi/T_s$  is the non-linear synchrotron (angular) frequency and is represented in Fig. I.4.34. The function  $K$  is the elliptic function of the first kind. The maximum amplitude in phase for a given particle is denoted by  $\phi_b$ .

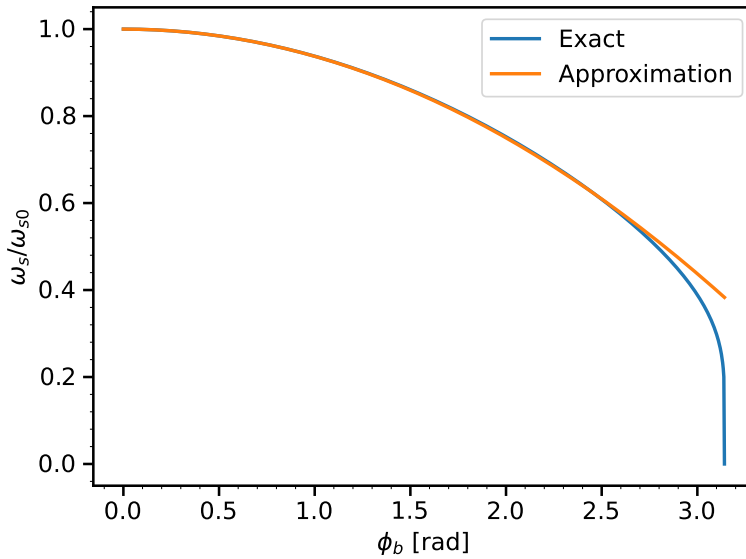


**Fig. I.4.34:** The non-linear synchrotron frequency distribution as a function of the maximum amplitude in phase of the particle, as obtained from Eq. (I.4.95).

As the particles at larger amplitude in the RF bucket take more time to perform a full synchrotron oscillation, the particles composing the bunch decohere with time until the particles occupy statistically the full area inside the trajectory of the particle with the largest longitudinal emittance. This is commonly called “filamentation” and is explained in Figs. I.4.35 and I.4.36. The bunch is considered matched if the density along an iso-Hamiltonian (constant Hamiltonian representing the particle trajectories) line is

constant. This can be expressed as

$$F(\phi, \Delta E/\omega_{\text{rf}}) = F(\mathcal{H}), \quad (\text{I.4.96})$$

where  $F$  is the bunch density in longitudinal phase space and only depends on  $\mathcal{H}$  and not on the angular position in phase space  $\psi$ .

The filamentation can typically happen at injection into a synchrotron, when the incoming bunch distribution is not well adjusted to the injection RF bucket. It can also happen in the case of non-adiabatic changes of the accelerator parameters, as discussed in Section I.4.5.1. In that case, during filamentation, the statistical emittance increases with respect to the starting bunch conditions. This is usually a degradation of the beam quality as the statistical emittance cannot be reduced later on (except in presence of synchrotron radiation, mostly for lepton synchrotrons) and can lead to particle loss if the filling factor cannot be maintained below one. Therefore, an important effort into the design of RF programs for hadron synchrotrons consists in ensuring a good matching of a bunch to its RF bucket.

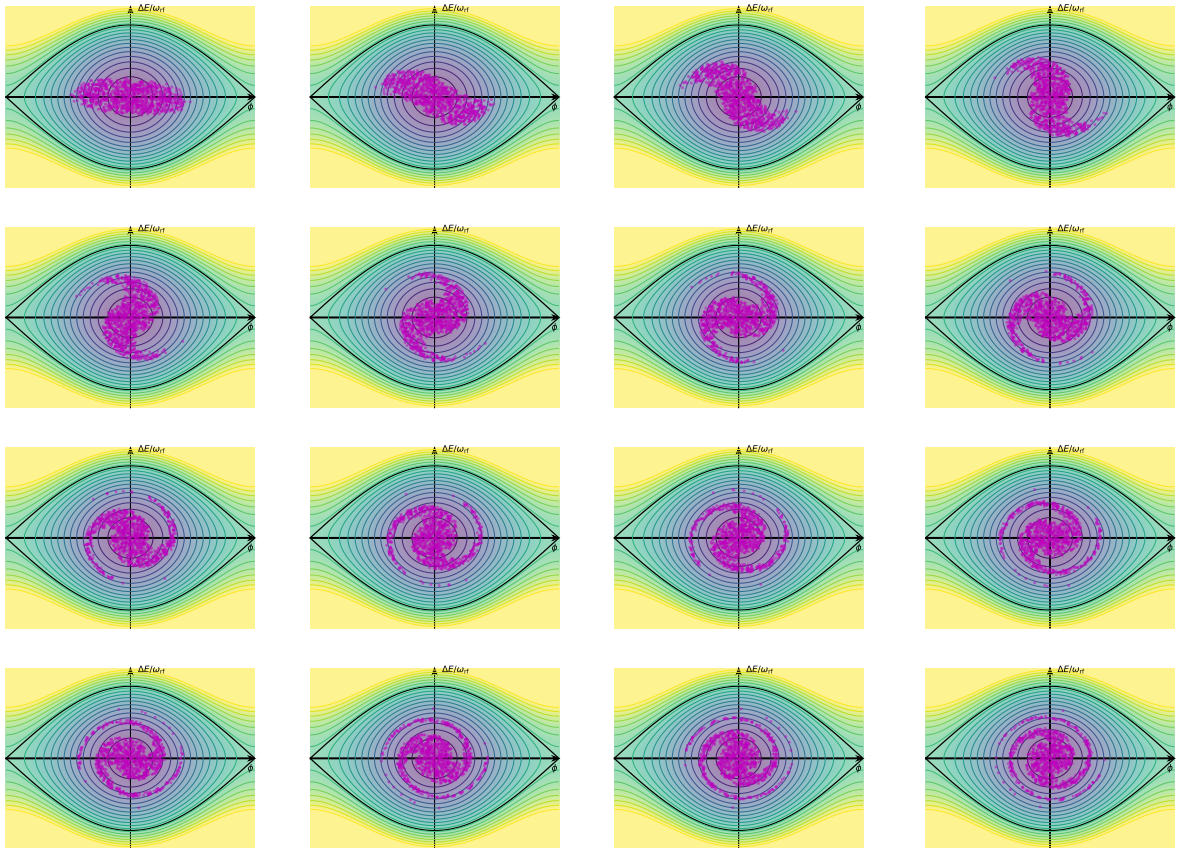


**Fig. I.4.35:** Evolution of the particle distribution (in purple) during the first few synchrotron periods (from left to right, then from one row to the next). The bunch starts with a mismatch (too high RF bucket compared to the energy spread of the bunch). The bunch experiences coherent synchrotron oscillations and filaments due to the non-linear synchrotron frequency (animated in [2]).

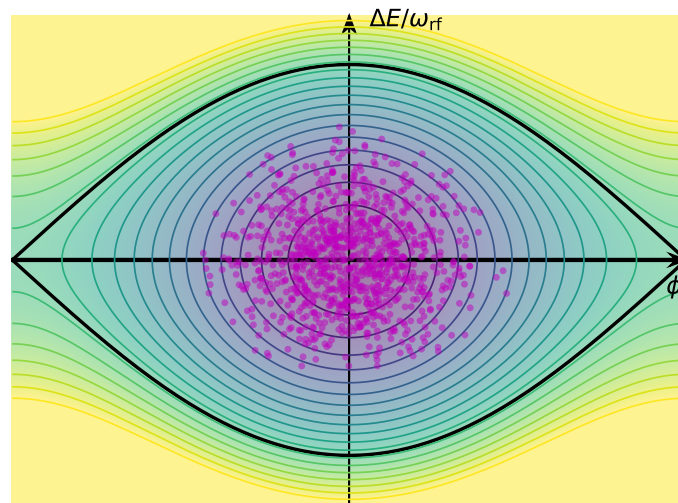


**Fig. I.4.36:** After many synchrotron periods, the bunch is completely filamented and the statistical emittance is increased with respect to the initial condition from Fig. I.4.35 (top left).

#### Exercise I.4.29

Following the parameter computation from Exercise I.4.26:

- Compute the RF bucket area (or acceptance) using the SPS parameters from Exercises I.4.18 and I.4.26.
- Compute the bucket height.
- Compute the filling factor for a 3 ns bunch at 14 GeV/c (use the linear approximation for the emittance calculation).
- The bunch length oscillations at injection indicate that the energy spread is too small by 10%. How much should the RF voltage be reduced to improve the matching?

## I.4.6 Applications

In this final section, we will set general applications of longitudinal beam dynamics. First, basic principles of longitudinal beam observation will be given, followed by examples of routine operation of RF systems in a synchrotron (injection oscillations). Then, more advanced concepts beyond the scope of the present course will be introduced, including RF manipulations and beam instabilities.

### I.4.6.1 Longitudinal beam observation

The longitudinal bunch profile can be measured using a wall current monitor (WCM), which converts the instantaneous beam current into a measurable voltage. The WCM measures the image current of the beam on the vacuum chamber. To do so, a small ceramic gap acting as a capacitor is opened and bridged with resistors. Inductors are installed to reduce the lower cutoff frequency. With this design, the device

provides a direct measurement of beam line density with a bandwidth covering from the kHz to the GHz range. More details on beam instrumentation are provided in Chapter II.9. An example of a WCM is displayed in the left-hand side of Fig. I.4.37.

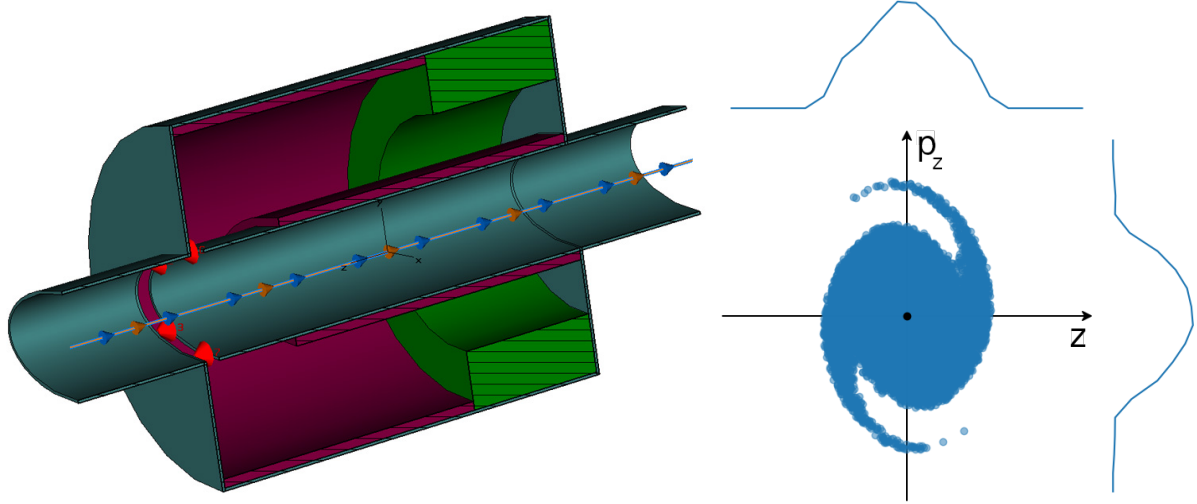


**Fig. I.4.37:** Inside view of a Wall Current Monitor to measure longitudinal profiles [17] (left). The beam path within the WCM is shown with the straight line and blue/orange arrows in the center of the device. The gap of the WCM is shown to the left of the equipment (red conical arrows) with the inductors made out of ferrite in green. The WCM provides measurements of the longitudinal line density (upper line in the right plot), corresponding to the projection in the longitudinal coordinate of the particle density in phase space (right plot).

The WCM is connected to a digitizer or an oscilloscope and triggered before the bunch passage to acquire the beam profile. The measured line density  $\lambda$  corresponds directly to the projection of the particle density in the longitudinal phase space along the energy axis (see the right-hand side of Fig. I.4.37), with the expression

$$\lambda(\phi) = \int_{-\infty}^{\infty} F(\phi, \Delta E/\omega_{\text{rf}}) d(\Delta E/\omega_{\text{rf}}). \quad (\text{I.4.97})$$

Therefore, combining the measured bunch profiles to the concepts of synchrotron motion exposed in the previous sections, the beam characteristics can be obtained and the parameters of the RF bucket adjusted to preserve the beam quality (e.g. avoiding unwanted mismatch and filamentation).

To measure and analyze the evolution of the particle bunches, a clock synchronized to the RF frequency provides the base for the triggers. Turn by turn, the bunch profile is measured to observe its evolution and, indirectly, the motion of the particles in the longitudinal phase space. An example acquisition is shown in Fig. I.4.38. In this example measured in the PS at CERN, the acquisition is started 170 ms after the beginning of the cycle, corresponding to the moment of beam injection. Each trace is an acquisition of 2000 ns duration, equivalent to one revolution period in that specific example (all bunches are hence measured). Acquisitions are triggered every six accelerator turns with a total of 300 traces acquired for this dataset. The total time span of the acquisition is about 4 ms, which was adjusted here to measure the first synchrotron periods as obtained from Eq. (I.4.75).

The example from Fig. I.4.38 illustrates the analysis of injection oscillations. Note that the first trace is a flat line with no signal, corresponding to the instant right before injection. Then, after beam

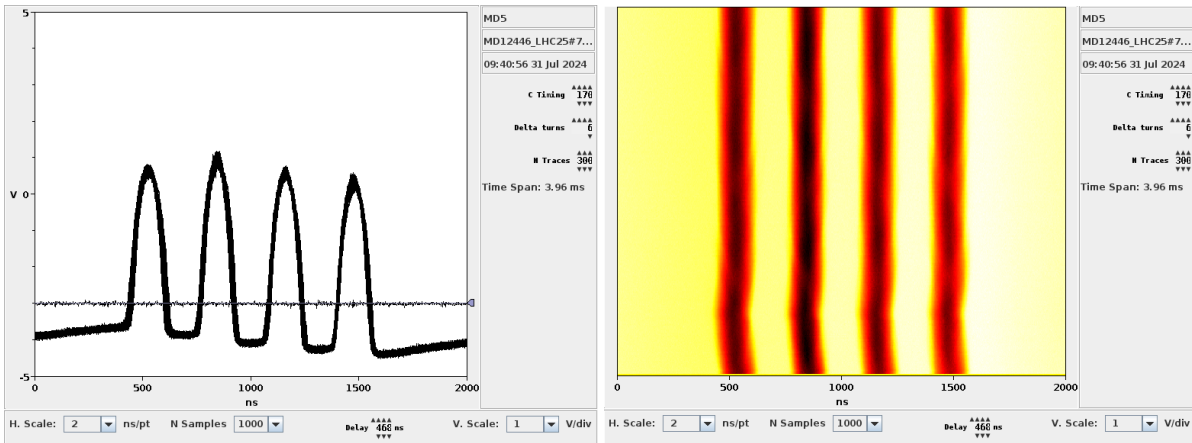


**Fig. I.4.38:** Example acquisition of longitudinal profiles with the Tomoscope application in the CERN PS. Both images represent the same data, once in oscilloscope view (left, each trace overlaid) and once as waterfall plot (right, each trace stacked vertically from bottom to top).

injection, the bunches appear to remain stationary. This is because bunches were injected well matched to the RF buckets.

### I.4.6.2 Injection oscillations

#### *Phase (dipole) oscillations*

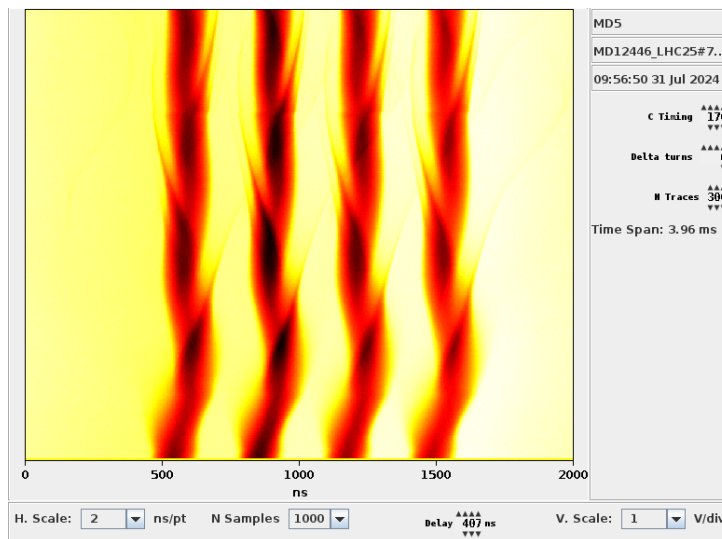


**Fig. I.4.39:** Bunch phase oscillations at injection. The bunches were not injected in the center of the RF bucket and particles perform coherent phase oscillations.

To achieve the good conditions shown previously, RF parameters must be regularly optimized during normal operation of a synchrotron, to ensure the best beam quality day to day. In this section, we will focus on the adjustment of injection oscillations to minimize the injection mismatch and resulting in filamentation. Figure I.4.39 displays an example where the bunches are not matched to the RF bucket. In that case, the bunches were injected into the RF bucket at the wrong RF phase and start to perform coherent oscillations.

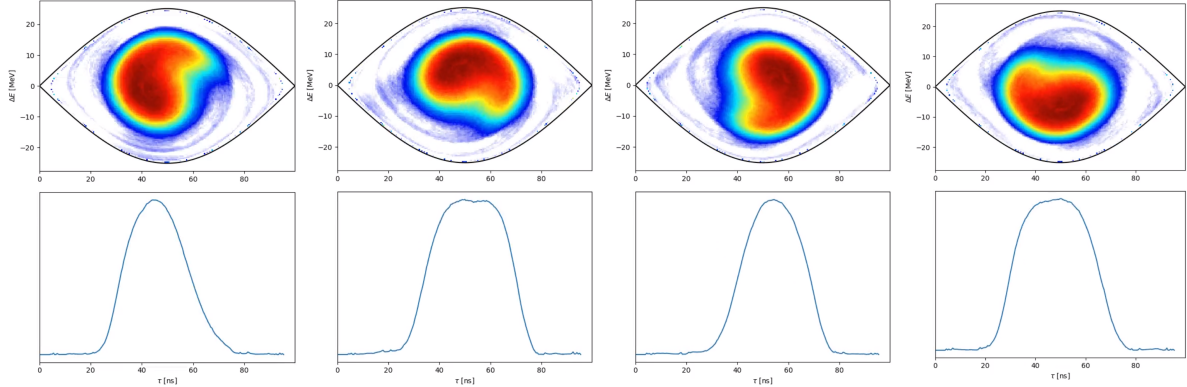


**Fig. I.4.40:** Bunch phase oscillations during one synchrotron period (from left to right), following an injection with an offset in phase with respect to the center of the RF bucket (or an offset with the expected beam energy). The center of mass of  $F$  (top plots, color represents particle density with white as low and red as high) rotates in phase space, causing the corresponding bunch profile  $\lambda$  (bottom plots) to arrive alternatively early and late (animated in [2]).

The motion of the bunches can be described as oscillations in time (or phase), where the bunches arrive alternatively early or late with respect to the expected revolution period (corresponding to left-right oscillations in Fig. I.4.39). In this scenario, the expected synchrotron frequency (obtained from Eq. (I.4.75)) in the PS is  $f_{s_0} = 580$  Hz, equal to a period of  $T_{s_0} = 1.72$  ms. In Fig. I.4.39, the bunches perform about two full synchrotron periods in a time span of 4 ms, close to the analytical calculation. One can nonetheless notice that the measured synchrotron period is closer to  $T_s \approx 2.0$  ms, which is larger than the analytical value. It is reminded that due to the non-linear nature of the synchrotron frequency (see Eq. (I.4.95)), the synchrotron frequency is reduced (and the synchrotron period increased) for particles at the larger amplitudes in the longitudinal phase space. It is therefore expected that the measured synchrotron period is larger than the linear evaluation, which is consistent with the measurement.

In longitudinal phase space, the oscillations of the particles and the bunch can be explained by Fig. I.4.40. Its images show the phase space density  $F$  together with the corresponding measured line density  $\lambda$  at four instants during the bunch oscillation: bunch is early in time (1), in time with a positive offset in energy (2), late in time (3) and in time with a negative offset in energy (4). The phase space density was reconstructed based on measured bunch profiles using a tomography method, which allows based on many measurements of  $\lambda$  to reconstruct numerically the only possible solution for  $F$ , reverting the integral in Eq. (I.4.97). More details of the longitudinal tomography algorithm can be found in Ref. [18].

All particles perform synchrotron oscillations coherently in the longitudinal phase space (at their synchrotron frequency), and the center of mass of the ensemble of particles  $F$  is alternatively late/early in time, and too high/low in energy. The center of mass oscillates at  $f_{s,m=1} = 1 \times f_s$  where  $m$  denotes a coherent mode of oscillation. The mode  $m = 1$  is usually referred to as “dipole” oscillations. Eventually, due to the non-linearity of the RF bucket, the bunch will filament, resulting in an increase in longitudinal emittance. In this case, the operational adjustment would either be to anticipate/delay the injection of the bunch, or to adjust the phase of the RF bucket to ensure that the bunch is injected in the center of the RF bucket. Note that the same oscillations would occur if the bunch was injected with an offset in energy.

**Bunch length (quadrupole) oscillations**

Another kind of incorrect adjustment of the RF settings at injection is represented in Fig. I.4.41. In that case, the bunches appear to be at the correct RF phase (no left-right oscillations in the measured time frame) but the bunch is alternatively large/short instead.

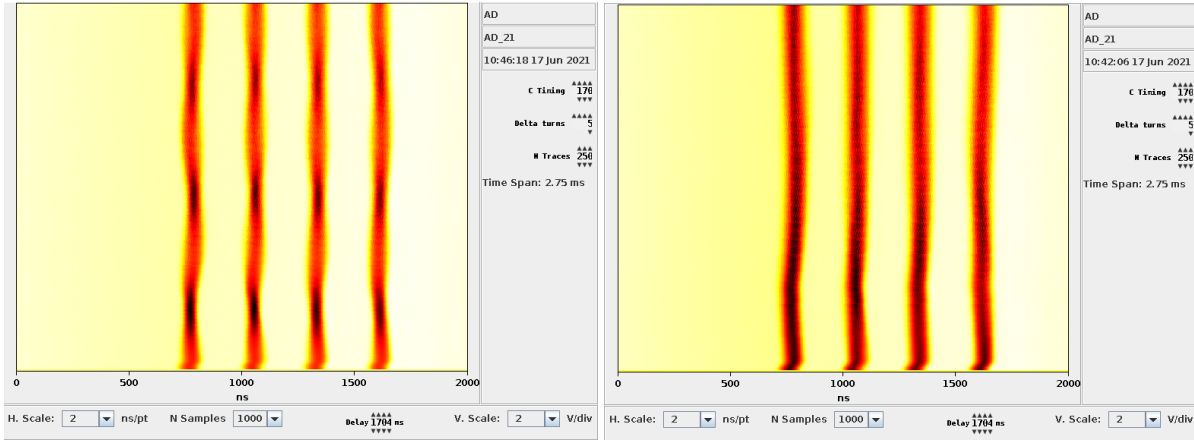


**Fig. I.4.41:** Bunch length oscillations at injection, following a too high RF voltage at injection (left). The distribution is mismatched with respect to the contour lines of the RF bucket and the bunch performs oscillations in bunch length. The oscillations can be mitigated by adjusting the RF voltage at injection (right, reduced RF voltage).

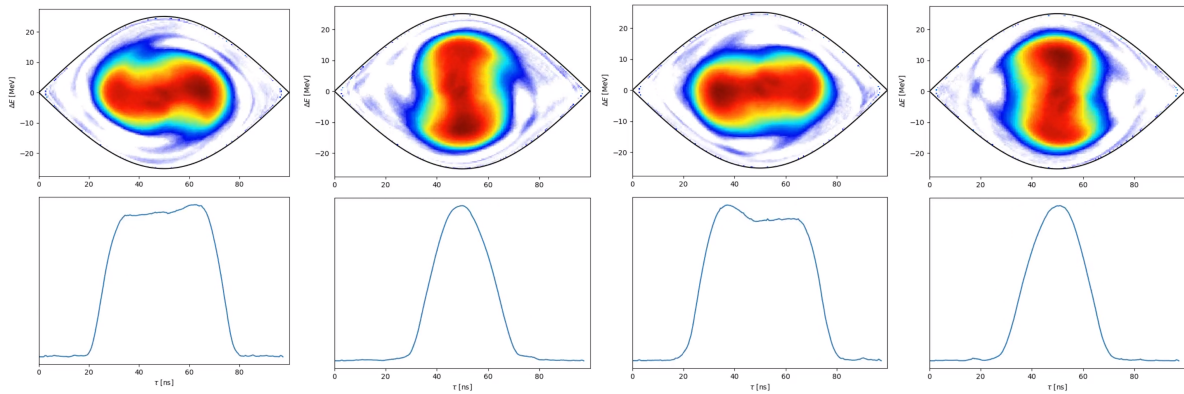


**Fig. I.4.42:** Bunch length oscillations during one synchrotron period (from left to right), following an injection with a mismatched (too large) RF voltage. Two “nodes” in density rotate around the center of mass of  $F$  (top plots, color represents particle density with red as high), leading to the corresponding bunch profile  $\lambda$  (bottom plots) to be alternatively short and large (animated in [2]).

In that example, the synchrotron frequency in the PS was  $f_{s_0} = 664$  Hz, and the period  $T_{s_0} = 1.51$  ms. In the measured time frame of 2.75 ms, the bunch performs slightly more than three periods of bunch length oscillations. Therefore, the bunch length oscillates at about twice the synchrotron frequency (including the non-linearity of the RF bucket). Like for the phase oscillations, these bunch oscillations in phase space can be analyzed using a tomographic reconstruction as shown in Fig. I.4.42. In this representation, the bunch is alternatively large with small momentum spread (1), then short with large momentum spread (2) and performs two bunch length oscillation periods in one synchrotron period (3 and 4). The distribution  $F$  can also be described as two “nodes” with higher density oscillating around

the center of the RF bucket (and bunch center of mass). Both nodes oscillate at the synchrotron frequency, but cannot be distinguished in the measured  $\lambda$  after the projection, leading to a resulting bunch length oscillation frequency of  $f_{s,m=2} = 2 \times f_s$ . The  $m = 2$  is usually referred to as the “quadrupole” mode of oscillations. One then remarks that any coherent bunch oscillations can then be described as a decomposition of modes  $m$  based on the synchrotron frequency  $f_s$ .

As for the phase oscillations, the settings of the RF system must be adjusted to avoid increasing the longitudinal emittance. In that case, the operational adjustment would be to adjust the amplitude of the RF voltage in order to match the shape of the RF bucket and the Hamiltonian contour lines closer to the density  $F$ , thereby better fulfilling the conditions of Eq. (I.4.96). Note that this configuration is identical to the one shown to illustrate the principle of filamentation in Fig. I.4.35.

### I.4.6.3 Advanced topics

At this stage, by following assiduously all steps of derivations and exercises, the student is expected to understand the main concepts behind longitudinal dynamics. Notably, the student understands how particles are accelerated in a synchrotron, how to compute the base parameters of an accelerating RF system, and applied knowledge on synchrotron motion and the RF bucket. Moreover, the analysis of the synchrotron motion in phase space, paired with longitudinal beam measurements, should allow the student to get a good representation of the coherent motion of a particle distribution. This can be analyzed and compared with tracking simulations, allowing to get a clear representation of the motion of any particle in the longitudinal phase space. From this basis, more advanced topics can be tackled.

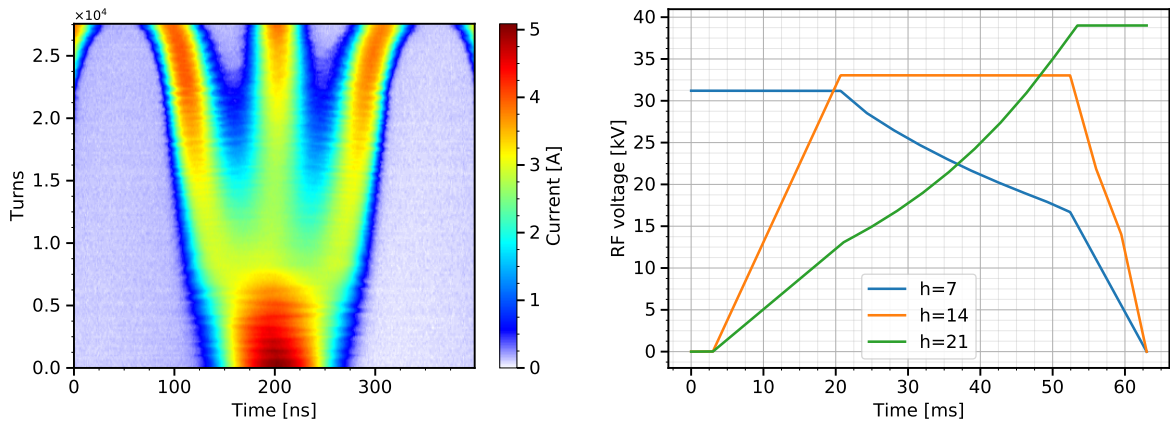


**Fig. I.4.43:** Waterfall plot of the bunch profile during triple splitting of a bunch in the longitudinal direction (left) together with the applied RF voltage program (right).

In the context of this lecture, the focus was put on synchrotrons with a single RF system designed for acceleration. However, as long as they can be physically accommodated in a straight section of the accelerator, any number of RF systems at different RF harmonics can be used. The contributions of the additional RF systems can be linearly added to the equation of motion (I.4.63) (note that the shape of the RF waveform can also be arbitrary and not just a sine wave!), which then results in a modification of the shape of the RF potential well and bucket in Eq. (I.4.86). Many RF manipulations are hence possible to shape the longitudinal distribution. In Fig. I.4.43, a simulated example is proposed where three RF

systems with RF harmonics  $h = 7$ ,  $h = 14$  and  $h = 21$  are used to split a bunch in three. The shape of the RF bucket together with the particles in the longitudinal phase space and the potential well during the manipulation are given in Fig. I.4.44. The beam is stretched longitudinally by the concomitant action

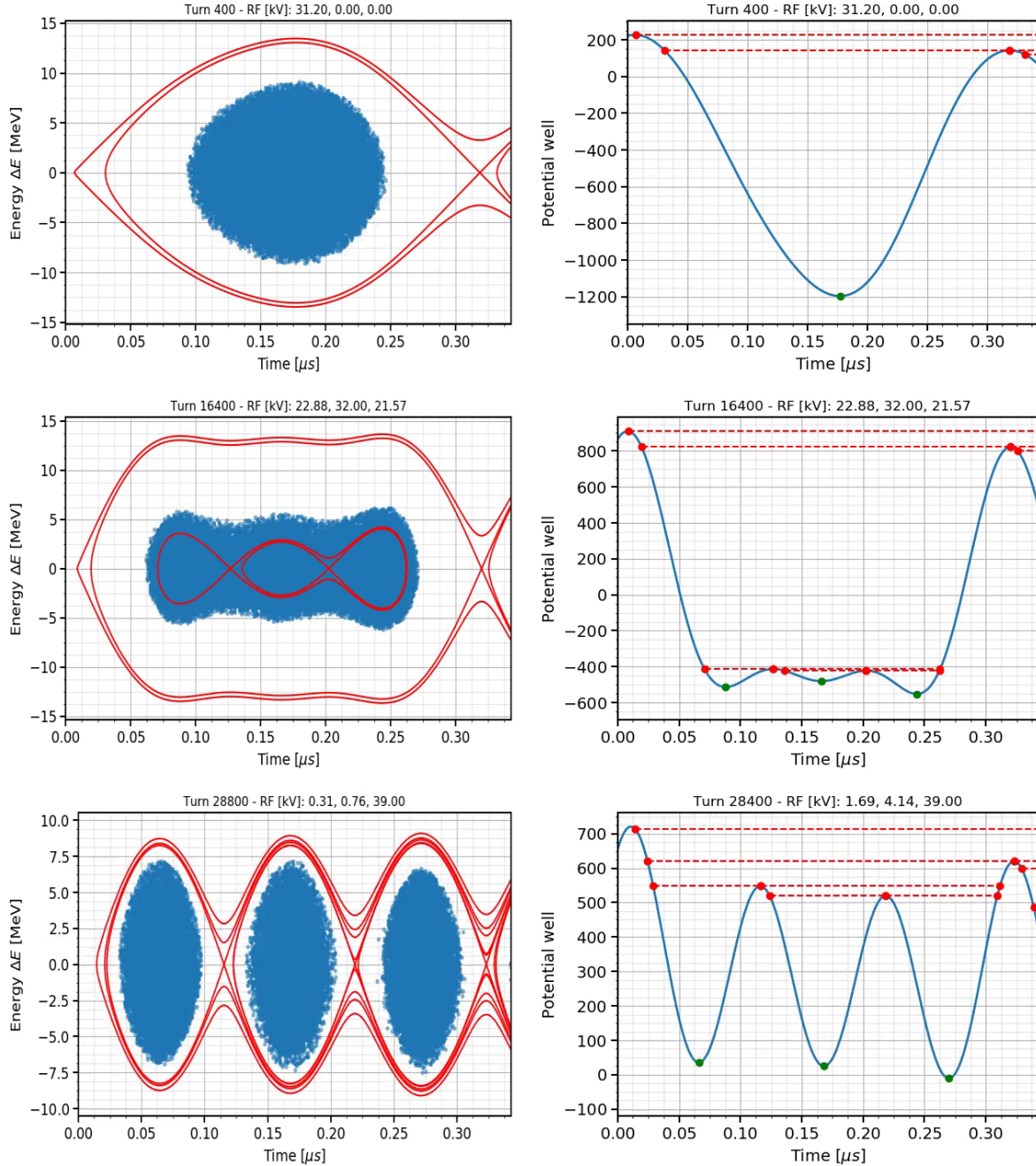


**Fig. I.4.44:** Longitudinal phase space distribution and RF buckets (left) and the corresponding RF potential well (right) during the triple splitting process (from top to bottom), including collective effects. The separatrix corresponding to the maxima of the potential well is shown in red (dashed lines are the projections of the unstable fixed points in the potential well), the minima of the potential well in green, while the particles are shown in blue (animated in [2]).

of the three RF systems yielding a flat RF potential and therefore RF bucket. Note that the relative phase of the RF systems must be carefully adjusted to ensure the symmetry of the potential well. The bunch is

finally cut in three by keeping only the contribution at  $h = 21$ . In this simulation, collective effects due to the action of the cavities was included leading to a distortion of the potential well and separatrices. The range of applications of multiple RF harmonics is very large, including splittings, bunch compression, phase displacement, etc. A dedicated course is available in [19].

Another important aspect are collective effects and beam instabilities. Just like the additional RF systems, the contribution from self-induced electric fields can be added linearly to the equation of motion (I.4.63) and lead to a distortion of the potential well. Depending on the characteristics of the beam and of the equipment in the accelerator leading to wakefields (beam coupling impedance), the perturbation can even lead to beam instabilities above a certain threshold in intensity. Many types of instabilities exist in synchrotrons, with single or multiple bunches, and even debunched beams. An example of instability where bunch oscillations are coupled is provided in Fig. I.4.45. In that example, bunches start to perform coherent oscillations leading to an increase in the longitudinal emittance. The bunches are coupled to each other due to the wakefields which are not decaying from one bunch to the next. The phase advance between each bunch can be seen from the dashed diagonal line in Fig. I.4.45.

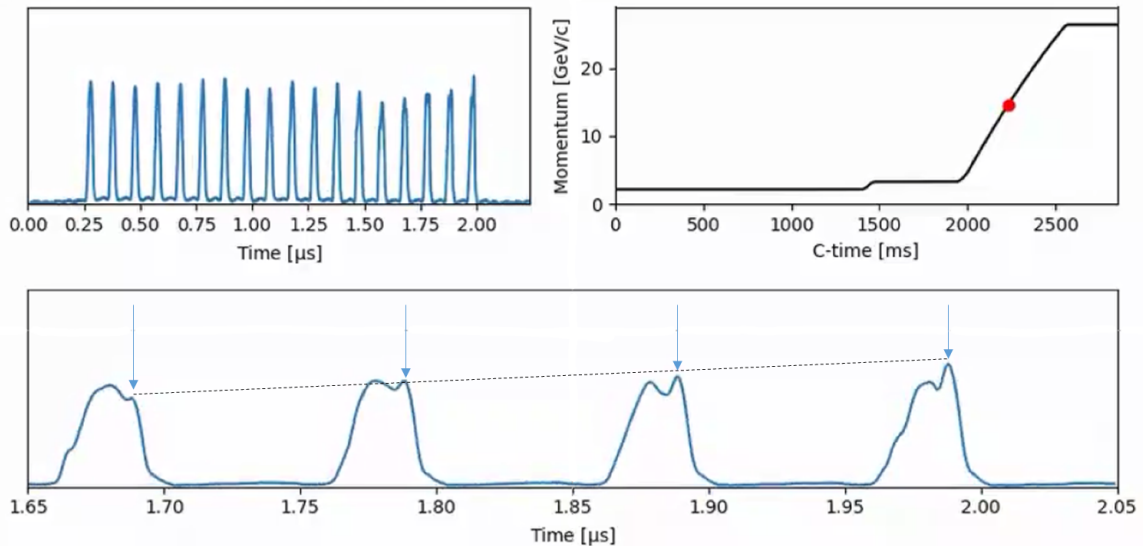


**Fig. I.4.45:** Measured beam line density (left) during the acceleration ramp (top right, red is the energy at the present acquisition). All bunches are represented on the top left while a zoom on the last four bunches is given on the bottom (animated in [2]).

Different types of coupled-bunch instabilities can be observed in more details as a function of time in Fig. I.4.46. The coherent oscillations can again be described based on the mode decomposition  $m$  with the synchrotron frequency as basis. However, unlike the mismatches at injection from the previous section, these oscillations are not triggered by wrong adjustments of the RF settings but by self-fields leading to instability. The perturbation enters in resonance with the beam-induced voltage generated by the perturbation from all bunches and grows exponentially. On the left side of Fig. I.4.46, the perturbation leading to instability manifests in the form of coherent dipole oscillations ( $m = 1$ ), while it performs quadrupole oscillations ( $m = 2$ ) on the right side of Fig. I.4.46. Note that the motion in the longitudinal phase space is the same as presented earlier in Figures I.4.42 and I.4.42. Each case can be driven by different sources of wakefields in the accelerator. In the more extreme cases, the instability can lead

to beam loss, in addition to beam quality degradation. This can again be studied through analytical developments derived from the synchrotron motion or advanced tracking simulations, and is essential for the design, analysis and study of limitations to improve the performance of an accelerator.

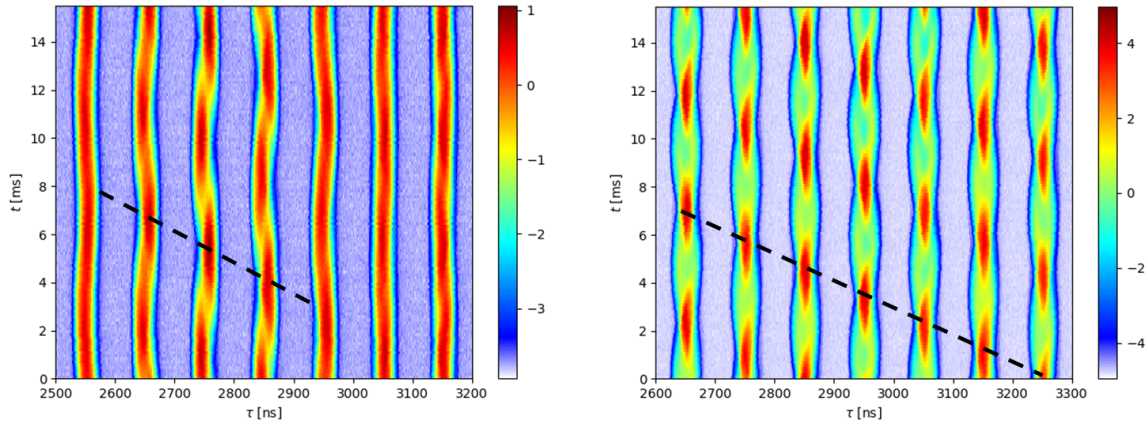


**Fig. I.4.46:** Coupled bunch instabilities of mode  $m = 1$  (left) and  $m = 2$  (right). The dashed black line represents the phase advance from one bunch to the next to highlight the coupled nature of the instability.

## I.4.7 Summary

### I.4.7.1 List of symbols

#### I.4.7.1.1 Constants

$c$ Speed of light	$\mu_0$ Vacuum permeability
$\epsilon_0$ Vacuum permittivity	$e$ Elementary charge

#### I.4.7.1.2 Coordinate system

$x$ Horizontal coordinate	$\rho$ Bending radius	$\theta$ Azimuth
$y$ Vertical coordinate	$R$ Mean radius / orbit	
$z$ Longitudinal coordinate	$C$ Circumference	$L$ Straight sections length

#### I.4.7.1.3 Forces, fields, energy

$t$ Time	
$\mathcal{E}$ Electric field	$\rho_q$ Charge density
$\mathcal{B}$ Magnetic field	$Q$ Total charge
$V$ Electric potential (voltage)	$j$ Current density
$q$ Charge	$I$ Beam current

$Z$  Particle charge number

$m_0$  Rest mass

$v$  Velocity

$E$  Total energy

$m$  Relativistic mass

$p$  Momentum

$E_0$  Rest energy

#### ***1.4.7.1.4 RF system***

$\rho_c$  Cavity radius

$\tau$  Time of arrival in the RF system

$\omega_{\text{rf}} = 2\pi f_{\text{rf}}$  RF (angular) frequency

$\phi$  Phase of arrival in the RF system

$T_{\text{rf}}$  RF period

$\delta E_{\text{rf}}$  Energy gain in RF gap

$V_{\text{rf}}$  RF voltage

$T_t$  Transit time factor

#### ***1.4.7.1.5 Synchrotron parameters***

$C$  Accelerator circumference

$\omega_{\text{rev}} = 2\pi f_{\text{rev}}$  Revolution (angular) frequency

$R$  Accelerator mean orbit

$T_{\text{rev}}$  Revolution period

$\mathcal{B}_y$  Dipole bending field

$h$  RF harmonic number

$\dot{\mathcal{B}}_y$  Magnetic field ramp rate

$\delta E_s$  Energy gain per turn

$\rho$  Bending radius in dipole magnets

$\phi_s$  Synchronous phase

$\alpha_p$  Momentum compaction factor

$\gamma_t$  Transition gamma

$\eta$  Phase slip factor

$\omega_s = 2\pi f_s$  Synchrotron (angular) frequency

(linear approximation with the subscript 0)

$Q_s$  Synchrotron tune

(linear approximation with the subscript 0)

$\Delta E_{\text{sep,m}}$  RF bucket height

$\mathcal{A}_{\text{bk}}$  RF bucket area

#### ***1.4.7.1.6 Beam parameters***

$\varepsilon_l$  Longitudinal emittance

(linear approximation with the subscript 0)

$\tau_l$  Bunch length

$\delta_p$  Momentum spread

#### **1.4.7.2 Summary of the Section 1.4.1**

– Lorentz force

$$\frac{d\vec{p}}{dt} = \vec{F} = q \left( \vec{\mathcal{E}} + \vec{v} \times \vec{\mathcal{B}} \right) \quad (\text{I.4.1})$$

- $\vec{\mathcal{E}}$  to accelerate and deflect
- $\vec{\mathcal{B}}$  to bend trajectories
- Assumptions:  $p_z \gg p_{x,y}$  and  $p \approx p_z$

### I.4.7.3 Summary of the Section I.4.2

#### *Fields and forces*

- Acceleration in an RF gap:

$$\delta E = \int q \mathcal{E}_z(\rho, z, t) dz = q V_{\text{rf}}(\rho, \tau) \quad (\text{I.4.11})$$

- Magnetic rigidity:

$$\mathcal{B}_y \rho = \frac{p}{q} \quad (\text{I.4.12})$$

$$\rightarrow p [\text{GeV}/c] \approx 0.3 Z \mathcal{B}_y [\text{T}] \rho [\text{m}] \quad (\text{I.4.17})$$

#### *Relativistic kinematics*

- Relativistic relationships ( $P = p c$ ):

$$E = E_{\text{kin}} + E_0 = \sqrt{P^2 + E_0^2} \quad (\text{I.4.13})$$

$$\beta = \frac{v}{c} = \frac{P}{E} \quad (\text{I.4.14})$$

$$\gamma = \frac{1}{\sqrt{1 - \beta^2}} = \frac{E}{E_0} \quad (\text{I.4.15})$$

$$\beta^2 + \frac{1}{\gamma^2} = 1 \quad (\text{I.4.16})$$

- Relativistic differential relationships

$$\frac{dE}{dp} = \beta c = v, \quad (\text{I.4.18})$$

$$\frac{dp}{p} = \frac{1}{\beta^2} \frac{dE}{E} = \frac{1}{\beta^2} \frac{d\gamma}{\gamma}, \quad (\text{I.4.19})$$

$$\frac{dp}{p} = \gamma^2 \frac{d\beta}{\beta}. \quad (\text{I.4.20})$$

### I.4.7.4 Summary of the Section I.4.3

#### *Energy gain in an RF system*

- RF energy gain

$$\delta E_{\text{rf}}(\tau) = V_{\text{rf},0} T_t \sin(\omega_{\text{rf}} \tau) \quad \rightarrow \quad \delta E_{\text{rf}}(\phi) = q V_{\text{rf}} \sin(\phi) \quad (\text{I.4.27})$$

- Transit time factor

$$T_t = \frac{\int_{-g/2}^{g/2} \mathcal{E}_0(\rho, z) \cos\left(\frac{\omega_{\text{rf}} z}{\beta c}\right) dz}{\int_{-g/2}^{g/2} \mathcal{E}_0(\rho, z) dz} \quad (\text{I.4.25})$$

- Assumptions:

- $\beta$  is not changing in the computation of  $T_t$
- The  $(\rho, \beta)$  dependence of  $T_t$  will be neglected

### ***The pillbox cavity***

- Time-varying electric field of a pillbox cavity

$$\mathcal{E}_z(\rho, t) = \mathcal{E}_0 J_0\left(\chi_0 \frac{\rho}{\rho_c}\right) \cos(\omega_{\text{rf}} t) \quad (\text{I.4.21})$$

$J_n$  Bessel function,  $\chi_0 \approx 2.405$ ,  $\omega_{\text{rf}} = \chi_0 c / \rho_c$

- Transit time factor of a pillbox cavity

$$T_t = \frac{\sin\left(\frac{\chi_0 g}{2\beta\rho_c}\right)}{\left(\frac{\chi_0 g}{2\beta\rho_c}\right)} \quad (\text{I.4.26})$$

### ***Other energy gain/loss in a ring***

- Induction acceleration (small in large synchrotrons)

$$\delta E_{\text{ind}}(\rho) = q \int_0^{2\pi} \int_0^\rho \frac{\partial \mathcal{B}_y(\rho', \theta, t)}{\partial t} \rho' d\rho' d\theta \quad (\text{I.4.28})$$

- Synchrotron radiation loss (relevant for lepton accelerators)

$$\delta E_{\text{sr}}(E, \rho) = \frac{q^2 \beta^3 E^4}{3\epsilon_0 \rho E_0^4} \quad (\text{I.4.30})$$

- Self-induced field

$$\delta E_{\text{ind}}(\tau) = qV_{\text{ind}}(\tau) = -qN_b(\lambda * \mathcal{W}) \quad (\text{I.4.31})$$

### ***Synchronism in synchrotrons***

- The revolution period

$$T_{\text{rev}} = \frac{C}{v} = \frac{2\pi R}{\beta c} \quad (\text{I.4.32})$$

- The revolution frequency

$$\omega_{\text{rev}} = 2\pi f_{\text{rev}} = \frac{2\pi}{T_{\text{rev}}} = \frac{\beta c}{R} \quad (\text{I.4.33})$$

- Synchronism condition with the RF frequency

$$\omega_{\text{rf}} = h\omega_{\text{rev},s} = h \frac{\beta_s c}{R_s} \quad (\text{I.4.34})$$

### Acceleration

- Acceleration rate (subscript  $s$  for synchronous particle)

$$\delta E_s = 2\pi q \rho_s R_s \dot{\mathcal{B}}_y \quad \text{and} \quad \phi_s = \arcsin \left( 2\pi \rho_s R_s \frac{\dot{\mathcal{B}}_y}{V_{\text{rf}}} \right) \quad (\text{I.4.39})$$

- RF frequency program

$$f_{\text{rf}}(t) = \frac{hc}{2\pi R_s} \sqrt{\frac{\mathcal{B}_y^2(t)}{\mathcal{B}_y^2(t) + \left(\frac{m_0 c}{\rho_s q}\right)^2}} \quad (\text{I.4.41})$$

- Assumptions: Acceleration with constant  $R_s$  and  $\rho_s$

### Radial displacement at constant $\mathcal{B}_y$

- Momentum compaction factor (subscript 0 for design orbit/momentum, transition gamma  $\gamma_t$ ), combined Eqs. (I.4.43) (I.4.46) (I.4.54)

$$\alpha_p = \frac{dR/R}{dp/p} = \frac{\langle D_x \rangle_\rho}{R} = \frac{1}{\gamma_t^2} \approx \frac{\Delta R/R_0}{\Delta p/p_0} \approx \frac{\Delta R/R_s}{\Delta p/p_s}$$

- Phase slip factor, combined Eqs. (I.4.51) (I.4.53)

$$\begin{aligned} \eta &= -\frac{d\omega_{\text{rev}}/\omega_{\text{rev}}}{dp/p} = \frac{dT_{\text{rev}}/T_{\text{rev}}}{dp/p} = \alpha_p - \frac{1}{\gamma^2} \\ &\approx -\frac{\Delta\omega_{\text{rev},0}/\omega_{\text{rev},0}}{\Delta p/p_0} \approx -\frac{\Delta\omega_{\text{rev},s}/\omega_{\text{rev},s}}{\Delta p/p_s} \end{aligned}$$

### Differential equations

(1) $\mathcal{B}_y, p, R$	$\frac{dp}{p} = \gamma_t^2 \frac{dR}{R} + \frac{d\mathcal{B}_y}{\mathcal{B}_y} \quad (\text{I.4.55})$
(2) $f_{\text{rev}}, p, R$	$\frac{dp}{p} = \gamma^2 \frac{df_{\text{rev}}}{f_{\text{rev}}} + \gamma^2 \frac{dR}{R} \quad (\text{I.4.56})$
(3) $\mathcal{B}_y, f_{\text{rev}}, p$	$\frac{d\mathcal{B}_y}{\mathcal{B}_y} = \gamma_t^2 \frac{df_{\text{rev}}}{f_{\text{rev}}} + \frac{\gamma^2 - \gamma_t^2}{\gamma^2} \frac{dp}{p} \quad (\text{I.4.57})$
(4) $\mathcal{B}_y, f_{\text{rev}}, R$	$\frac{d\mathcal{B}_y}{\mathcal{B}_y} = \gamma^2 \frac{df_{\text{rev}}}{f_{\text{rev}}} + (\gamma^2 - \gamma_t^2) \frac{dR}{R} \quad (\text{I.4.58})$

#### I.4.7.5 Summary of the Section I.4.4

*The longitudinal equations of motion (continuous, single RF system, linear momentum compaction factor)*

$$\frac{d}{dt} \left( \frac{\Delta E}{\omega_{\text{rev},s}} \right) = \frac{qV_{\text{rf}}}{2\pi} [\sin(\phi) - \sin(\phi_s)] \quad (\text{I.4.63})$$

$$\frac{d\phi}{dt} = \frac{h\eta\omega_{\text{rev},s}^2}{\beta_s^2 E_s} \left( \frac{\Delta E}{\omega_{\text{rev},s}} \right) \quad (\text{I.4.66})$$

*The longitudinal equations of motion (discrete, several RF systems, non-linear momentum compaction factor)*

$$\Delta E^{(n+1)} = \Delta E^{(n)} + \sum_{k=1}^{n_{\text{rf}}} qV_{\text{rf},k}^{(n)} \sin \left( \omega_{\text{rf},k}^{(n)} \Delta\tau^{(n)} + \phi_k^{(n)} \right) - \delta E_s^{(n \rightarrow n+1)} + \delta E_{\text{other}} \quad (\text{I.4.70})$$

$$\Delta\tau^{(n+1)} = \Delta\tau^{(n)} + T_{\text{rev},d}^{(n+1)} \left[ \left[ 1 + \sum_l \alpha_l^{(n+1)} \left( \frac{\Delta p}{p_d^{(n+1)}} \right)^l \right] \frac{\Delta p/p_d^{(n+1)}}{\Delta E/E_d^{(n+1)}} - 1 \right] \quad (\text{I.4.72})$$

#### I.4.7.6 Summary of the Section I.4.5

*Linear synchrotron motion*

- Linear synchrotron frequency

$$\omega_{s_0} = 2\pi f_{s_0} = \sqrt{-\frac{qV_{\text{rf}}\omega_{\text{rf}}^2 \eta \cos \phi_s}{2\pi h \beta_s^2 E_s}} \quad (\text{I.4.75})$$

- Linear synchrotron tune

$$Q_{s_0} = \frac{\omega_{s_0}}{\omega_{\text{rev},s}} = \sqrt{-\frac{qV_{\text{rf}} h \eta \cos \phi_s}{2\pi \beta_s^2 E_s}} \quad (\text{I.4.77})$$

- Phase stability condition

$$\eta \cos \phi_s < 0 \quad (\text{I.4.76})$$

*Linear oscillation amplitude and emittance*

- Oscillation amplitude ratio

$$\frac{(\Delta E/\omega_{\text{rf}})_m}{\Delta\phi_m} = \frac{\beta_s^2 E_s}{|\eta| \omega_{\text{rf}}^2} \omega_{s_0} = \frac{\beta_s^2 E_s}{|\eta| h^2 \omega_{\text{rev},s}} Q_{s_0} \quad (\text{I.4.79})$$

- Approximate longitudinal emittance

$$\varepsilon_{l_0} = \pi \Delta E_m \frac{\tau_l}{2} = \frac{\pi \beta_s^2 E_s}{4 |\eta|} \omega_{s_0} \tau_l^2 = \frac{\pi |\eta|}{\beta_s^2 E_s \omega_{s_0}} \Delta E_m^2 \quad (\text{I.4.82})$$

**Bunch parameters linear scaling laws**

- Bunch length

$$\tau_l \propto \varepsilon_{l_0}^{1/2} V_{\text{rf}}^{-1/4} h^{-1/4} E_s^{-1/4} \eta^{1/4} \quad (\text{I.4.84})$$

- Energy deviation

$$\Delta E_m \propto \varepsilon_{l_0}^{1/2} V_{\text{rf}}^{1/4} h^{1/4} E_s^{1/4} \eta^{-1/4} \quad (\text{I.4.85})$$

**Hamiltonian of non-linear synchrotron motion**

$$\mathcal{H} = \frac{\eta \omega_{\text{rf}}^2}{2\beta_s^2 E_s} \left( \frac{\Delta E}{\omega_{\text{rf}}} \right)^2 + \frac{q V_{\text{rf}}}{2\pi h} [\cos \phi - \cos \phi_s + (\phi - \phi_s) \sin \phi_s] \quad (\text{I.4.86})$$

**RF bucket parameters**

- RF bucket height

$$\Delta E_{\text{sep,m}} = \sqrt{\frac{2qV_{\text{rf}}\beta_s^2 E_s}{\pi h |\eta|} \left| -\cos \phi_s + \frac{(\pi - 2\phi_s)}{2} \sin \phi_s \right|^{1/2}} \quad (\text{I.4.88 I.4.89})$$

- RF bucket area (acceptance)

$$\mathcal{A}_{\text{bk}} \approx \frac{8}{\omega_{\text{rf}}} \sqrt{\frac{2qV_{\text{rf}}\beta_s^2 E_s}{\pi h |\eta|} \frac{1 - \sin \phi_s}{1 + \sin \phi_s}} \quad (\text{I.4.92})$$

- For the stationary RF bucket, the RF bucket length is  $2\pi$  and  $\mathcal{A}_{\text{bk}} = 8\Delta E_{\text{sep,m}}/\omega_{\text{rf}}$ .

- Non-linear synchrotron frequency distribution

$$\frac{\omega_s}{\omega_{s_0}} = \frac{\pi}{2K\left(\sin \frac{\phi_b}{2}\right)} \approx 1 - \frac{\phi_b^2}{16} \quad (\text{I.4.95})$$

**I.4.8 Solutions to exercises**
**I.4.8.1 Correction of exercises from the Section I.4.1**

**I.4.1:** At this stage it is impossible to answer! The notion of slippage factor is required. Intuitively, the ratio of the particles trajectories to their velocity determines the time it takes to complete a full revolution in the accelerator. However, the velocity being close to the speed of light will lead to a second regimes where the increase in path length becomes more important than the increase in velocity.

**I.4.8.2 Correction of exercises from the Section I.4.2**

**I.4.2:** Using Eq. (I.4.7) and (I.4.8)

- An accelerator has a potential of 20 MV, what is the corresponding energy gain of the beam in Joules?

$$20 \cdot 10^6 \cdot 1.609 \cdot 10^{-19} = 3.2 \cdot 10^{-12} \text{ J}$$

- What is the total energy of the beam stored in the LHC

$$2808 \cdot 1.15 \cdot 10^{11} \cdot 7 \cdot 10^{12} \cdot 1.609 \cdot 10^{-19} = 364 \text{ MJ}$$

- What is the equivalent speed of a high speed train ( $E_{\text{LHC}} = E_{\text{kin,train}}$ )

$$v_{\text{train}} = \sqrt{2E_{\text{LHC}}/m_{\text{train}}} = \sqrt{2 \cdot 364 \cdot 10^6 / (400 \cdot 10^3)} = 154 \text{ km/h}$$

- What is the power delivered to the LHC beam (1800 s)

$$2808 \cdot 1.15 \cdot 10^{11} \cdot (7 - 0.450) \cdot 10^{12} \cdot 1.609 \cdot 10^{-19} / 1800 = 189 \text{ kW}$$

**I.4.3:** Assuming azimuthal symmetry and a vertical magnetic field  $\vec{\mathcal{B}} = -\mathcal{B}_y(\rho, t) \vec{e}_y$  at a constant orbit  $\rho_0$ , we seek to derive an equation for  $\mathcal{E}_\theta$  and the corresponding  $\frac{dp_\theta}{dt}$ . We introduce the magnetic flux  $\Phi_{S,\rho_0}$  and an averaged magnetic field in the betatron core  $\langle \mathcal{B}_y \rangle_{S,\rho_0}$ :

$$\Phi_{S,\rho_0} = 2\pi \int_0^{\rho_0} \mathcal{B}_y(\rho) \rho d\rho = \pi \rho_0^2 \langle \mathcal{B}_y \rangle_{S,\rho_0}.$$

The equilibrium condition for a constant  $p_\theta$  is given by:

$$\mathcal{B}_y \rho = \frac{p_\theta}{q} = \frac{p}{q}.$$

With the assumption of azimuthal symmetry and a vertical magnetic field  $\vec{\mathcal{B}} = -\mathcal{B}_y(\rho, t) \vec{e}_y$  at a constant orbit  $\rho_0$ , Faraday's law for induction (I.4.4) gives:

$$\begin{aligned} \int_0^{2\pi} \mathcal{E}_\theta \rho d\theta &= \frac{d}{dt} \int_0^{2\pi} \int_0^{\rho_0} \mathcal{B}_y(\rho, t) \rho d\rho d\theta \\ 2\pi \rho_0 \mathcal{E}_\theta &= \frac{d\Phi_{S,\rho_0}}{dt} \\ \mathcal{E}_\theta &= \frac{1}{2\pi \rho_0} \frac{d\Phi_{S,\rho_0}}{dt} \end{aligned}$$

where  $\Phi_{S,\rho_0}$  is the magnetic flux in the contour enclosed in the orbit  $\rho_0$ . The obtained acceleration is:

$$\begin{aligned} \frac{dp_\theta}{dt} &= q\mathcal{E}_\theta = \frac{q}{2\pi \rho_0} \frac{d\Phi_{S,\rho_0}}{dt} \\ p_\theta &= \frac{q}{2\pi \rho_0} \Phi_{S,\rho_0}. \end{aligned}$$

Using the magnetic rigidity  $p_\theta = q\mathcal{B}_y(\rho_0) \rho_0$ , we obtain:

$$\begin{aligned} q\mathcal{B}_y(\rho_0) \rho_0 &= \frac{q}{2\pi \rho_0} \Phi_{S,\rho_0} \\ \mathcal{B}_y(\rho_0) &= \frac{1}{2} \frac{\Phi_{S,\rho_0}}{\pi \rho_0^2}. \end{aligned}$$

Introducing an averaged magnetic field in the betatron core  $\langle \mathcal{B}_y \rangle_{S,\rho_0}$ , we have:

$$\begin{aligned}\Phi_{S,\rho_0} &= 2\pi \int_0^{\rho_0} \mathcal{B}_y(\rho) \rho d\rho = \pi \rho_0^2 \langle \mathcal{B}_y \rangle_{S,\rho_0} \\ \mathcal{B}_y(\rho_0) &= \frac{1}{2} \frac{\Phi_{S,\rho_0}}{\pi \rho_0^2} = \frac{1}{2} \langle \mathcal{B}_y \rangle_{S,\rho_0}.\end{aligned}\quad (\text{I.4.9})$$

I.4.4: Using Fig. I.4.2, in cylindrical coordinates (overdot is derivative with time  $d/dt$ )

$$\begin{aligned}v_\rho &= \dot{\rho} \\ v_\theta &= \rho \dot{\theta} = \rho \omega \\ v_y &= \dot{y}\end{aligned}$$

and if  $\dot{m} = 0$

$$\begin{aligned}\dot{p}_\rho &= m \left( \ddot{\rho} - \rho \dot{\theta}^2 \right) \\ \dot{p}_\theta &= m \left( \rho \ddot{\theta} + 2\dot{\rho} \dot{\theta} \right) \\ \dot{p}_y &= m \ddot{y}.\end{aligned}$$

The force from a magnetic field is always orthogonal to the particle direction, in cylindrical coordinates and with a constant  $v = v_\theta$  (implying  $p = p_\theta$ ,  $\dot{m} = 0$ ), and a magnetic field  $\vec{\mathcal{B}} = -\mathcal{B}_y \vec{e}_y$ , we get

$$\begin{aligned}\frac{d\vec{p}}{dt} &= \vec{F}_{\mathcal{B}} = q \left( \vec{v} \times \vec{\mathcal{B}} \right) \\ \text{in } \vec{e}_\rho &\implies m \left( \ddot{\rho} - \rho \dot{\theta}^2 \right) = -qv_\theta \mathcal{B}_y, \quad (\dot{\rho} = 0) \\ &\implies m \frac{v_\theta^2}{\rho} = qv_\theta \mathcal{B}_y, \quad (v_\theta = \rho \dot{\theta}) \\ &\implies p_\theta = q\mathcal{B}_y \rho \\ &\implies \mathcal{B}_y \rho = \frac{p_\theta}{q} = \frac{p}{q}\end{aligned}\quad (\text{I.4.12})$$

I.4.5: The (unitless) magnitude of a variable is noted in ||

$$p [\text{Ns}] = e [\text{C}] Z \mathcal{B}_y [\text{T}] \rho [\text{m}]$$

$$p [\text{Ns}] c [\text{m/s}] = c [\text{m/s}] e [\text{C}] Z \mathcal{B}_y [\text{T}] \rho [\text{m}]$$

$$P [\text{Nm}] = c [\text{m/s}] e [\text{C}] Z \mathcal{B}_y [\text{T}] \rho [\text{m}]$$

$$P [\text{Nm}] / |e| = 1 [\text{C}] c [\text{m/s}] Z \mathcal{B}_y [\text{T}] \rho [\text{m}]$$

$$P [\text{eV}] / (1 [\text{m/s}]) = |c| 1 [\text{C}] Z \mathcal{B}_y [\text{T}] \rho [\text{m}]$$

$$p [\text{GeV}/c] \approx 0.3 Z \mathcal{B}_y [\text{T}] \rho [\text{m}]$$

I.4.6:

Machine	$E_0$ [MeV]	$E_{\text{kin}}$ [GeV]	$E$ [GeV]	$\gamma$	$\beta$	$p$ [GeV/c]	$\mathcal{B}_y \rho$ [Tm]
PSB inj (p+)	938	0.160	1.098	1.17	0.52	0.57	1.90
PSB ext (p+)	938	2	2.938	3.13	0.95	2.78	9.30
SPS ( $^{208}\text{Pb}^{82+}$ )	193751	1940.50	2134.25	11.0	0.996	2125.44	86.4
LHC (p+)	938	6999	7000	7460	0.999...	6999.99...	23333
LEP (e+/e-)	0.511	99.99	100	195695	0.999...	99.99...	333.33

I.4.7: Eq. (I.4.18)

$$\begin{aligned} E^2 &= P^2 + E_0^2 \\ \implies d(E^2) &= d(P^2) + d(E_0^2) \\ \implies 2EdE &= 2PdP = 2pdpc^2 \\ \implies \frac{dE}{dp} &= \frac{pc^2}{E} \\ \implies \frac{dE}{dp} &= \beta c = v \end{aligned}$$

Eq. (I.4.19)

$$\begin{aligned} EdE &= pdpc^2 \\ \implies \frac{dE}{E} &= \frac{pc^2}{E^2} dp \\ \implies \frac{dE}{E} &= \left(\frac{pc}{E}\right)^2 \frac{dp}{p} \\ \implies \frac{dE}{E} &= \beta^2 \frac{dp}{p} \\ \implies \frac{dp}{p} &= \frac{1}{\beta^2} \frac{dE}{E} = \frac{1}{\beta^2} \frac{d\gamma}{\gamma} \end{aligned}$$

Eq. (I.4.20)

$$\begin{aligned} \beta^2 &= 1 - \frac{1}{\gamma^2} \\ \implies d(\beta^2) &= d\left(1 - \frac{1}{\gamma^2}\right) \\ \implies 2\beta d\beta &= 2\gamma^{-3} d\gamma \\ \implies \frac{d\beta}{\beta} &= \left(\frac{1}{\beta\gamma}\right)^2 \frac{d\gamma}{\gamma} \\ \implies \frac{d\beta}{\beta} &= \frac{1}{\gamma^2} \frac{dp}{p} \end{aligned}$$

### I.4.8.3 Correction of exercises from the Section I.4.3

I.4.8: We will assume a solution of the form  $\mathcal{E}_z = \mathcal{E}_0(\rho) \cos(\omega_{\text{rf}}t)$ . Reminder: in cylindrical coordinates

$$\Delta \vec{\mathcal{E}} = \frac{\partial^2 \mathcal{E}_z}{\partial z^2} + \frac{1}{\rho} \frac{\partial \mathcal{E}_z}{\partial \rho} + \frac{\partial^2 \mathcal{E}_z}{\partial \rho^2}.$$

Reminder: the Bessel differential equation

$$x^2 \frac{\partial^2 y}{\partial x^2} + x \frac{\partial y}{\partial x} + \left( \frac{x}{x_0} - n \right)^2 y = 0 \rightarrow y = y_0 J_n \left( \frac{x}{x_0} \right).$$

The wave equation in cylindrical coordinates becomes

$$\frac{\partial^2 \mathcal{E}_z}{\partial z^2} + \frac{1}{\rho} \frac{\partial \mathcal{E}_z}{\partial \rho} + \frac{\partial^2 \mathcal{E}_z}{\partial \rho^2} - \frac{1}{c^2} \frac{\partial^2 \mathcal{E}_z}{\partial t^2} = 0.$$

Assuming a solution of the form  $\mathcal{E}_z = \mathcal{E}_{z,\rho}(\rho) \cos(\omega_{\text{rf}}t)$  leads to

$$\begin{aligned} & \frac{1}{\rho} \frac{\partial \mathcal{E}_{z,\rho}}{\partial \rho} \cos(\omega_{\text{rf}}t) + \frac{\partial^2 \mathcal{E}_{z,\rho}}{\partial \rho^2} \cos(\omega_{\text{rf}}t) - \frac{1}{c^2} \frac{\partial^2 \cos(\omega_{\text{rf}}t)}{\partial t^2} \mathcal{E}_{z,\rho} = 0 \\ \implies & \frac{\partial^2 \mathcal{E}_{z,\rho}}{\partial \rho^2} \cos(\omega_{\text{rf}}t) + \frac{1}{\rho} \frac{\partial \mathcal{E}_{z,\rho}}{\partial \rho} \cos(\omega_{\text{rf}}t) + \left( \frac{\omega_{\text{rf}}}{c} \right)^2 \mathcal{E}_{z,\rho} \cos(\omega_{\text{rf}}t) = 0 \\ \implies & \rho^2 \frac{\partial^2 \mathcal{E}_{z,\rho}}{\partial \rho^2} + \rho \frac{\partial \mathcal{E}_{z,\rho}}{\partial \rho} + \left( \frac{\rho \omega_{\text{rf}}}{c} \right)^2 \mathcal{E}_{z,\rho} = 0. \end{aligned}$$

The differential equation

$$\rho^2 \frac{\partial^2 \mathcal{E}_{z,\rho}}{\partial \rho^2} + \rho \frac{\partial \mathcal{E}_{z,\rho}}{\partial \rho} + \left( \frac{\rho \omega_{\text{rf}}}{c} \right)^2 \mathcal{E}_{z,\rho} = 0$$

is the Bessel differential equation which has a solution for  $\mathcal{E}_{z,\rho}$  given by

$$\mathcal{E}_{z,\rho} = \mathcal{E}_0 J_0 \left( \frac{\rho \omega_{\text{rf}}}{c} \right)$$

where  $\mathcal{E}_0$  is the amplitude of the field at  $\rho = 0$ . The boundary condition for electrical fields implies that  $\mathcal{E}_z(\rho = \rho_c) = 0$ . We reformulate the electric field

$$\mathcal{E}_{z,\rho} = \mathcal{E}_0 J_0 \left( \chi_0 \frac{\rho}{\rho_c} \right)$$

where  $\chi_0 = \rho_c \omega_{\text{rf}}/c \approx 2.405$  is the first zero of the Bessel function  $J_0$ . Finally,

$$\mathcal{E}_z(\rho, t) = \mathcal{E}_0 J_0 \left( \chi_0 \frac{\rho}{\rho_c} \right) \cos(\omega_{\text{rf}}t)$$

with  $\omega_{\text{rf}} = \chi_0 c/\rho_c \approx 2.405 c/\rho_c$ .

I.4.9: Starting from

$$\delta E_{\text{rf}} = q \int_{-g/2}^{g/2} \mathcal{E}_0(\rho, z) \cos \left[ \omega_{\text{rf}} \left( \frac{z}{\beta c} \right) - \omega_{\text{rf}} \tau \right] dz.$$

Using the trigonometric relationship

$$\delta E_{\text{rf}} = q \int_{-g/2}^{g/2} \mathcal{E}_0(\rho, z) \left[ \cos\left(\frac{\omega_{\text{rf}} z}{\beta c}\right) \cos(\omega_{\text{rf}} \tau) + \sin\left(\frac{\omega_{\text{rf}} z}{\beta c}\right) \sin(\omega_{\text{rf}} \tau) \right] dz.$$

The sin function is odd and cancels in the integral. We get

$$\delta E_{\text{rf}} = q \cos(\omega_{\text{rf}} \tau) \int_{-g/2}^{g/2} \mathcal{E}_0(\rho, z) \cos\left(\frac{\omega_{\text{rf}} z}{\beta c}\right) dz.$$

We define the maximum possible accelerating potential (no variation with time during particle passage) as

$$V_{\text{rf},0} = \int_{-g/2}^{g/2} \mathcal{E}_0(\rho, z) dz.$$

We define the transit time factor as the ratio between the accelerating potential including the time variation of the field and the maximum potential

$$T_t = \frac{\int_{-g/2}^{g/2} \mathcal{E}_0(\rho, z) \cos\left(\frac{\omega_{\text{rf}} z}{\beta c}\right) dz}{V_{\text{rf},0}}.$$

The energy gain in the gap finally becomes

$$\delta E_{\text{rf}}(\tau) = q V_{\text{rf},0} T_t \cos(\omega_{\text{rf}} \tau) = q V_{\text{rf}} \cos(\omega_{\text{rf}} \tau).$$

The cos can be interchanged with sin depending on the convention used (linac vs. synchrotrons).

**I.4.10:** Including the expression of the pillbox cavity field in the transit time factor

$$\begin{aligned} T_t &= \frac{\int_{-g/2}^{g/2} \mathcal{E}_0(\rho, z) \cos\left(\frac{\omega_{\text{rf}} z}{\beta c}\right) dz}{\int_{-g/2}^{g/2} \mathcal{E}_0(\rho, z) dz} \\ \Rightarrow T_t &= \frac{\mathcal{E}_0 J_0(\rho) \int_{-g/2}^{g/2} \cos\left(\frac{\omega_{\text{rf}} z}{\beta c}\right) dz}{\mathcal{E}_0 J_0(\rho) \int_{-g/2}^{g/2} dz} \\ \Rightarrow T_t &= \frac{1}{g} \int_{-g/2}^{g/2} \cos\left(\frac{\omega_{\text{rf}} z}{\beta c}\right) dz. \end{aligned}$$

Including the expression of the pillbox cavity field in the transit time factor

$$\begin{aligned} \Rightarrow T_t &= \frac{1}{g} \int_{-g/2}^{g/2} \cos\left(\frac{\omega_{\text{rf}} z}{\beta c}\right) dz \\ \Rightarrow T_t &= \frac{\beta c}{\omega_{\text{rf}} g} \left[ \sin\left(\frac{\omega_{\text{rf}} g}{2\beta c}\right) - \sin\left(\frac{-\omega_{\text{rf}} g}{2\beta c}\right) \right] \\ \Rightarrow T_t &= \frac{\sin\left(\frac{\omega_{\text{rf}} g}{2\beta c}\right)}{\left(\frac{\omega_{\text{rf}} g}{2\beta c}\right)} = \frac{\sin\left(\frac{\chi_0 g}{2\beta \rho c}\right)}{\left(\frac{\chi_0 g}{2\beta \rho c}\right)} \end{aligned}$$

I.4.11: Applying Eq. (I.4.23) to get the radius from the rf frequency

$$\rho_c = \frac{2.405 \cdot 3 \cdot 10^8}{2\pi \cdot 80 \cdot 10^6} = 1.4 \text{ m}$$

$$\rho_c = \frac{2.405 \cdot 3 \cdot 10^8}{2\pi \cdot 1.4 \cdot 10^9} = 8.2 \text{ cm}$$

I.4.12: Starting from

$$\begin{aligned} \frac{d}{dt} (\mathcal{B}_y \rho_s) &= \frac{\dot{p}_s}{q} \\ \implies \dot{\mathcal{B}}_y \rho_s + \mathcal{B}_y \dot{\rho}_s &= \frac{\dot{E}_s}{q\beta_s c} \end{aligned}$$

Assuming  $\dot{\rho}_s = 0$

$$\implies \dot{\mathcal{B}}_y \rho_s = \frac{V_{\text{rf}}}{\beta_s c T_{\text{rev},s}} \sin(\phi_s) = \frac{V_{\text{rf}}}{2\pi R_s} \sin(\phi_s)$$

$$\implies 2\pi q R_s \rho_s \dot{\mathcal{B}}_y = q V_{\text{rf}} \sin(\phi_s) = \delta E_s$$

I.4.13: Expression of  $\beta_s$

$$\begin{aligned} \beta_s(t) &= \frac{pc}{E} = \frac{pc}{\sqrt{(pc)^2 + E_0^2}} \\ &= \frac{\mathcal{B}_y \rho_s qc}{\sqrt{(\mathcal{B}_y \rho_s qc)^2 + (m_0 c^2)^2}} \\ &= \frac{\mathcal{B}_y}{\sqrt{(\mathcal{B}_y)^2 + \left(\frac{m_0 c^2}{\rho_s qc}\right)^2}} \\ &= \sqrt{\frac{\mathcal{B}_y^2}{\mathcal{B}_y^2 + \left(\frac{m_0 c}{\rho_s q}\right)^2}} \end{aligned}$$

Leading to

$$\begin{aligned} f_{\text{rf}}(t) &= \frac{\omega_{\text{rf}}(t)}{2\pi} = \frac{hc}{2\pi R_s} \beta_s(t) \\ &= \frac{hc}{2\pi R_s} \sqrt{\frac{\mathcal{B}_y^2(t)}{\mathcal{B}_y^2(t) + \left(\frac{m_0 c}{\rho_s q}\right)^2}} \end{aligned}$$

I.4.14:

Machine	SPS inj. p+	SPS ext. p+	SPS inj. Pb	SPS ext. Pb
$p$ [GeV/c]	26	450	2132	36900
$E$ [GeV]	26.0169	450.001	2140.786	36900.509
$\beta$	0.99935	0.999...	0.9959	0.999..
$T_{\text{rev}}$ [ $\mu\text{s}$ ]	23.0693	23.0543	23.1493	23.0546
$f_{\text{rf}}$ [MHz]	200.266	200.396	199.574	200.394

– Energy gain per turn in the SPS ( $\dot{\mathcal{B}}_y = 0.7 \text{ T/s}$ )

–  $6911.50 \cdot 741.35 \cdot 1 \cdot 0.7 = 3.59 \text{ MeV}$  for p+

$$- 6911.50 \cdot 741.35 \cdot 82 \cdot 0.7 = 294 \text{ MeV for Pb}$$

– Smallest RF voltage to accelerate the synchronous particle

$$- 3.59 \text{ MV for p+ and Pb } (\delta E_{\text{rf}}/q)$$

I.4.15: The total path length increase due to dispersion is

$$\begin{aligned} dC &= 2\pi dR = \int_0^{2\pi} x_D(z) d\theta \\ \implies dR &= \frac{1}{2\pi} \int_0^{2\pi R} D_x(z) \frac{dp}{p} \frac{dz}{\rho(z)} \quad , (dz = \rho(z) d\theta) \\ \implies \frac{dR}{R} \frac{p}{dp} &= \frac{1}{2\pi R} \int_0^{2\pi R} \frac{D_x(z)}{\rho(z)} dz \\ \implies \alpha_p &= \frac{1}{2\pi R} \int_0^{2\pi R} \frac{D_x(z)}{\rho(z)} dz. \end{aligned}$$

I.4.16: The local radial offset where  $D_x$  is max is about  $x_D \approx 1 \text{ cm}$ . The corresponding elongation of the trajectory is  $\Delta C = \alpha_p (p/p_0) C = 0.124 \cdot 10^{-3} \cdot 78.54 \approx 9.7 \text{ mm}$ .

I.4.17: Starting from

$$\begin{aligned} \langle \mathcal{B}_y \rangle &= \frac{1}{2\pi R} \int_0^{2\pi R} \mathcal{B}_y dz \\ &= \frac{1}{2\pi R} \int_0^{2\pi R} \frac{p}{q\rho} dz \\ &= \frac{1}{2\pi R} \frac{p}{q} \int_0^{2\pi R} \frac{dz}{\rho(z)} \\ &= \frac{1}{2\pi R} \frac{p}{q} \frac{2\pi\rho}{\rho} \quad \rho \rightarrow \infty \text{ in straight sections, otherwise constant} \\ \langle \mathcal{B}_y \rangle R &= \frac{p}{q} \end{aligned}$$

then differentiating

$$\begin{aligned} p &= q \langle \mathcal{B}_y \rangle R \\ \implies \frac{dp}{p} &= \frac{d\langle \mathcal{B}_y \rangle}{\langle \mathcal{B}_y \rangle} + \frac{dR}{R} \\ \implies \frac{dp/p}{dR/R} &= \frac{d\langle \mathcal{B}_y \rangle / \langle \mathcal{B}_y \rangle}{dR/R} + 1 \\ \implies \frac{1}{\alpha_p} &= -\langle n \rangle + 1 \\ \implies \langle n \rangle &= 1 - \frac{1}{\alpha_p} \end{aligned}$$

I.4.18:

	SPS injection	SPS extraction
Momentum [GeV/c]	14	450
$E$ [GeV]	14.03	450
$\gamma$	14.95	479.6
$T_{\text{rev}}$ [ $\mu\text{s}$ ]	23.11	23.05
$\alpha_p$ [ $10^{-3}$ ]		3.086
$E_t$ [GeV]		16.89
$\eta$ [ $10^{-3}$ ]	-1.385	3.082

**I.4.19:** The mean radial offset is  $\Delta R = 3.086 \cdot 10^{-3} \cdot 6911.50 / (2 \cdot 3.14) \cdot (-10^{-4}) = -0.34$  mm and the corresponding change in the revolution period is

– Low  $E$ :  $\Delta T_{\text{rev}} = -1.385 \cdot 10^{-3} \cdot 23.11 \cdot 10^{-6} \cdot (-10^{-4}) = 3.2$  ps (late)

– High  $E$ :  $\Delta T_{\text{rev}} = 3.082 \cdot 10^{-3} \cdot 23.05 \cdot 10^{-6} \cdot (-10^{-4}) = -7.1$  ps (early)

**I.4.20:**

(1) Directly the definition from the momentum compaction factor Eq. (I.4.44).

(2) Combining

$$\frac{dp}{p} = \gamma^2 \frac{d\beta}{\beta} \quad \text{and} \quad \frac{d\beta}{\beta} = \frac{df_{\text{rev}}}{f_{\text{rev}}} + \frac{dR}{R}$$

(3) Substituting  $\frac{dR}{R}$  from (1) in (2)

(4) Substituting  $\frac{dp}{p}$  from (1) in (2)

#### I.4.8.4 Correction of exercises from the Section I.4.4

**I.4.21:** Expressing with  $T_{\text{rev}}$  instead of  $\omega_{\text{rev}}$

$$\begin{aligned}
 \dot{E}T_{\text{rev}} - \dot{E}_s T_{\text{rev},s} &= (\dot{E}_s + \Delta \dot{E}) (T_{\text{rev},s} + \Delta T_{\text{rev}}) - \dot{E}_s T_{\text{rev},s} \\
 &= \dot{E}_s T_{\text{rev},s} + \dot{E}_s \Delta T_{\text{rev}} + \Delta \dot{E} T_{\text{rev},s} + \Delta \dot{E} \Delta T_{\text{rev}} - \dot{E}_s T_{\text{rev},s} \\
 &\quad \text{(dropping second order terms)} \\
 &\approx \dot{E}_s \Delta T_{\text{rev}} + \Delta \dot{E} T_{\text{rev},s} \\
 &\quad \text{(Assumption: linearizing } \Delta T_{\text{rev}} \text{ around the synchronous particle)} \\
 &\approx \left( \frac{dE}{dt} \right)_s \left( \frac{dT_{\text{rev}}}{dE} \right)_s \Delta E + \Delta \dot{E} T_{\text{rev},s} \\
 &\approx \dot{T}_{\text{rev},s} \Delta E + \Delta \dot{E} T_{\text{rev},s} \\
 &\approx \frac{d}{dt} (\Delta E T_{\text{rev},s}) \\
 \rightarrow \frac{\dot{E}}{\omega_{\text{rev}}} - \frac{\dot{E}_s}{\omega_{\text{rev},s}} &\approx \frac{d}{dt} \left( \frac{\Delta E}{\omega_{\text{rev},s}} \right)
 \end{aligned}$$

I.4.22: Resuming from the above solution from Ex. I.4.21 we get

$$\frac{\dot{E}}{\omega_{\text{rev}}} - \frac{\dot{E}_s}{\omega_{\text{rev},s}} \approx \frac{\Delta \dot{E}}{\omega_{\text{rev},s}} + \frac{1}{2\pi} \dot{E}_s \Delta T_{\text{rev}}.$$

Including  $\omega_{\text{rev},s}$  inside the derivative with time

$$\begin{aligned} \frac{\Delta \dot{E}}{\omega_{\text{rev},s}} + \frac{1}{2\pi} \dot{E}_s \Delta T_{\text{rev}} &= \frac{d}{dt} \left( \frac{\Delta E}{\omega_{\text{rev},s}} \right) - \Delta E \frac{d}{dt} \left( \frac{1}{\omega_{\text{rev},s}} \right) + \frac{1}{2\pi} \dot{E}_s \Delta T_{\text{rev}} \\ &= \frac{d}{dt} \left( \frac{\Delta E}{\omega_{\text{rev},s}} \right) + \frac{\Delta E}{\omega_{\text{rev},s}} \frac{\dot{\omega}_{\text{rev},s}}{\omega_{\text{rev},s}} + \frac{1}{2\pi} \dot{E}_s \Delta T_{\text{rev}} \\ &= (1) + (2) + (3) \end{aligned}$$

Expressing (2), using  $dE = v dp = \omega R dp$  (Eq. (I.4.18)) and differentiating  $\omega = \beta c/R$

$$\frac{\Delta E}{\omega_{\text{rev},s}} \frac{\dot{\omega}_{\text{rev},s}}{\omega_{\text{rev},s}} = R_s \Delta p \left( \frac{\dot{\beta}_s}{\beta_s} - \frac{\dot{R}_s}{R_s} \right).$$

Expressing (3), using  $dE = v dp = \omega R dp$  and  $\eta = \alpha_p - \gamma^{-2} = (dT_{\text{rev}}/T_{\text{rev}}) / (dp/p)$

$$\begin{aligned} \frac{1}{2\pi} \dot{E}_s \Delta T_{\text{rev}} &= \frac{1}{2\pi} \omega_{\text{rev},s} R_s \dot{p}_s \eta \frac{\Delta p}{p_s} T_{\text{rev},s} \\ &= R_s \Delta p \left( \alpha_p - \frac{1}{\gamma_s^2} \right) \frac{\dot{p}_s}{p_s}. \end{aligned}$$

Summing (2) + (3) and with  $d\beta/\beta = \gamma^{-2} dp/p$

$$(2) + (3) = R_s \Delta p \left( \alpha_p \frac{\dot{p}_s}{p_s} - \frac{\dot{R}_s}{R_s} \right).$$

Using the synchrotron differential equation Eq (I.4.55)

$$R_s \Delta p \left( \alpha_p \frac{\dot{p}_s}{p_s} - \frac{\dot{R}_s}{R_s} \right) = R_s \Delta p \alpha_p \frac{\dot{\mathcal{B}}_{y,s}}{\mathcal{B}_{y,s}}.$$

From the relativistic differential relationship  $dE = \beta c dp$  (Eq. (I.4.18)),  $\beta = P/E$  and the definition of the angular revolution frequency  $\omega = \beta c/R$

$$\begin{aligned} \dots &= R_s \frac{\Delta E}{\beta_s c} \alpha_p \frac{\dot{\mathcal{B}}_{y,s}}{\mathcal{B}_{y,s}} \\ &= \left( \frac{\Delta E}{\omega_{\text{rev},s}} \right) \alpha_p \frac{\dot{\mathcal{B}}_{y,s}}{\mathcal{B}_{y,s}} \end{aligned}$$

Finally

$$\frac{\dot{E}}{\omega_{\text{rev}}} - \frac{\dot{E}_s}{\omega_{\text{rev},s}} = \frac{d}{dt} \left( \frac{\Delta E}{\omega_{\text{rev},s}} \right) + \alpha_p \frac{\dot{\mathcal{B}}_{y,s}}{\mathcal{B}_{y,s}} \left( \frac{\Delta E}{\omega_{\text{rev},s}} \right)$$

I.4.23: Using the Eq. (I.4.65) The difference in the magnetic flux in the surface between the paths of an

arbitrary particle and the synchronous one is

$$\begin{aligned}
 \frac{q}{2\pi} \int_0^{2\pi} \int_{\rho_s}^{\rho} \frac{\partial \mathcal{B}_y}{\partial t} \rho' d\rho' d\theta &\approx \frac{q}{2\pi} \int_0^{2\pi} \frac{\partial \mathcal{B}_{y,s}}{\partial t} \int_{\rho_s}^{\rho} \rho' d\rho' d\theta \\
 &= \frac{q}{2\pi} \int_0^{2\pi} \frac{\partial \mathcal{B}_{y,s}}{\partial t} \frac{\rho^2 - \rho_s^2}{2} d\theta \\
 &= \frac{q}{2\pi} \int_0^{2\pi} \frac{\partial \mathcal{B}_{y,s}}{\partial t} \frac{(\rho_s + x_D)^2 - \rho_s^2}{2} d\theta \quad (\text{2nd order in } \rho \text{ neglected}) \\
 &\approx \frac{q}{2\pi} \int_0^{2\pi} \frac{\partial \mathcal{B}_{y,s}}{\partial t} \rho_s x_D d\theta
 \end{aligned}$$

Using Eq. (I.4.46) and  $dz = \rho d\theta$

$$\begin{aligned}
 \frac{q}{2\pi} \int_0^{2\pi} \frac{\partial \mathcal{B}_{y,s}}{\partial t} \rho_s x_D d\theta &= \frac{q}{2\pi} \dot{\mathcal{B}}_{y,s} \rho_s \int_0^{2\pi} D_x \frac{\Delta p}{p} d\theta \\
 &= \frac{q}{2\pi} \dot{\mathcal{B}}_{y,s} \rho_s 2\pi R_s \alpha_p \frac{\Delta p}{p_s} \\
 &= \alpha_p \frac{q \rho_s}{p_s} \dot{\mathcal{B}}_{y,s} R_s \Delta p \\
 &= \alpha_p \frac{\dot{\mathcal{B}}_{y,s}}{\mathcal{B}_{y,s}} R_s \frac{\Delta E}{\beta_s c} \\
 &= \alpha_p \frac{\dot{\mathcal{B}}_{y,s}}{\mathcal{B}_{y,s}} \left( \frac{\Delta E}{\omega_{\text{rev},s}} \right).
 \end{aligned}$$

#### I.4.8.5 Correction of exercises from the Section I.4.5

I.4.24: Starting from

$$\begin{aligned}
 \Delta\phi(t) &= \Delta\phi_m \sin(\omega_{s_0} t) \\
 \Rightarrow \Delta\dot{\phi} &= \Delta\phi_m \omega_{s_0} \cos(\omega_{s_0} t) \\
 \Rightarrow \frac{\eta \omega_{\text{rf}}^2}{\beta_s^2 E_s} \left( \frac{\Delta E}{\omega_{\text{rf}}} \right)_m \cos(\omega_{s_0} t) &= \Delta\phi_m \omega_{s_0} \cos(\omega_{s_0} t)
 \end{aligned}$$

We obtain

$$\frac{(\Delta E / \omega_{\text{rf}})_m}{\Delta\phi_m} = \frac{\beta_s^2 E_s}{|\eta| \omega_{\text{rf}}^2} \omega_{s_0} = \frac{\beta_s^2 E_s}{|\eta| h^2 \omega_{\text{rev},s}} Q_{s_0}.$$

We took  $|\eta|$  to obtain positive phase/energy maximum amplitudes.

I.4.25: Replacing  $\Delta E_m$  and using  $\Delta\phi_m = \omega_{\text{rf}}\tau_l/2$ 

$$\begin{aligned}\varepsilon_{l_0} &= \pi \Delta E_m \frac{\tau_l}{2} = \pi \omega_{\text{rf}} \Delta\phi_m \frac{\beta_s^2 E_s}{|\eta| \omega_{\text{rf}}^2} \omega_{s_0} \frac{\tau_l}{2} = \pi \frac{\omega_{\text{rf}} \tau_l}{2} \frac{\beta_s^2 E_s}{|\eta| \omega_{\text{rf}}} \omega_{s_0} \frac{\tau_l}{2} \\ \varepsilon_{l_0} &= \frac{\pi \beta_s^2 E_s}{4 |\eta|} \omega_{s_0} \tau_l^2 \\ &= \frac{\pi \beta_s^2 E_s}{4 |\eta|} \sqrt{-\frac{q V_{\text{rf}} \omega_{\text{rf}}^2 \eta \cos \phi_s}{2\pi h \beta_s^2 E_s}} \tau_l^2 \\ &= \tau_l^2 \sqrt{-\frac{\pi \omega_{\text{rev},s}^2 \beta_s^2 E_s}{32 \eta} q V_{\text{rf}} h \cos \phi_s}.\end{aligned}$$

 Replacing  $\Delta\phi_m$ 

$$\begin{aligned}\varepsilon_{l_0} &= \frac{\pi}{\omega_{\text{rf}}} \Delta E_m \Delta\phi_m = \frac{\pi}{\omega_{\text{rf}}} \Delta E_m \frac{1}{\omega_{s_0}} \frac{|\eta| \omega_{\text{rf}}^2}{\beta_s^2 E_s} \left( \frac{\Delta E}{\omega_{\text{rf}}} \right)_m \\ \varepsilon_{l_0} &= \frac{\pi |\eta|}{\beta_s^2 E_s} \frac{1}{\omega_{s_0}} \Delta E_m^2 \\ &= \frac{\pi |\eta|}{\beta_s^2 E_s} \sqrt{-\frac{2\pi h \beta_s^2 E_s}{q V_{\text{rf}} \omega_{\text{rf}}^2 \eta \cos \phi_s}} \Delta E_m^2 \\ &= \Delta E_m^2 \sqrt{-2\pi^3 \frac{\eta}{\omega_{\text{rev},s}^2 \beta_s^2 E_s} \frac{1}{q V_{\text{rf}} h \cos \phi_s}}\end{aligned}$$

## I.4.26:

*Linear synchrotron frequency and tune*

Low energy:

$$\begin{aligned}f_{s_0} &= \frac{1}{2 \cdot 3.14} \sqrt{\frac{1 \cdot 4.5 \cdot 10^6 \cdot (4620 \cdot 2 \cdot 3.14 / 23.11 \cdot 10^6)^2 \cdot 1.385 \cdot 10^{-3}}{2 \cdot 3.14 \cdot 4620 \cdot (14/14.03)^2 \cdot 14.03 \cdot 10^9}} \\ &\approx 784 \text{ Hz}\end{aligned}$$

$$Q_{s_0} = 784 \cdot 23.11 \cdot 10^{-6} \approx 1.81 \cdot 10^{-2}$$

High energy:

$$\begin{aligned}f_{s_0} &= \frac{1}{2 \cdot 3.14} \sqrt{\frac{1 \cdot 4.5 \cdot 10^6 \cdot (4620 \cdot 2 \cdot 3.14 / 23.05 \cdot 10^6)^2 \cdot 3.082 \cdot 10^{-3}}{2 \cdot 3.14 \cdot 4620 \cdot 1 \cdot 450 \cdot 10^9}} \\ &\approx 206 \text{ Hz}\end{aligned}$$

$$Q_{s_0} = 206 \cdot 23.05 \cdot 10^{-6} \approx 4.76 \cdot 10^{-3}$$

*Linear emittance*

$$\varepsilon_{l_0} = \frac{3.14 \cdot (14/14.03)^2 \cdot 14.03 \cdot 10^9}{4 \cdot 1.385 \cdot 10^{-3}} 2 \cdot 3.14 \cdot 784 \cdot (3 \cdot 10^{-9})^2 \approx 0.35 \text{ eVs}$$

### Energy spread

$$\begin{aligned}\delta_p &= 2 \frac{\Delta E_m}{\beta_s^2 E_s} = 4 \frac{\varepsilon_{l_0}}{\pi \tau_l \beta_s^2 E_s} = \frac{4 \cdot 0.35}{3.14 \cdot 3 \cdot 10^{-9} (14/14.03)^2 \cdot 14.03 \cdot 10^9} \\ &\approx 1.06 \times 10^{-2}\end{aligned}$$

### Adiabatic damping

$$\tau_{l,\text{high}} = \tau_{l,\text{low}} \left( \frac{E_{\text{high}}}{E_{\text{low}}} \right)^{-1/4} = 3 \cdot \left( \frac{450}{14.03} \right)^{-1/4} \approx 1.26 \text{ ns}$$

### Transition

The bunch length would tend to zero while the energy spread diverge to infinity! Non-adiabatic theory needed to better evaluate bunch parameters at transition crossing.

### Adiabatic bunch shortening

$$\begin{aligned}\tau_{l,\text{high}} &= \tau_{l,\text{low}} \left( \frac{V_{\text{high}}}{V_{\text{low}}} \right)^{-1/4} \\ \implies V_{\text{high}} &= V_{\text{low}} \left( \frac{\tau_{l,\text{high}}}{\tau_{l,\text{low}}} \right)^{-4} = V_{\text{low}} \times 16\end{aligned}$$

The required voltage increase is a factor 16! Not very efficient shortening.

**I.4.27:** The potential well at  $\pi - \phi_s$ , using the trigonometric identity, is

$$\begin{aligned}\mathcal{U}(\pi - \phi_s) &= \frac{qV_{\text{rf}}}{2\pi h} [\cos(\pi - \phi_s) - \cos \phi_s + (\pi - 2\phi_s) \sin \phi_s] \\ &= \frac{qV_{\text{rf}}}{2\pi h} [\cos \pi \cos \phi_s + \sin \pi \sin \phi_s - \cos \phi_s + (\pi - 2\phi_s) \sin \phi_s] \\ &= \frac{qV_{\text{rf}}}{2\pi h} [-2 \cos \phi_s + (\pi - 2\phi_s) \sin \phi_s] \\ &= \frac{qV_{\text{rf}}}{\pi h} \left[ -\cos \phi_s + \frac{(\pi - 2\phi_s)}{2} \sin \phi_s \right].\end{aligned}$$

**I.4.28:** The bucket area  $\mathcal{A}_{\text{bk}}$  is defined as:

$$\begin{aligned}\mathcal{A}_{\text{bk}} &= 2 \sqrt{\frac{2\beta_s^2 E_s}{|\eta| \omega_{\text{rf}}^2}} \int_{\phi_u}^{\phi_m} \sqrt{\mathcal{U}(\pi - \phi_s) - \mathcal{U}(\phi)} d\phi \\ &= 2 \sqrt{\frac{qV_{\text{rf}} \beta_s^2 E_s}{\pi h |\eta| \omega_{\text{rf}}^2}} \int_{\phi_u}^{\phi_m} \sqrt{\dots} d\phi\end{aligned}$$

where the integrand is given by:

$$\begin{aligned}
 \dots &= [\cos(\pi - \phi_s) - \cos \phi_s + (\pi - 2\phi_s) \sin \phi_s] \\
 &\quad - [\cos \phi - \cos \phi_s + (\phi - \phi_s) \sin \phi_s] \\
 &= [-2 \cos \phi_s + (\pi - 2\phi_s) \sin \phi_s] \\
 &\quad - [\cos \phi - \cos \phi_s + (\phi - \phi_s) \sin \phi_s] \\
 &= -\cos \phi_s - \cos \phi + (\pi - \phi - \phi_s) \sin \phi_s.
 \end{aligned}$$

Finally  $\Gamma(\phi_s)$  is defined as:

$$\begin{aligned}
 \Gamma(\phi_s) &= \frac{1}{4\sqrt{2}} \int_{\phi_u}^{\phi_m} \sqrt{-\cos \phi_s - \cos \phi + (\pi - \phi - \phi_s) \sin \phi_s} d\phi \\
 &\approx \frac{1 - \sin \phi_s}{1 + \sin \phi_s}.
 \end{aligned}$$

I.4.29:

*Low energy 14 GeV/c*

RF Bucket area

$$\begin{aligned}
 A_{\text{bk}} &= \frac{8}{4620 \cdot 2 \cdot 3.14 / 23.11 \cdot 10^6} \cdot \\
 &\quad \sqrt{\frac{2 \cdot 1 \cdot 4.5 \cdot 10^6 \cdot (14/14.03)^2 \cdot 14.03 \cdot 10^9}{3.14 \cdot 4620 \cdot 1.385 \cdot 10^{-3}}} \\
 &\approx 0.50 \text{ eVs}
 \end{aligned}$$

RF Bucket height (half height)

$$\begin{aligned}
 \Delta E_{\text{sep,m}} &= \sqrt{\frac{2 \cdot 1 \cdot 4.5 \cdot 10^6 \cdot (14/14.03)^2 \cdot 14.03 \cdot 10^9}{3.14 \cdot 4620 \cdot 1.385 \cdot 10^{-3}}} \\
 &\approx 79.1 \text{ MeV}
 \end{aligned}$$

*High energy 450 GeV/c*

RF Bucket area

$$\begin{aligned}
 A_{\text{bk}} &= \frac{8}{4620 \cdot 2 \cdot 3.14 / 23.05 \cdot 10^6} \cdot \\
 &\quad \sqrt{\frac{2 \cdot 1 \cdot 4.5 \cdot 10^6 \cdot 1 \cdot 450 \cdot 10^9}{3.14 \cdot 4620 \cdot 3.082 \cdot 10^{-3}}} \\
 &\approx 1.91 \text{ eVs}
 \end{aligned}$$

RF Bucket height (half height)

$$\begin{aligned}
 \Delta E_{\text{sep,m}} &= \sqrt{\frac{2 \cdot 1 \cdot 4.5 \cdot 10^6 \cdot 1 \cdot 450 \cdot 10^9}{3.14 \cdot 4620 \cdot 3.082 \cdot 10^{-3}}} \\
 &\approx 301 \text{ MeV}
 \end{aligned}$$

**Filling factor:** From the previous module exercise, the longitudinal emittance is 0.35 eVs. The

filling factor in area is

$$0.35/0.50 \approx 70\%$$

**Matching:** The bunch length and energy spread are fixed at injection. In order to match the bunch, the bucket height should be reduced by 10%. The RF voltage can be reduced to reduce the bucket height, with a scaling  $\sqrt{V_{\text{rf}}}$

$$\frac{\Delta E_{\text{sep},m,2}}{\Delta E_{\text{sep},m,1}} = 0.9 = \sqrt{\frac{V_{\text{rf},2}}{V_{\text{rf},1}}} \rightarrow V_{\text{rf},2} = 0.9^2 V_{\text{rf},1} \approx 0.81 V_{\text{rf},1}$$

The RF voltage should be reduced by 20% (useful tip:  $(1 - \epsilon)^n \approx 1 - n\epsilon \rightarrow (1 - 0.1)^2 \approx 1 - 2 \cdot 0.1$ ).

## References

- [1] E.D. Courant and H.S. Snyder, Theory of the alternating-gradient synchrotron, *Ann. Phys.* **3** (1958) 1–48, doi:10.1016/0003-4916(58)90012-5.
- [2] A. Lasheen, Animations of the Longitudinal Beam Dynamics lecture, presented at the Joint Universities Accelerator School (JUAS), Zenodo, Aug. 2024, doi:10.5281/zenodo.13222635.
- [3] F. Hinterberger, Electrostatic accelerators, in Proc. CERN Accelerator School and KVI: Specialised CAS Course on Small Accelerators, Zeegse, The Netherlands, 24 May–2 Jun. 2005, Edited by D. Brand, CERN-2006-012 (CERN, Geneva, 2006), pp. 95–112, doi:10.5170/CERN-2006-012.95.
- [4] Wikipedia - Cathode-ray tube, [https://en.wikipedia.org/wiki/Cathode-ray\\_tube](https://en.wikipedia.org/wiki/Cathode-ray_tube), last accessed 14 Nov. 2024.
- [5] Wikipedia - Paschen's law, [https://en.wikipedia.org/wiki/Paschen%27s\\_law](https://en.wikipedia.org/wiki/Paschen%27s_law), last accessed 14 Nov. 2024.
- [6] F. Bordry *et al.*, Accelerator engineering and technology: accelerator technology, in Particle physics reference library: Volume 3: Accelerators and colliders, Edited by S. Myers and H. Schopper (Springer, Cham, 2020), pp. 337–517, doi:10.1007/978-3-030-34245-6\_8.
- [7] CERN PS panorama, [online], <https://panoramas-outreach.cern.ch/viewer?fov=90&id=43087505&lat=-0.72&lon=36.00>, last accessed 14 Nov. 2024.
- [8] E. Jensen, RF cavity design, in Proc. CAS Advanced Accelerator Physics, Trondheim, Norway, 18–29 Aug. 2013, Edited by W. Herr, CERN-2014-009 (CERN, Geneva, 2014), pp. 405–429, doi:10.5170/CERN-2014-009.405, and slides pres. in Darmstadt, 2009.
- [9] CERN Optics repository, LEIR Optics, [online], [https://acc-models.web.cern.ch/acc-models/leir/2021/scenarios/nominal/2\\_flat\\_top/](https://acc-models.web.cern.ch/acc-models/leir/2021/scenarios/nominal/2_flat_top/), last accessed 14 Nov. 2024.
- [10] C. Bovey *et al.*, A selection of formulae and data useful for the design of A.G. synchrotrons, CERN-MPS-SI-Int-DL-70-4 (CERN, Geneva, 1970), doi:10.17181/CERN-MPS-SI-Int-DL-70-4.
- [11] J.A. MacLachlan and J.-F. Ostiguy, User's guide to ESME 2001, FERMILAB-TM-2132 (Fermilab, Batavia, IL, 2000), [Inspire](https://arxiv.org/abs/2001.00001).

- [12] H. Timko *et al.*, Beam longitudinal dynamics simulation studies, *Phys. Rev. Accel. Beams* **26** (2023) 114602, doi:[10.1103/PhysRevAccelBeams.26.114602](https://doi.org/10.1103/PhysRevAccelBeams.26.114602).
- [13] A. Oeftiger, An overview of PyHEADTAIL, CERN-ACC-NOTE-2019-0013 (CERN, Geneva, 2019), doi:[10.17181/CERN-ACC-NOTE-2019-0013](https://doi.org/10.17181/CERN-ACC-NOTE-2019-0013).
- [14] G. Iadarola *et al.*, Xsuite: An integrated beam physics simulation framework, in Proc. 68th Adv. Beam Dyn. Workshop High-Intensity High-Brightness Hadron Beams (HB'23), JACoW (CERN, Geneva, 2024), pp. 73–80, doi:[10.18429/JACoW-HB2023-TUA211](https://doi.org/10.18429/JACoW-HB2023-TUA211).
- [15] A. Shishlo *et al.*, The particle accelerator simulation code PyORBIT, *Procedia Comput. Sci.* **51** (2015) 1272–1281, doi:[10.1016/j.procs.2015.05.312](https://doi.org/10.1016/j.procs.2015.05.312).
- [16] S.Y. Lee, Accelerator Physics, 4th ed. World Scientific, 2019, doi:[10.1142/11111](https://doi.org/10.1142/11111).
- [17] J.M. Belleman, W. Andreatza, and A.A. Nosych, A new Wall Current Monitor for the CERN Proton Synchrotron, in Proc. of International Beam Instrumentation Conference (IBIC'16), Barcelona, Spain: JACoW, Feb. 2017, pp. 143—146, doi:[10.18429/JACoW-IBIC2016-MOPG41](https://doi.org/10.18429/JACoW-IBIC2016-MOPG41).
- [18] S. Hancock, A simple algorithm for longitudinal phase space tomography, CERN-PS-RF-NOTE-97-06 (CERN, Geneva, 1997), doi:[10.17181/CERN-PS-RF-Note-97-06](https://doi.org/10.17181/CERN-PS-RF-Note-97-06).
- [19] R. Garoby, RF gymnastics in synchrotrons, in Proc. CERN Accelerator School: RF for Accelerators, Ebeltoft, Denmark, 8–17 Jun. 2010, Edited by R. Bailey, CERN-2011-007 (CERN, Geneva, 2011), pp. 431–446, doi:[10.5170/CERN-2011-007.431](https://doi.org/10.5170/CERN-2011-007.431).
- [20] H. Bruck, *Accélérateurs circulaires de particules: introduction à la théorie* (Institut National des Sciences et Techniques Nucléaires, Saclay, Presses Universitaires de France, 1966), English translation [LA-TR-72-10-Rev](https://doi.org/10.17181/CERN-PS-RF-Note-97-06).
- [21] J.A. MacLachlan, Difference equations for longitudinal motion in a synchrotron, FERMILAB-FN-0529 (Fermilab, Batavia, IL, 1989) [Inspire](https://doi.org/10.17181/CERN-PS-RF-Note-97-06).
- [22] J.A. MacLachlan, Differential equations for longitudinal motion in a synchrotron, FERMILAB-FN-0532 (Fermilab, Batavia, IL, 1990), [Inspire](https://doi.org/10.17181/CERN-PS-RF-Note-97-06).
- [23] E. Metral, Elias Metral's personal web site (JUAS courses, exercises, exams and corrections), [online], <http://emetral.web.cern.ch/>, last accessed 14 Nov. 2024.
- [24] B. Holzer, Introduction to longitudinal beam dynamics, in Proc. CERN Accelerator School: Course on Superconductivity for Accelerators, Erice, Italy, 24 Apr.–4 May 2013, CERN-2014-005 (CERN, Geneva, 2014), Edited by R. Bailey, pp. 41–56, doi:[10.5170/CERN-2013-007.47](https://doi.org/10.5170/CERN-2013-007.47).
- [25] H. Damerau, Introduction to non-linear longitudinal beam dynamics, in Proc. CERN Accelerator School 2019: Introduction to Accelerator Physics, Vysoke-Tatry, Slovakia, 8–21 Sep. 2019, doi:[10.48550/arXiv.2108.04497](https://doi.org/10.48550/arXiv.2108.04497).
- [26] W. Pirkel, Longitudinal beam dynamics, in Proc. CERN Accelerator School: 5th Advanced Accelerator Physics Course, Rhodes, Greece, 20 Sep.–1 Oct. 1993, Edited by S. Turner, CERN-95-06 (CERN, Geneva, 1995), pp. 233–257, doi:[10.5170/CERN-1995-006.233](https://doi.org/10.5170/CERN-1995-006.233).
- [27] L. Rinolfi, Longitudinal beam dynamics application to synchrotron, Pres. Joint Universities Accelerator School; 1st Course on Accelerator Physics, Archamps, France, 10 Jan.–12 Feb. 2000, CERN-PS-2000-008-LP (CERN, Geneva, 2000), doi:[10.17181/CERN-PS-2000-008-LP](https://doi.org/10.17181/CERN-PS-2000-008-LP).

- [28] J. Le Duff, Longitudinal beam dynamics in circular accelerators, in Proc. CERN Accelerator School: 5th General Accelerator Physics Course, Jyväskylä, Finland, 7–18 Sep 1992, Edited by S. Turner, CERN-94-01 (CERN, Geneva, 1994), pp. 289–311, [doi:10.5170/CERN-1994-001.289](https://doi.org/10.5170/CERN-1994-001.289).
- [29] F. Tecker, Longitudinal beam dynamics in circular accelerators, in Proc. CERN Accelerator School 2019: Introduction to Accelerator Physics, Vysoke-Tatry, Slovakia, 8–21 Sep. 2019, [doi:10.48550/arXiv.2011.02932](https://doi.org/10.48550/arXiv.2011.02932).
- [30] H. Wiedemann, *Particle accelerator physics*, 4th ed. (Springer Cham, 2015), [doi:10.1007/978-3-319-18317-6](https://doi.org/10.1007/978-3-319-18317-6).
- [31] S. Humphries, *Principles of charged particle acceleration* (Wiley, New York, NY, 1999), [Internet Archive](#).
- [32] T.P. Wangler, *RF linear accelerators* (Wiley, New York, NY, 2008), [doi:10.1002/9783527623426](https://doi.org/10.1002/9783527623426).
- [33] B.W. Montague, Single particle dynamics: Hamiltonian formulation, in Proc. 1st Int. School of Particle Accelerators “Ettore Majorana”, Erice, Italy, 10–22 Nov. 1976, Edited by M.H. Blewett, CERN-77-13 (CERN, Geneva, 1977), pp. 37–51, [doi:10.5170/CERN-1977-013.37](https://doi.org/10.5170/CERN-1977-013.37).
- [34] A.A. Kolomensky and A.N. Lebedev, *Theory of cyclic accelerators*, (North-Holland, Amsterdam, 1966), [Internet Archive](#).
- [35] G. Dôme, Theory of RF acceleration, in Proc. CERN Accelerator School: Accelerator Physics, Oxford, UK, 16–27 Sep. 1985, Edited by S. Turner, CERN-87-03-V-1 (CERN, Geneva, 1987), pp. 110–158, [10.5170/CERN-1987-003-V-1.110](https://doi.org/10.5170/CERN-1987-003-V-1.110).
- [36] H.G. Hereward, What are the equations for the phase oscillations in a synchrotron?, CERN, Geneva, CERN-66-06 (CERN, Geneva, 1966), [doi:10.5170/CERN-1966-006](https://doi.org/10.5170/CERN-1966-006).